Entwicklung eines Modells zur Simulation der Bodenerosion bei Starkregen auf Grundlage eines zweidimensionalen HN-Modellansatzes

Development of a Model for the Simulation of Soil Erosion due to Heavy Precipitation based on a Two-dimensional HN Model Approach

Dissertation

zur Erlangung des akademischen Grades
einer Doktorin der Naturwissenschaften der Fakultät für
Empirische Humanwissenschaften und Wirtschaftswissenschaften
der Universität des Saarlandes

vorgelegt von

Rebecca Hinsberger

aus Neunkirchen

Saarbrücken, 2026

Dekan

Univ.-Prof. Dr. Axel Mecklinger, Universität des Saarlandes

Berichterstatter

Univ.-Prof. Dr. rer. nat. Jochen Kubiniok, Universität des Saarlandes

Prof. Dr.-Ing. Alpaslan Yörük, Hochschule für Technik und Wirtschaft des Saarlandes (htw saar)

Univ.-Prof. Dr. rer. nat. Florian Weber, Universität des Saarlandes

Tag der Disputation

15. Dezember 2025

Summary

Heavy precipitation is a natural and extreme event that has gained public attention in recent years. The hazards and risks posed by these extreme events present a significant challenge. An additional concern is soil erosion on cropland, often caused by heavy precipitation. Flash floods transport soil material, posing a risk of soil loss and negative effects on other ecosystems, such as streams, which are polluted by the influx of sediment. In addition, the sedimentation of soil material in urban areas increases the damage caused by flash floods.

German municipalities are increasingly involved in managing the risks of heavy precipitation, which includes assessing the dangers and risks associated with it. Two-dimensional hydrodynamic numerical models (2D models) are used for this purpose, accurately calculating the hydraulics of surface runoff. Additionally, erosion models are available to estimate erosion hazards. However, these models use erosion approaches with simplified hydraulic calculations. To date, no analysis has been conducted that combines precisely calculated hydraulic forces acting on the soil with a process-oriented approach to soil erosion. Therefore, this thesis aims to demonstrate that accurately calculating hydraulics using a 2D model can enhance soil erosion modeling to a greater degree of accuracy than previously possible.

Various methods were used to test this hypothesis, and corresponding results were obtained. First, the hydraulics of the 2D model were examined independently of the erosion approach. The flow resistance of the surface, known as roughness, plays a significant role in the flow process. This was investigated in laboratory experiments to better estimate suitable values for surface runoff. The results show that the ratio of vegetation height to water depth is particularly decisive for the roughness value. The resistance increases with increasing runoff at water depths less than the vegetation height. It reaches a maximum value when the water depth corresponds to the vegetation height, then decreases until the water depth exceeds approximately 5 to 7 times the vegetation height. Beyond this point, constant roughness values can be determined.
For the combined 2D hydraulic and erosion calculation, a suitable approach for calculating sediment transport capacity in surface runoff was first selected and then coupled with the existing 2D model HydroAS GS. The transport capacity approach by Govers (1990) was used, resulting in the new, coupled HydroAS GS–Govers model. Erosion data was collected over three years to calibrate and validate the new model. In particular, linear erosion that occurred after a heavy precipitation event was recorded using an unmanned aerial vehicle (UAV) and analyzed in terms of spatial distribution and the amount of erosion in rills. A total of 11 fields with 32 rills were examined. The data was used to test the existing erosion

models with simplified hydraulics, RUSLE2 and EROSION-3D, and the new HydroAS GS–Govers model. A comparison of the model results showed a significant improvement in rill erosion, both in terms of rill generation, spatial location, and erosion volumes, compared to the observed erosion data.

Furthermore, this work examined the accuracy of UAV-generated digital elevation models (DEMs) of croplands with erosion to estimate the extent of error in the calibration and validation data. A key finding was that rill depths were underestimated in the DEMs generated compared to manual measurements, resulting in an average underestimation of erosion of 10%.

The proposed coupled 2D hydraulic and erosion model, HydroAS GS–Govers, can be used for a detailed analysis of erosion on arable land caused by heavy precipitation. This model allows for the spatial and quantitative determination of rill erosion, which is a significant contributor to total erosion. Consequently, the model can verify the dangers and damaging effects of extreme heavy precipitation. Potential applications of the model include using simulation results as a basis for developing erosion countermeasures and assessing their effectiveness, as well as estimating sediment-bound nutrient and pollutant inputs from arable land into neighboring ecosystems.

Zusammenfassung

Starkregen ist ein natürliches, extremes Ereignis, das in den vergangenen Jahren in den Fokus der Öffentlichkeit gerückt ist. Die Gefahren und Risiken dieser Extremereignisse stellen eine ernstzunehmende Herausforderung dar. Eine zusätzliche Problematik ergibt sich durch die häufig mit Starkregen einhergehende Bodenerosion auf Ackerflächen. Sturzfluten transportieren Bodenmaterial und verursachen dadurch nicht nur ein Risiko für Bodenverluste, sondern auch negative Auswirkungen für andere Ökosysteme, wie Fließgewässer, die durch den Eintrag von Sedimenten belastet werden. Gleichzeitig erhöht der Sedimenteintrag in Siedlungsräume die Schadwirkung von Starkregenereignissen.

Zurzeit wird in deutschen Kommunen vermehrt Starkregenrisikomanagement (SRRM) betrieben, wobei die Gefahren und Risiken bei Starkregen bewertet werden. Dazu werden zweidimensionale hydrodynamisch-numerische Modelle (2D-Modelle) herangezogen, die die Hydraulik der Oberflächenabflüsse präzise berechnen können. Parallel dazu liegen Erosionsmodelle vor, die zur Abschätzung von Erosionsgefahren angewendet werden. Hierbei werden allerdings Erosionsansätze mit vereinfachter hydraulischer Berechnung genutzt. Bisher liegt keine kombinierte Betrachtung von präzise berechneten hydraulischen Kräften, die auf den Boden wirken, und einem prozess-orientieren Bodenerosionsansatz vor. Daher soll in dieser Arbeit gezeigt werden, dass durch die akkurate Berechnung der Hydraulik mittels 2D-Modell auch die Bodenerosion besser abgebildet werden kann als bisher möglich.

Zur Überprüfung dieser Hypothese wurden verschiedene Methoden angewendet. Zunächst wurde die Hydraulik des 2D-Modells unabhängig von dem Erosionsansatz untersucht. Eine signifikante Rolle im Fließprozess wird durch den Fließwiderstand der Oberfläche dargestellt, der sogenannten Rauheit. Diese wurde zur besseren Abschätzung geeigneter Rauheitswerte im Labor untersucht. Die Ergebnisse zeigen, dass besonders das Verhältnis von Vegetationshöhe zu Wassertiefe entscheidend für die Festlegung des Rauheitswertes ist. Bei Wassertiefen geringer als die Vegetationshöhe nimmt der Widerstand mit steigendem Abfluss zu. Der Widerstand erreicht einen maximalen Wert, wenn die Wassertiefe der Vegetationshöhe entspricht und nimmt wieder ab, bis die Wassertiefe die Vegetationshöhe um das 5-bis 7-fache übersteigt. Danach kann von einem konstanten Rauheitswert ausgegangen werden.
Zur kombinierten 2D-Hydraulik- und Erosionsberechnung wurde zunächst ein geeigneter Ansatz zur Berechnung der Sedimenttransportkapazität bei Oberflächenabfluss ausgewählt und mit dem bestehenden 2D-Modell HydroAS GS gekoppelt. Hierbei kam der Ansatz nach

Govers (1990) zur Anwendung, wodurch das neue, gekoppelte HydroAS GS–Govers Modell entstand. Zur Kalibrierung und Validierung des neuen Modells wurden über drei Jahre Erosionsdaten gesammelt. Hierbei wurde insbesondere die lineare Erosion, die nach einem Starkregenereignis auftrat, mithilfe einer Drohne aufgenommen und im Hinblick auf die räumliche Verteilung sowie die Erosionsmenge der Rinnen analysiert. Insgesamt konnten 11 Felder mit 32 Rinnen untersucht werden. Die Daten wurden genutzt, um die bereits existierenden Erosionsmodelle mit vereinfachten hydraulischen Ansätzen, RUSLE2 und EROSION-3D, und das neue HydroAS GS–Govers Modell zu prüfen. Ein Vergleich der Modellergebnisse mit den beobachteten Daten zeigte eine signifikante Verbesserung der Rinnenerosion, sowohl in der Rinnengenerierung, ihrer räumlicher Lage und der Erosionsmengen.

Weiterhin wurde die Genauigkeit der durch Drohnenaufnahmen generierten, digitalen Geländemodelle (DGM) von Ackerflächen mit Erosion betrachtet, um das Fehlerausmaß der Kalibrierungs- und Validierungsdaten abzuschätzen. Ein entscheidendes Ergebnis stellte dabei die Unterschätzung der Rinnentiefe in Drohnen-generierten DGMs im Vergleich zu händischen Messungen dar. Insgesamt ist im Mittel mit einer Unterschätzung der Erosionsmenge von 10 % zu rechnen.

Das neu erstellte, gekoppelte 2D-Hydraulik- und Erosionsmodell HydroAS GS–Govers kann zur detaillierten Analyse von Erosion auf Ackerflächen, ausgelöst durch Starkregenereignisse, genutzt werden. Dadurch kann insbesondere die Rinnenerosion, die einen Großteil der Gesamterosion ausmacht, räumlich und mengenmäßig bestimmt werden. Die Gefahren und Schadauswirkungen, die ein extremes Starkregenereignis haben kann, können dadurch verifiziert werden. Mögliche Einsatzmöglichkeiten des Modells sind die Nutzung der Simulationsergebnisse als Basis zur Erarbeitung von Gegenmaßnahmen von Erosion und zu deren Wirksamkeitsnachweis sowie die Abschätzung sedimentgebundener Nähr- und Schadstoffeinträge von Ackerflächen in benachbarte Ökosysteme.

Danksagung

Mein erster und besonderer Dank geht an Prof. Dr. Alpaslan Yörük, der mich während meines Studiums und der Promotion stets gefördert und gefordert und mir immer sein vollstes Vertrauen geschenkt hat. Danke für die Wertschätzung während meiner gesamten Htw-Zeit. Ein ebenso großer Dank geht an Prof. Dr. Jochen Kubiniok, der mir alle Freiheiten bei der Bearbeitung geschenkt hat, stets für alle Fragen offen war und mir immer mit Rat zur Seite stand, wenn ich ihn brauchte.
Danke an beide für die vielen fachlichen Ratschläge und Ideen und die Möglichkeiten der persönlichen und fachlichen Entwicklung, die mir während meiner Promotionszeit geschenkt wurden. Ich konnte mich glücklich schätzen, gleich zwei Doktorväter an meiner Seite zu wissen.
Herrn Prof. Dr. Florian Weber danke ich für die Bereitschaft dieses Promotionsverfahren als weiterer Gutachter zu übernehmen.

Mein Dank gilt zudem Andreas Biehler, der einen entscheidenden Beitrag dazu geleistet hat, dass ich schon früh meinen Weg in die Forschungsgruppe Wasser gefunden habe. Danke für den Glauben in mich seit Stunde eins und jede erdenkliche Unterstützung während meiner gesamten Zeit im Team. Besonders danken möchte ich auch meinen Kolleg*innen, insbesondere Volker Mißler, Yannick Brach, Joshua Becker und Anton Petry, sowohl für die gute Zusammenarbeit als auch für die Ablenkung in den Pausen. Danke an Martin Engel, der mich besonders in meiner Anfangszeit im Geotechniklabor unterstützt hat und an alle studentischen und wissenschaftlichen Hilfskräfte für die Hilfe bei Laborversuchen und Feldstudien.
Vielen Dank an alle Hydrotec‘ler, die mich im Laufe der Zeit mit ihren Erfahrungen und Fachkenntnissen unterstützt haben. Mein Dank geht insbesondere an Andreas Förster und Dr. Eva Loch für jegliche Unterstützung und Hilfe beim Verständnis von Feststofftransportsimulationen und Frédéric Connotte für das Korrekturlesen meiner Arbeit.

Ein ganz besonderer Dank gilt meiner Familie, auf deren Einsatz ich immer setzen konnte, sowohl mental als auch aktiv bei meinen Feldstudien und allen anderen Herausforderungen. Danke, dass ihr mich zu dem Menschen gemacht habt, der ich heute bin.

Der größte Dank gilt meinem Partner Markus, der mich in allen Phasen meiner Arbeit unermüdlich unterstützt und ermutigt hat. Danke für das Lesen meiner Texte, dem Feiern kleiner und großer Erfolge und für Deine Geduld mit mir. Ohne Dich wäre diese Arbeit so nicht möglich gewesen.

Danke!

Table of Contents

List of Figures

List of Tables

List of Abbreviations

Abbreviation	Description
ABAG	Allgemeine Bodenabtragsgleichung
CORR	Corrected
DEM	Digital elevation model
E3D	EROSION-3D
EUROSEM	European Soil Erosion Model
FEWS	Flood Early Warning System
GCP	Ground Control Point
GIS	Geo-information system
GNSS	Global Navigation Satellite System
IPCC	Intergovernmental Panel on Climate Change
LISEM	Limburg Soil Erosion Model
MAE	Mean absolute error
MUSLE	Modified USLE
P4	Phantom 4
RMSE	Root mean square error
RoG	Rain-on-Grid
RTK	Real-time kinematic
SfM	Structure from motion
SMS	Surface-water Modeling System
SRTM	Shuttle radar topography mission
RUSLE	Revised Universal Soil Loss Equation
UAV	Unmanned aerial vehicle
USLE	Universal Soil Loss Equation
WEPP	Water Erosion Prediction Project
2D	Two-dimensional

List of Symbols

Symbol	Unit	Description
A	m^2	Cross-sectional area
A	t/(ha*a)	Soil loss (USLE family models)
C	-	Crop cover and management factor (USLE family models)
C_D	-	Bulk drag coefficient
D_H	m	Hydraulic diameter
d_{veg}	m	Diameter of the vegetation
D_{veg}	pcs/m^2	Density of the vegetation
f	-	Friction factor (Darcy–Weisbach)
f '	-	Bottom friction factor
f "	-	Vegetation friction factor
Fr	-	Froude number
g	m/s^2	Gravitational acceleration
h	m	Water depth
H	m	Water level above reference level
h_{veg}	m	Vegetation height
I_R	-	Friction slope
I_S	-	Bed slope
K	-	Soil erodibility factor (USLE family models)
k_N	m	Equivalent sand-grain roughness (Nikuradse)
k_S	$m^{1/3}/s$	Strickler roughness coefficient
L	-	Slope length factor (USLE family models)
ν	m^2/s	Viscosity
P	-	Protection factor (USLE family models)
p_r	-	Shape coefficient
Q	m^3/s	discharge
R	-	Rainfall erosivity factor (USLE family models)
R_H	m	Hydraulic radius
Re	-	Reynolds number
S	-	Channel slope / Slope gradient factor (USLE family models)
t	-	Time
τ	Pa	Shear stress
τ_{cr}	Pa	Critical shear stress
u	m/s	Flow velocity in x direction

Symbol	Unit	Description
v	m/s	Flow velocity in y direction
x	-	Longitudinal direction along the flume
y	-	Transverse direction of the flume
v	m/s	Flow velocity
ω	$kg*m^2/s^3$	Stream power
ω_{cr}	$kg*m^2/s^3$	Critical stream power

1 Introduction

1.1 Relevance and Motivation

In recent decades, extreme events, such as droughts, floods, and flash floods, have increased, leading to adverse consequences for human settlements, infrastructure, and the environment. Regarding floods and flash floods in Germany, the events in July 2021, with persistent and heavy precipitation, resulted in floodings, particular in the federal states of Rhineland–Palatinate and North Rhine–Westphalia. In addition, several heavy precipitation events and flash floods have occurred in Germany over the past few years. Media-effective events occurred in Simbach (Bayern, Germany) and Braunsbach (Baden–Württemberg, Germany) in 2016. In the federal state of Saarland, Germany, which is the area in which this study was conducted, flash floods occurred in Eppelborn in 2016 and Kleinblittersdorf in 2018. Figure 1-1 shows the flow path of a flash flood on a road in Eppelborn municipality.

Figure 1-1: Runoff across a road caused by a heavy precipitation event in Eppelborn in 2016 (Feuerwehr Eppelborn (n.d.), Photo: Gerd Maron).

Different reasons for the increased occurrence of these events have been proposed in the literature. CO_2-driven climate change could increase the number of heavy precipitation events (IPCC, 2023; Robinson et al., 2021). An increase in temperature increases the atmospheric water-holding capability. Therefore, the amount of water that can potentially be provided for precipitation also increases (Held and Soden, 2006; Trenberth et al., 2003). Additionally, framework changes such as land use and soil management can affect the consequences of these events (Auerswald et al., 2025).

Regardless of the reason for the occurrence, frequent heavy precipitation events with increasing rainfall lead to flash floods that negatively impact the environment, infrastructure and humans (IPCC, 2021; Nunes & Nearing, 2011). Thus, hydraulic models have been

used to simulate the water flow in rivers and overland flows to better understand and counteract the risks of flash floods (Al-Fugara et al., 2023; Hu and Song, 2018; Huang et al., 2015; Liang et al., 2016). There is a wide range of models with low levels of accuracy and quick results, up to those with higher levels of accuracy, which are associated with longer computing times. A balanced relationship between accuracy and speed can be achieved using two-dimensional (2D) state-of-the-art hydrodynamic numerical models for flood and flash flood simulations. These models solve complete shallow water equations and consider the turbulence and acceleration terms.

In addition, soil erosion can have negative consequences both on- and off-site. On-site soil that is eroded from croplands is lost to future cultivation. Erosion rates often exceed the rates of regeneration and new soil formation many times (Amelung et al., 2018). In addition, the actual crop yield can be drastically reduced. Off-site, eroded sediments can cause severe damage to infrastructure and buildings and affect adjacent ecosystems, such as rivers, through pollution, primarily caused by pesticides and eutrophication from nutrients. In particular, a single heavy precipitation event can cause a high degree of erosion (Parkin et al., 2008). Soil erosion remains a challenge for both farmers and other ecosystems. Therefore, predictive models have been developed to forecast and implement measures for reducing soil erosion. Soil erosion modeling has been conducted for more than 50 years. Empirical (universal soil loss equation (USLE)) and process-based (Water Erosion Prediction Project (WEPP) and European Soil Erosion Model (EUROSEM)) models have been developed. Process-based models use a hydraulic approach to estimate water forces acting on the soil. As stated by Morgan et al. (1998b), soil erosion predictions are only as accurate as the hydraulic results. Nevertheless, the aforementioned models use simplified hydraulic approaches to calculate the forces acting on the soil. Thus, errors are part of the simulation owing to imprecise hydraulic results.

Currently, the physical bases of the hydraulic and erosion models used are not at the same level.

1.2 Background and Knowledge Gaps

Water flow and soil erosion are closely related. In this section, the frameworks of these processes and the potential for their modeling are discussed. Currently, hydraulic models can be used to simulate water flow, and erosion models are available to simulate the detachment, transport, and deposition of sediments in rivers or on arable land. Based on this analysis, knowledge gaps are identified.

1.2.1 Fundamentals of Water Flow and Erosion Processes

1.2.1.1 Fundamentals of Water Flow

Hydrological and hydraulic processes on Earth include precipitation, runoff generation and concentration, and flood routing. Precipitation leads to surface runoff, in which two primary flow processes can be distinguished: unchanneled overland flow and channeled stream flow. Overland flow is characterized by shallow water of a few centimeters and high slopes of several percent, whereas stream flow or river flow indicates a water depth of decimeters and low slopes in the range of per mil (‰).

Similar to the different flow processes, a distinction was made between the resulting hazards and risks. Heavy and intense precipitation can lead to strong overland flows and flash floods, which are particularly hazardous to slopes in catchment areas. Heavy precipitation events were defined as those with an intensity of at least 15 mm/h (DWA, n.d.). In contrast, heavy and continuous rain accumulates almost harmlessly in the catchment area, leading to an increase in the water level of the stream in larger catchments. This can potentially result in flooding that endangers the known floodplains.

Overland and stream flows are influenced by the surface over which they flow. This factor is referred to as roughness. For overland flow, land use is a significant factor in determining roughness, whereas for streams, flume conditions, such as vegetation or concrete, are crucial. Roughness factors cannot be physically described and are therefore empirically derived. However, existing studies have primarily focused on stream flow conditions, and research on transferability is limited. Nevertheless, roughness values based on stream flows have also been used for flow calculations in flash flood modeling (Costabile et al., 2021; David and Schmalz, 2020; Zeiger and Hubbart, 2021).

Sediment is a common surface condition that occurs in both overland flows and streams. These sediments form the surface and are influenced by water forces acting on the soil surface. The frameworks and consequences of these forces are discussed in the following sections.

1.2.1.2 Fundamentals of Soil Erosion Processes

Sediment aggregates can be detached, transported by the water flow, and deposited when the water force decreases. All subprocesses contribute to the complexity of erosion. Erosion can occur in streams or on arable land. The principles of the forces acting on the soil are similar for both processes. However, as the focus of this study was soil erosion on arable land, this topic should be discussed in more detail.

Figure 1-2 illustrates relevant soil erosion processes (beige boxes) and their influencing factors (white boxes).

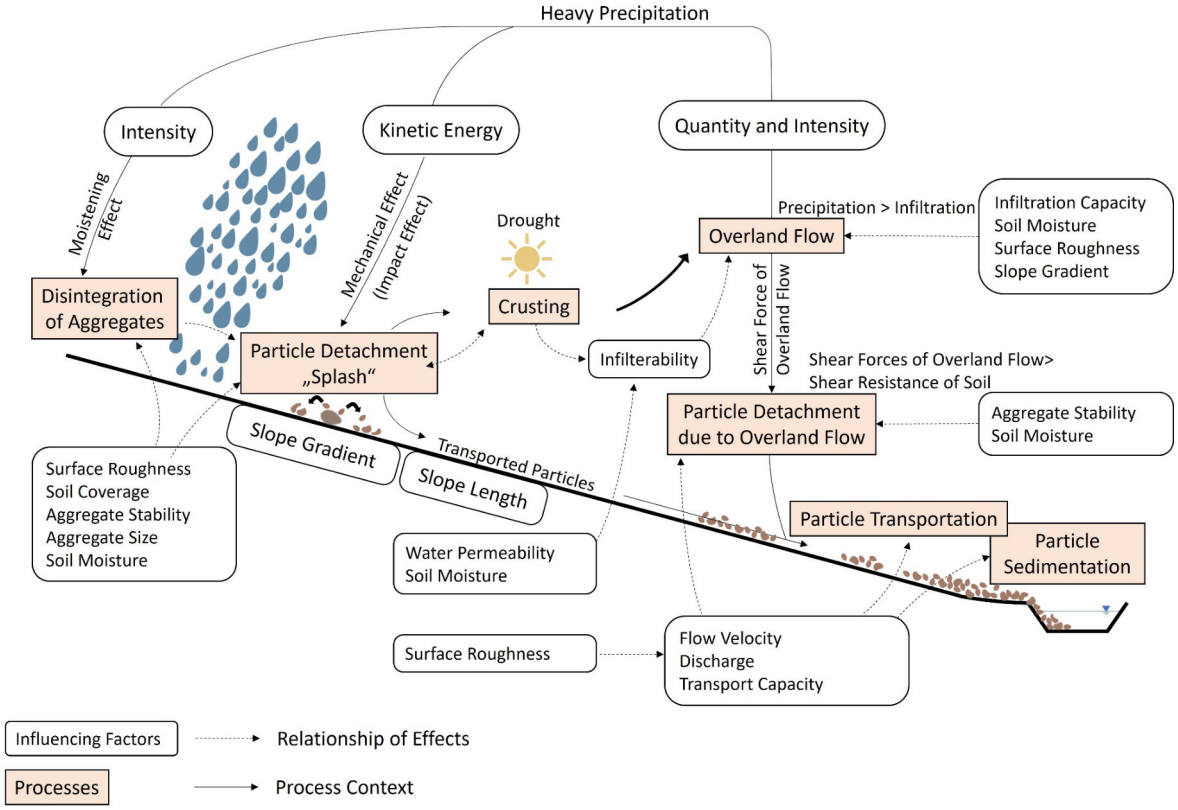

Figure 1-2: Processes and influencing factors of the soil erosion processes (Duttmann, 2001; modified)

In principle, soil detachment occurs when the raindrop or water flow forces exceed the holding force of the soil. The flow exerts a driving force on the particles in the direction of the flow, causing them to detach. These forces are counteracted by holding forces, such as weight, cohesion, and adhesion.

Owing to the impact of raindrops on the soil, soil aggregates disintegrate and are displaced. This process is often referred to as splash erosion (Prasuhn, 1991). The impact of the raindrop energy load depends on the amount and intensity of precipitation as well as on the size of the raindrops. In particular, high-energy loads are caused by heavy precipitation with high intensity and large raindrops up to 3 mm in diameter. The raindrops disintegrate and detach soil aggregates and particles. As a result, particles are infiltrated with water, washed into the pores, and the soil is silted, hindering further infiltration. This silt layer can reduce the infiltration capacity by 90 %. Consequently, surface runoff increases, leading to additional forces acting on the soil. The largest portion of the total erosion is contributed by the accumulated runoff in rills, with erosion due to splash and shallow water accounting for only 20 %, which further decreases with time and slope steepness (Govers and Poesen, 1988).

The erosion processes and arable land conditions play a significant role in determining erosion characteristics. Erosion can occur broadly in sheets and is concentrated in the rills or gullies.

The sediments provided by the detachment of raindrops and flows are transported by runoff. The transport capacity (TC) of a flow determines its ability to transport sediment. This capacity is the maximum a flow can carry and depends primarily on the grain size and flow velocity. When the velocity decreases owing to changes in topography or discharge, the sediments become detached. Sedimentation mostly occurs at the base of hillslopes and in adjacent areas and ecosystems such as streams.

Given that heavy precipitation events in Europe often occur during early summer (Auerswald and v. Perger, 1998), arable lands with specific crops may have little vegetation, making the soil vulnerable to drying and raindrop exposure. In particular, dry soils are prone to splash erosion owing to their water-repellent properties and low stability, leading to higher silting compared to regular precipitation events. The infiltration rates are significantly reduced and are less important for the flow process. These fundamentals align with the research of Parkin et al. (2008), which suggests that a few heavy and single events contribute the most to total erosion over time.

1.2.2 Hydraulic and Erosion Modeling

In general, models are simplified versions of reality. Different model types can be distinguished according to different degrees of accuracy and determination, and spatial and temporal distributions (Hebel, 2003; Tügel, 2023).

Degree of determination:

- Empirical models (Blackbox)
  The input and output parameters depend only on empirically determined relationships without considering different processes or process dynamics. These models are easy to use but cannot be transferred to other areas or framework conditions in which they are found. These models are often the easiest to develop.
- Process-oriented models (Graybox)
  Both physically based and empirically derived equations are part of the model. The validity, regardless of location and time, can be improved compared with empirical equations. Empirical equations complete these and prevent high parameterization input in physically based equations.

- Physically based models (Whitebox)
  Model in which all parameters are solved using physically based mathematical equations. These models require a large amount of high-quality input data, which may limit their practicality.

Spatial distribution

- Lumped
  No horizontal distribution of the input and output parameters.
- Distributed
  Spatial distribution is defined by sections or mesh elements.

Temporal distribution

- Continuous
  Long-term simulation of several events.
- Discrete
  Event-based simulation.

The models were developed and used to address various research objectives and practical questions. Model complexity is often accompanied by change in computational efficiency (Hu et al., 2019; Wu et al., 2023). Therefore, the cost–benefit ratio is always crucial for determining an adequate model.

1.2.2.1 Hydraulic Modeling

Hydraulic modeling was conducted for a wide range of questions. Different model approaches are available depending on the aims of the research or practical questions.

The basis for calculating hydraulics and flow conditions are the conservation laws of mass and momentum. The conservation of mass is mathematically realized using the continuity equation, and the conservation of momentum is represented by the Navier–Stokes equations.

Both the continuity and Navier–Stokes equations describe the flow of compressible, unsteady, and frictional fluids. However, these equations were simplified. The primary simplification was the assumption of incompressibility of water, which is reasonable because the volumetric change in a fluid due to pressure change is negligible.

Further simplifications lead to different equations:

- The **Reynolds equations** consider a time-related average for flow parameters and a Reynolds stress term for turbulent fluctuations.
- The depth-averaged **shallow water equations** contain additional simplifications, such as neglecting the vertical velocity and acceleration terms and assuming a uniform velocity distribution. These are known as 2D models.
- The **1D Saint–Venant equations** were further simplified using width averaging, where the depth-averaged transverse velocity and acceleration terms were zero. An even greater simplification can be achieved by regressing dynamic, diffuse, and kinematic wave approximation to normal flow (Maniak, 2016).

In this work, a 2D hydrodynamic numerical model, referred to as the HydroAS model, was used. According to the HydroAS model manual, the following 2D shallow water equations were used for the simulation (Hydrotec, 2024a):

$$\frac{\partial \mathbf{w}}{\partial t} + \frac{\partial \mathbf{f}}{\partial x} + \frac{\partial \mathbf{g}}{\partial y} + \mathbf{s} = 0 \tag{1-1}$$

with

$$\mathbf{w} = \begin{bmatrix} H \\ uh \\ \mathrm{v}h \end{bmatrix} \tag{1-2}$$

$$\mathbf{f} = \begin{bmatrix} uh \\ u^2h + 0.5gh^2 - \nu h\dfrac{\partial u}{\partial x} \\ u\mathrm{v}h - \nu h\dfrac{\partial \mathrm{v}}{\partial x} \end{bmatrix} \tag{1-3}$$

$$\mathbf{g} = \begin{bmatrix} \mathrm{v}h \\ u\mathrm{v}h - \nu h\dfrac{\partial u}{\partial y} \\ \mathrm{v}^2h + 0.5gh^2 - \nu h\dfrac{\partial \mathrm{v}}{\partial y} \end{bmatrix} \tag{1-4}$$

$$\mathbf{s} = \begin{bmatrix} 0 \\ gh(I_{Rx} - I_{Sx}) \\ gh\left(I_{Ry} - I_{Sy}\right) \end{bmatrix} \tag{1-5}$$

where t is the time, and x and y represent the streamwise and transverse directions, respectively. H is the water level above a reference level; h is the water depth; u and v are components of the flow velocity in x and y directions, respectively; g is gravitational acceleration; and Greek letter nu (ν) is the viscosity. The source term s contains the friction (I_R) and bed (I_S) slopes.

This model provides water depths and flow velocities at each model node and time step.

Currently, this model is used to simulate both overland and stream flow. However, the mathematical alignment and simplifications require a limitation of the slope to ≤ 0.01 (Maniak, 2016; Yörük, 2008). This value can be exceeded in overland flow modeling. The study area was partially affected by this limitation.

Hydraulic modeling can be conducted to simulate runoff, or rain-on-grid modeling. For runoff simulations, the flow amount must be provided as an input parameter and can be derived from hydrological models or statistical values (such as recurrence intervals, for example, 100 years). By contrast, the rain-on-grid model simulates runoff generation from precipitation inputs. This is particularly useful in flash flood modeling. The amount of precipitation can be reduced using the initial losses and discharge coefficients for effective precipitation.

Calibrating these models using gauges in streams is advisable.

1.2.2.2 Soil Erosion Modeling

Similar to hydraulic models, erosion models have a wide range of scopes and accuracies. Over the last six decades, erosion modeling has continuously evolved. Wischmeier and Smith (1978) developed the **Universal Soil Loss Equation (USLE)** as an empirical model using 10,000 trial years of soil erosion observations at 50 locations in the United States between 1930 and 1952. From the observed erosion data, the USLE equation (Equation (1-6)) was derived based on six influencing factors.

$$A = R * K * LS * C * P \tag{1-6}$$

where *A* is the soil loss, *R* is the rainfall erosivity factor, *K* is the soil erodibility factor, *L* and *S* are topographic factors (slope length and gradient, respectively), *C* is the cover and management factor, and *P* is the support practice factor.

The USLE was adapted to German conditions by Schwertmann et al. (1987), and is referred to as the “Allgemeine Bodenabtragsgleichung” (ABAG). These parameters were defined according to DIN 19708 (2017).

In addition, the USLE serves as the basis for several subsequent revised versions, such as the MUSLE (Modified USLE), RUSLE (Revised USLE), and RUSLE2, for single events. Models within the USLE family are commonly used in many research projects because of their ease of use (Batista, 2025).

Process-based models have been developed to provide more precise and comprehensive analyses.

Various approaches have been developed for sediment detachment, transport, and deposition. When considering soil detachment approaches, it is important to consider detachment from channeled flow in rills, and from raindrops and sheet flow in interrill areas. In their review, Knapen et al. (2007) distinguished three primary approaches to flow detachment: i) simple hydraulic indicators, ii) TC deficit approaches, and iii) probability density functions.

The simplified hydraulic indicators include excess shear stress and stream power models. Flow detachment capacity is calculated based on the excess of hydraulic shear stress (τ) and the critical shear stress (τ_{cr}), or the stream power (ω) and the critical stream power (ω_{cr}). The excess shear stress model is used in models such as WEPP (Laflen et al., 1991) and Chemical Runoff and Erosion from Agricultural Management Systems (CREAMS) (Knisel, 1980). To determine the soil detachment rate, the calculated detachment capacity must be considered in relation to the sediment load and TC.

Models such as EUROSEM (Morgan et al., 1998a), Limburg Soil Erosion Model (LISEM) (De Roo et al., 1994), and Kineros (Woolhiser et al., 1990) use TC deficit approaches. In these models, the detachment and transportation processes are linked, with detachment being dependent on the sediment load in the flow. Multiple TC approaches are available. Commonly used and well-established TC approaches are empirically derived from flume experiments such as those of Meyer–Peter and Müller (Meyer–Peter and Müller, 1948), Engelund–Hansen (Engelund and Hansen, 1967) and Yalin (Yalin, 1963). Wainwright et al. (2015) reviewed the existing geomorphological TC concepts.

In Germany, EROSION-3D (E3D) (Schmidt, 1996) is widely used to predict soil erosion. The detachment approach implemented in the E3D model is based on comparing the holding forces of a critical momentum flux and momentum fluxes transmitted by the flow and raindrops. The E3D model requires a relatively large input for parameterization. Michael (2000) provides an extensive parameter catalog that determines the input parameters.

Review articles such as those by Andualem et al. (2023) and Borelli et al. (2021) provide detailed lists of existing erosion models for various purposes.

Regardless of the soil erosion approaches used in the presented models, all models calculate the hydraulic factors that affect the soil and are responsible for detachment, transport, and sedimentation. In these models, hydraulic calculations were simplified to various degrees. For the LISEM (Hessel et al., 2011), WEPP (Stone et al., 1995) and EUROSEM (Morgan et al., 1998b) models, overland flow calculation is primarily based on the kinematic

wave equation (Section 1.2.2.1). E3D uses normal flow calculation in a geoinformation system (GIS) in the regular version and a kinematic wave approach in an add-on module (GeoGnostics, n.d., a).

1.2.3 Knowledge Gaps

Currently, hydraulic and erosion models coexist. Hydraulic models are used to calculate the water flow, whereas erosion models are used to calculate soil detachment, transport, and deposition. Hydraulic parameters play a crucial role in calculating erosion parameters because erosion calculations rely significantly on water forces acting on the soil (Morgan et al., 1998b; Smith et al., 1999). Therefore, accurately calculated hydraulics are essential for accurate erosion modeling.

Given that this study focuses on soil erosion caused by heavy precipitation events and flash floods, two areas of research emerged from this assessment: combining hydraulic models with known erosion processes.

First, hydraulic models must calculate the parameters used for soil erosion modeling precisely and with reasonable effort. As mentioned in the background section, hydraulic models are used for flood and flash flood modeling. In practice, some input data, such as the mesh resolution, differ between the two simulation bases. However, one parameter that was used independently of the model's purpose was the surface roughness. This parameter influences the flow behavior and, thus, the hydraulic parameters acting on the soil. Roughness is an empirically derived parameter, and many studies have investigated the roughness of different surfaces using the framework conditions of stream flow, that is, high water depth and low slope. As flash flood models consider overland flow, these conditions are not met. This results in the first knowledge gap regarding the **transferability of roughness parameters** from stream to overland flow.

Second, existing erosion models use simplified hydraulic approaches to calculate the water forces acting on the soil (Section 1.2.2.2). Most soil erosion models use kinematic wave equations. However, when modeling flash floods, the use of depth-averaged shallow water equations in 2D models is state-of-the-art in Germany and involves a reasonable computational effort. Thus, a combination of 2D hydraulic and soil erosion models can improve the accuracy of the hydraulic input for erosion calculations. To date, the **influence of improved hydraulics on soil erosion prediction** has not been investigated. Rill erosion accounts for most of the total erosion. Understanding the location and extent of soil erosion caused by rills is essential for implementing effective preventive measures.

1.3 Objectives

The objective of this work was to combine the simulation of erosion on arable land and overland flow caused by flash floods. The existing soil erosion models consider simplified hydraulics. However, a detailed hydraulic approach using a 2D model is essential for the accurate calculation of hydraulic parameters. This thesis aimed to accurately model heavy precipitation-induced linear and sheet erosion.

To ensure the accuracy of hydraulic modeling, roughness parameters that influence the flow conditions were investigated for flash flood modeling. The hypothesis was that overland flow conditions, such as shallow water depth and steep slopes, affect the roughness value assumptions. Laboratory experiments were conducted to test this hypothesis by varying the degree of discharge, slope, and bed roughness. The aim of these experiments was to determine appropriate roughness values for overland flow modeling.

The following research questions (RQ) were raised:

- RQ1: How do water depth and slope influence roughness parameters for hydraulic modeling?
- RQ2: Which roughness values are most suitable for an accurate calculation?

To combine erosion and hydraulic modeling, appropriate approaches for both components must be selected. The state-of-the-art hydraulic modeling for flash floods is a 2D model that calculates shallow water equations, and there are various approaches available for erosion modeling, as outlined in Section 1.2.2.2, which led to the following research question:

- RQ3: Which erosion approach is suitable for heavy precipitation framework conditions?

After selection and implementation of the combined model, it was calibrated and validated to evaluate its suitability. Therefore, data on soil erosion caused by heavy precipitation is appropriate in this context. One objective of this thesis was to collect and analyze soil erosion data caused by heavy precipitation at the field scale using an unmanned aerial vehicle (UAV). The new model and two existing erosion models were applied to erosion fields. These objectives led to the following research questions.

- RQ4: How accurately can soil erosion be recorded using a UAV?
- RQ5: How well can existing erosion models using simplified hydraulics simulate erosion caused by heavy precipitation?
- RQ6: Can the use of an improved hydraulic approach also enhance soil erosion predictions compared with existing erosion models?

- RQ7: Can rills be simulated in terms of their location and quantity without differentiating between rill and interrill areas, as in existing models?

1.4 Approach and Thesis Outline

This thesis is organized into six sections. The introduction provides an overview of the thesis topic and outlines the objectives and research questions of this thesis, representing **Section 1**. Following the introduction, the primary components of this work are described in Sections 2 to 5, which are divided into four journal articles. Three of these articles have already been published, and one is accepted for publication in peer-reviewed, international, and scientific journals.

Figure 1-3 shows a schematic overview of the thesis sections.

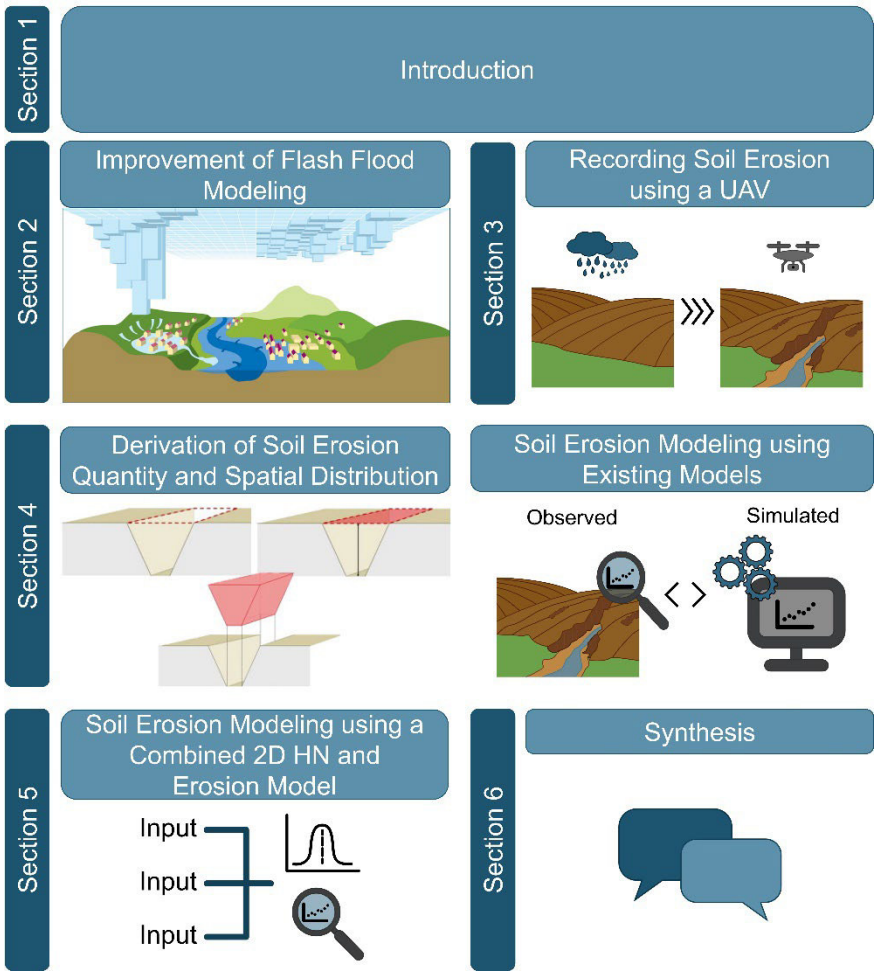

Figure 1-3: Schematic overview of the thesis outline (Figure in Section 2: LUBW, 2016; Figures in Section 3: Kathrin Hinsberger; Figures in Section 4, left: Peter et al., 2014, modified, right: Kathrin Hinsberger; Figures in Sections 5 and 6: Kathrin Hinsberger).

Section 2 addresses the knowledge gap regarding the transferability of roughness parameters from literature to flash flood conditions. Research questions RQ1 and RQ2 were investigated. This section includes laboratory experiments on roughness under overland flow conditions, specifically shallow water depths and steep slopes.

Section 3 examines the accuracy of soil erosion data generated by the UAV 'Phantom 4 RTK', that were used for the generation of calibration data in this study. This assessment aims to evaluate recording errors, as outlined in RQ4.

Section 4 explains the approach and analysis method for generating calibration data caused by heavy precipitation and provides the results of the spatial distribution and quantity of rill erosion. In addition, two existing soil erosion models, RUSLE2 and EROSION-3D, were applied to three previously recorded and analyzed erosion fields to evaluate the quality of these models using simplified hydraulic approaches, addressing RQ5.

Section 5 presents the combined soil erosion and 2D hydraulic model. This new model was used to analyze the recorded soil erosion fields, and the results were compared with those obtained from RUSLE2 and EROSION-3D. This section addresses RQ3, RQ6, and RQ7.

Section 6 summarizes the key findings, assesses these findings, clarifies limitations, and offers practical applications and an outlook for further research.

2 Influence of Water Depth and Slope on Roughness – Experiments and Roughness Approach for Rain-on-Grid Modeling

Two-dimensional (2D) models have become a well-established tool for channel flow, as well as rain-induced overland flow simulations. In channel flow simulations, slopes are usually less than a few percent and water depths are over several meters, while overland flow simulations show steep slopes and flow of a few centimeters. Despite these discrepancies, modelers transfer roughness coefficients, validated for channel flow, to overland flow. One purpose of this study is to verify whether roughness values from the literature are also valid for overland flow simulations. Laboratory experiments with different degrees of bed roughness, various discharges and a range of experimental flume slopes were carried out. For a given discharge, water depth was measured, and bed roughness was derived. Experimental results reveal that roughness shows no clear dependence on slope but is strongly dependent on water depth for vegetated surfaces. To verify the influence of different roughness approaches, they were implemented in a 2D model. A comparison of different simulation results indicates differences in the hydrograph. Here, consideration of water depth-related roughness coefficients leads to retention and translation effects. With the results of the following study, modelers may enhance the precision of the hydraulic component in overland flow simulations.

Rebecca Hinsberger, Andreas Biehler and Alpaslan Yörük

Water, 2022, 14(24), 4017
Special Issue: Hydraulics and Hydrodynamics of Overland Flow – Catchment, Subcatchment, Plot Scale and Experimental Approach
DOI: 10.3390/w14244017

2.1 Introduction

2.1.1 Modeling Extreme Events

Due to the excessive human impact on the environment, the global temperature has steadily increased. In the recent past, natural disasters, such as drought, storms, flooding or heavy precipitation have become more frequent. According to the IPCC Report (2021), these extreme events are a consequence of climate change, and their frequencies will rise in the future.

Fluvial flooding are events that occur on every stream in different periods and intensities. Therefore, maps were created to show areas at risk and to make provisions against extreme events. To identify affected areas, parts of the examined stream are built in a model and loaded with a certain discharge. Simulations are often carried out with two-dimensional hydrodynamic numerical models (2D models). This approach has been state of the art in Germany for several years (Yörük and Sachen, 2014).

In contrast to fluvial flooding, where water rises in streams, flash floods lead to overland flow. Surface conditions vary from mountain areas to lowlands, and therefore, there is an enormous range in slope, bed roughness and discharge. In the last few years, 2D models that were and are used for fluvial flooding have also been used for pluvial and flash flood simulations (Bellos et al., 2020; Caviedes-Vouillème et al., 2012). With these models, vulnerable areas can be identified, and corresponding safety precautions can be installed. In contrast to fluvial flooding models, which only rebuild specific channel sections and river forelands, flash flood models have to rebuild the entire catchment area to generate overland flow due to precipitation. The approach for assessing pluvial and flash floods is well-known as “Direct Rainfall Modeling” or “Rain-on-Grid” (RoG). RoG simulations combine hydrological and hydrodynamic flood processes.

Previous studies have simulated RoG using 2D models to investigate the impact of uniform and non-uniform, triangular and quadrilateral meshes (Gibson et al., 2016), the influence of different mesh resolutions (Caviedes-Vouillème et al., 2012), flow velocity (Barbero et al., 2022; Taccone et al., 2020), and comparisons of experimental data and simulations (Taccone et al., 2020). Several studies have focused on the influence of resistance coefficients. Abderrezzak et al. (2009) simulated two events and examine the influence of different Strickler roughness coefficients. They conclude that a sufficient roughness parameter is a relevant issue to improve the model. A sensitivity analyses by Huang et al. (2015) also shows a considerable impact of roughness on hydrographs. The mentioned literature along with other studies (Costabile et al., 2021; Zeiger and Hubbart, 2021) have assumed uniform

and constant roughness coefficients for their simulations, and sometimes with spatial distribution. García-Pintado et al. (2009) considered time-varying roughness coefficients in channels. David and Schmalz (2020) revealed that the RoG approach provides realistic information on overland flows. However, they indicated that constant roughness values, which were selected for natural channels and floodplains, did not fit and needed to be increased, to provide higher friction (David and Schmalz, 2020). Currently, modelers of RoG transfer roughness values, valid for channels, to overland flow simulations, irrespective of the differences in water depth and slope conditions. Rain induced overland flow is characterized by shallow sheets of water (Abrahams et al., 1990) and steep slopes as opposed to channel flow with water depths up to several meters and low slopes of a few per mill. However, the consideration of friction is the main factor affecting the calculation of water depth, flow velocity, and the overall catchment response (Barbero et al., 2022). Cea et al. (2014) asserted that the accuracy of a hydrograph does not ensure the correct determination of the hydraulics in the entire model. Therefore, a correct approach for friction is essential for obtaining precise results at each point in the model.

2.1.2 Aim of the Study

The present study addresses two aims. For the first part, laboratory experiments were carried out to study the influence of water depth and bottom slope on bed roughness. Water sheets with shallow depths, up to 10 cm, are of particular interest. A 2D simulation of an existing RoG model shows that the largest percentage of area is covered with water depths lower than 10 cm, so areas with these water depths are essential for modeling overland flow until water reaches channels. Steep slope could be another influencing factor for roughness coefficients. In the conducted experiments, the range of the bottom slope reaches 40%, which represents very steep hills. The objective of these experiments is to determine whether existing values for roughness, which are based on channels and the given conditions, are also suitable for overland flow. A wide range of different bed roughness values, from solid and smooth to dense vegetation with a high resistance, were used to represent different conditions.

Previous studies point out the considerable impact of roughness in 2D models. Therefore, some results of the laboratory experiments are used for the second part of this study, which focuses on roughness in 2D models. Simulations of a 2D model quantify the effect of applying different roughness approaches on a hydrograph in the catchment area. These results can provide insight into the sensitivity and influence of roughness on the response time. With a more accurate approach for roughness, the quality of the simulated water depth and flow velocity at each point in the model could be improved.

Common flow equations are presented in Section 2.2. As mentioned in previous studies, roughness parameters are important impact factors and calibration parameters (Abrahams et al., 1990; Augustijn et al., 2008; García-Pintado et al., 2009). Therefore, a literature review on approaches to consider roughness and studies on vegetation resistance is presented, as well as studies on overland flow conditions. All Materials and Methods for the experimental study are presented in Section 2.3. The Results and Discussion on experiments and 2D modeling for submerged vegetation are part of Section 2.4.1; the Results and Discussion for emergent vegetation and solid surfaces are parts of Sections 2.4.2 and 2.4.3, respectively. The Conclusion is provided in Section 2.5.

2.2 Background

2.2.1 Flow Equations

For water flow calculations and simulations, there are a few fundamental and well known equations, such as the Gauckler–Manning–Strickler equation (Manning's equation) or the Darcy–Weisbach equation. Typically, different materials and surfaces in the course and the bank of a stream are considered with roughness coefficients, such as the Darcy–Weisbach friction factor f, Nikuradse's equivalent sand–grain roughness k_N or the Strickler roughness coefficient k_S. In principle, these coefficients consider the total resistance. The only dimensionless factor is Darcy–Weisbach's friction factor f, which is the most general and valid for all states of flow (Abrahams et al., 1994; Huthoff and Augistijn, 2006). The friction factor f is part of the following Darcy–Weisbach equation:

$$Q = \sqrt{\frac{8\,g\;R_H\,S}{f}}\,A \tag{2-1}$$

Here, Q is the discharge, g is the gravitational acceleration, R_H is the hydraulic radius, S is the channel slope and A is the cross-sectional area. There are different possibilities to calculate the friction factor f. According to Prandtl (2009), the friction factor depends on the Reynolds number Re for hydraulically smooth areas and laminar flow, and according to Nikuradse (1933), it depends on the relative roughness k_N/D_H (hydraulic diameter) for the hydraulically rough flow regime. For the experiments conducted in this study, only the hydraulically rough flow regime is valid (see Reynolds numbers in Table 2-1). In addition to the friction factor f, another coefficient to analyze roughness is used here, the equivalent sand–grain roughness k_N, by Nikuradse.

$$\frac{1}{\sqrt{f}} = -2\;log\left(\frac{k_N}{4\;R_H\;p_r}\right) \tag{2-2}$$

Here, the parameter p_r is influenced by channel shape. For surface runoff with the assumption of an infinitely wide channel bed, the parameter can be estimated to be $p_r = 3.05$ (Aigner and Bollrich, 2015).

To calculate roughness, extensive experimental work was performed. Roughness values for specific bed or surface materials (Aigner and Bollrich, 2015; Chow, 1959; Zanke, 2013) and approaches to calculate Manning's n (Abood et al., 2006), Darcy–Weisbach's friction factor f (Ferro, 2019) or Nikuradse's k_N (Gualtieri et al., 2018; Huthoff, 2012) are available. The influence of roughness on the flow differs depending on the surface and bed conditions. There is resistance due to bed roughness, such as concrete in channels, and vegetation resistance, where vegetation is either emergent or submerged. In the literature, roughness for solid surfaces is assumed to be a constant, empirically calculated coefficient, whereas the consideration of vegetation depends on the submergence of vegetation structures.

2.2.2 Vegetation Resistance

Vegetation resistance was investigated in several studies with field and laboratory flumes and different conditions: artificial plants (Nepf and Vivoni, 2000), real vegetation (Abood et al., 2006), vegetation surrogates (Gualtieri et al., 2018; Tang et al., 2018; Wang et al., 2019b), and rigid and flexible vegetation (Huthoff et al., 2007; Järvelä, 2004). From the existing experiments, equations and approaches were derived. An overview of possibilities to model vegetation effects is given by Vargas-Luna et al. (2015). According to Ferguson (2021a), there are two ways to specify roughness in existing models: roughness as a constant or roughness as a function of relative submergence (h/h_{veg}). This submergence ratio depends on the water depth h and vegetation height h_{veg}. Other studies state that conventional flow resistance equations with constant values are not valid for vegetated flow (Augustijn et al., 2008; Gualtieri et al., 2018) because vegetation resistance depends on vegetation type and water depth (Huthoff et al., 2007). By analyzing the performance of different models in vegetated channels, Vargas-Luna et al. (2015) concluded that a separate consideration of emergent and submerged conditions offers the best results. One possibility to describe different resistance conditions is a distinction in a resistance layer (flow through vegetation) and a surface layer (flow above vegetation) (Augustijn et al., 2008; Huthoff et al., 2007). This two-layer approach has been proposed by several studies (Baptist et al., 2007; Huthoff et al., 2007; Van Velzen et al., 2003).

For submerged vegetation, researchers have explored Nikuradse's roughness coefficient and derived equations depending, for example, on the height, shape and/or density of obstacles. Schröder (1990) published a summary of information connected to roughness. He describes the dependence of k_N on a shape parameter, the roughness density and the

height for selective roughness. Huthoff (2012) presents an equation for k_N that is based on a resistance coefficient, the ratio of the frontal cylinder area and the specific volume between roughness elements (product of the specific bed surface area and the height of roughness elements). Another approach for k_N was proposed by Gualtieri et al. (2018). To formulate a constant roughness coefficient k_N, roughness height and density are used. Gualtieri et al.'s approach is valid for submergence ratios (water depth/obstacle height) of 5 and higher and therefore represents strongly inundated vegetation. Another approach is provided by Ferro and Guida (2022). They used a new resistance approach for the friction factor f and validated it with experimental data by Bond et al. (2020) for grassland. This approach has a calibration parameter for different types and properties of grass and depends on slope, Reynolds number and Froude number. For experiments by Bond et al. (2020), the calibration parameter ranges from 0.273 to 0.314. Conversely, solving the equation yields a very similar form of the Darcy–Weisbach equation (Equation (2-1)).

All listed literature limits the utilization to submerged vegetation. The approaches mentioned above are used for comparisons with the experimental results in the section "Consideration of Roughness for Submerged Vegetation".

To consider emergent vegetation, bed roughness and drag effects of vegetation must be taken into account (Huthoff et al., 2007). In addition to the friction of the flow and channel bottom, the resistance of a rigid object or vegetation can be included in the equation. Then, the total friction factor f is the sum of f' for the frictional resistance of the bottom and f'' for the object or vegetation cover, the form drag. Here, f' is a solid surface, usually without vegetation, and can be assumed with a constant roughness k_N and Equation (2-2). f'' can be calculated with Equation (2-3); in the following "vegetation approach" (Aigner and Bollrich, 2015; Baptist et al., 2007):

$$f'' = 4 * C_D * R_H * d_{veg} * D_{veg} \tag{2-3}$$

where C_D is the bulk drag coefficient. Factors d_{veg} (diameter of vegetation) and D_{veg} (density of vegetation or roughness elements [pieces per area]) represent the specific frontal area of the vegetation in the x-direction, the roughness density (Nepf, 2012).

The hydraulic response shows differences for emergent and submerged conditions in channels. For emergent flow, Manning's n increases with increasing water depth, whereas for submerged flow, Manning's n decreases with increasing water depth (Nepf, 2012). This phenomenon is also presented by Abrahams et al. (1990, 1994) for overland flow. They observe 2 types of shapes for the relationship between the Reynolds number Re and Darcy–Weisbach's friction factor f: (a) a convex-upward function for progressive inundation

of roughness and therefore an increase in roughness with increasing water depth and (b) a negatively sloping function for progressive increase in water depth over inundated parts of the bed and therefore a decrease in roughness. An increase in roughness with increasing water depth results from a domination of form resistance instead of bed roughness. The individual function depends on surface and vegetation properties (Abrahams et al., 1994). When inundation and therefore the submergence ratio is high (h/h_{veg} >5), resistance will transform to conventional equations, which are not dependent on water depth but are constant in their values (Augustijn et al., 2008; Gualtieri et al., 2018; Huthoff et al., 2007).

2.2.3 Conditions for Overland Flow

While roughness in channel flow has been investigated extensively, information on roughness related to overland flow is limited (Ferro and Guida, 2022). Existing rainfall simulations and overland flow experiments were carried out with grassland and shrubland on deserted hillslopes (Abrahams et al., 1990, 1994), brush and grassland areas (Polyakov et al., 2018) and grass to different seasonal conditions (Bond et al., 2020). Recently, a novel open channel flow equation for the Darcy–Weisbach friction factor was proposed (Ferro, 2017, 2019). Subsequent studies estimate a surface-dependent coefficient Γ with different experiments for smooth beds (Nicosia et al., 2020), grass-like vegetation in channels (Ferro, 2019), different soil textures (Carollo et al., 2021; Palmeri et al., 2018), erosion rills (Di Stefano et al., 2019a, 2019b, 2021; Nicosia et al., 2019), vegetated beds (Nicosia et al., 2021) and grassland habitats (Ferro and Guida, 2022).

As a consequence of less common hillslope measurements (Bond et al., 2020), empirical roughness values are derived from laboratory and field experiments with bottom slopes in the range of per mill or a few percent (Cheng, 2011; Dunn et al., 1996; Murphy et al., 2007). Experiments in steep river channels or flumes with high slopes are rare. Comiti et al. (2007) investigated steep slopes in predominantly step-pool channels. However, due to the persisting lack of experimental data on overland flow, modelers of pluvial and flash floods currently use roughness coefficients based on stream experiments (Schubert et al., 2008; Tyrna et al., 2018). Although the influence of water depth and submergence on vegetation resistance is well known in the literature, modelers of flash floods transferred constant roughness values from channel flow with mostly high submergence to overland flow. For only a few years, a guideline for flash flood modelers published by a federal state of Germany (LUBW, 2020) have suggested roughness coefficients influenced by water depth for some bed roughness. Regarding what has been discussed in the literature about vegetation, this approach is reasonable.

2.3 Materials and Methods

To investigate different degrees of bed roughness depending on the water depth and bottom slope, laboratory experiments were carried out. All experiments were conducted at the laboratory of hydraulic engineering at the University of Applied Sciences in Saarbrücken, Germany. Figure 2-1 shows a sketch of the closed water circuit that proceeds with the experiments; 70 m³ water is stored in an underground reservoir (Figure 2-1, no. 1) and is transported by two pumps through a pipe system to an inlet reservoir and the experimental setup. The channel (Figure 2-1, no. 7) is 10 m long and contains a cross-section of 1 × 1 m without any slope. At the transition of the inlet reservoir to the channel, a flood protection system is installed to separate both elements. This system is composed of several beams to dam the water in the reservoir to different heights.

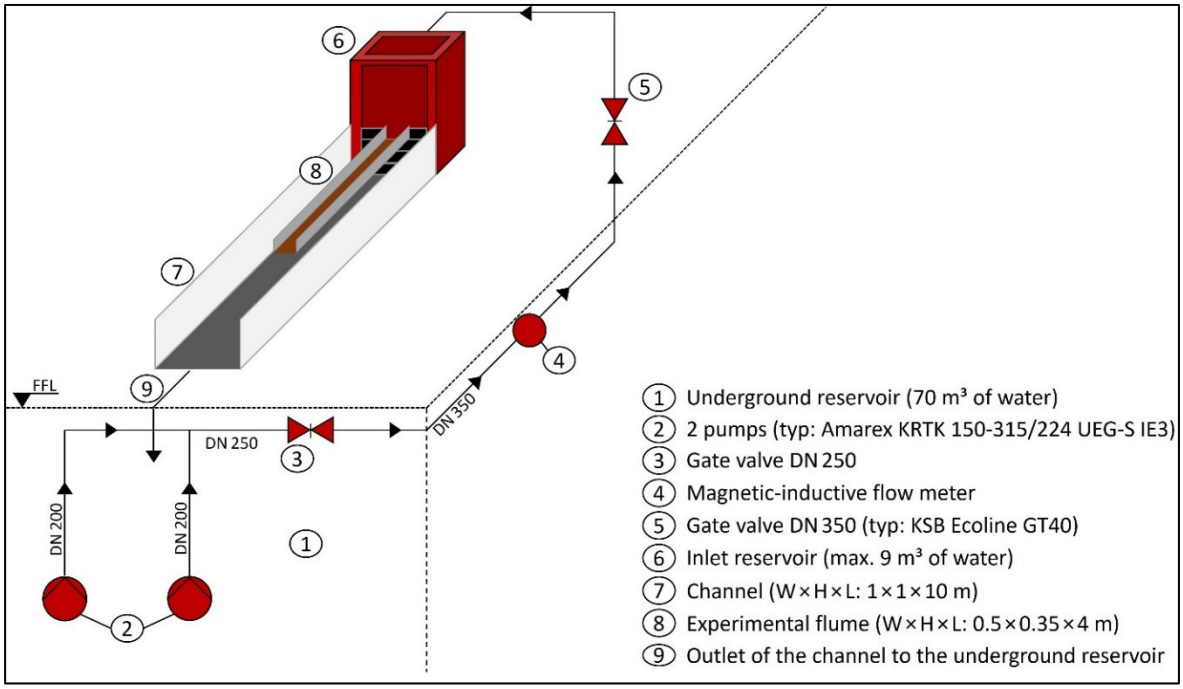

Figure 2-1: Sketch of the experimental setup.

For the experiments of this study, a second, smaller channel, the experimental flume (Figure 2-1, no. 8), was installed. The experimental flume has a length of 4 m and a cross-section of 0.5 × 0.35 m. Its bottom is a coated plywood plate, and the walls are made of aluminum. For the roughness experiments, the whole bottom was covered with insets. The experimental flume is stabilized at the upstream end of the flume to a handle at the topmost beam of the flood protection system and can therefore align the slope. With the help of a mobile crane at the downstream end of the flume, the slope can be further adjusted. A digital clinometer is supposed to measure the flume's slope with a precision of 1%. For the entire setup, a range of slopes from 0% to a maximum of 40% (21.8°) is possible (see Figure 2-2f).

The flume is charged by the inlet reservoir, which reduces the turbulence of the flow. A perforated plate evenly conducts the water stream over the whole width of the flume.

Figure 2-2: Photos of the experimental flume with different surfaces: (a) artificial grass, (b) wheat, (c) cement-based coating, (d) asphaltic emulsion, (e) exposed aggregate concrete, and (f) aluminum.

In the experimental procedures, the discharge was controlled by gate valves (Figure 2-1, no. 3 and no. 5) and measured by a magnetic-inductive flow meter (Figure 2-1, no. 4). The measurements of the water depth were conducted with a point gauge that signals (visually and acoustically) contact with water (Richter Deformationsmesstechnik GmbH, Frauenstein, Germany). A frame with the point gauge was positioned in the middle of the flume to avoid an influence from the inlet and outlet areas. The position was determined by preliminary tests. Water depths were measured in a longitudinal section of the experimental flume, and areas influenced by inlet and outlet were detected. For the final experiments, water depth values are single measurements. When vegetation stalks were higher than the flume walls (Figure 2-2b), the stalks were slightly bent at the top to fit through openings of the

frame. Then, the water depth was measured as in previous experiments using the acoustics of the point gauge when water was touched.

As the objective of this study was to investigate different degrees of bed roughness, the sidewall influence of the flume must be considered. As a preliminary test, aluminum plates were used as insets (Figure 2-2f). Hence, in addition to the flume walls, the whole experimental flume is covered with aluminum so the material specific roughness can be determined to take the wall roughness for all subsequent experiments into consideration. For the results of bed roughness, wall roughness is considered via the wetted perimeter to use only the specific bottom friction for analyses. All bed roughness and surfaces used in this study are illustrated in Figure 2-2.

In the present study, flow above solid surfaces as well as flow through and above vegetation is investigated. Artificial grass represents submerged vegetation with a flow above the vegetational layer. For experiments with wheat, the water flows through the wheat stalks, so it is defined as emergent vegetation. Further surfaces are described as “solid”. For each surface, a short description of the configuration details, flow conditions and the range of discharges, water depths and bottom slopes are given in Table 2-1.

Table 2-1: Experimental configurations.

Reference		Artificial Grass	Wheat	Cement-Based Coating	Asphaltic Emulsion	Exposed Aggregate Concrete	Aluminum
Description		Nubby blade of grass: length: 2.5 cm height: 1.5 cm predominantly rigid	Dried wheat height: 0.5 m 500 pc/m² fixed in 3 cm Styrodur and on top: 2 cm cement-based coating predominantly rigid (bending was avoided)	Mixture of masonry mortal and tile adhesive (ratio 1:2)	Grain size: 0–8 mm	Texture: gravel grain size: 5–20 mm	Plates 2 mm thick
Installation		Sticked and tightened to a coated plywood plate	4 separate boxes	4 separate boxes	4 separate boxes	4 pieces	4 pieces sealed with silicone
Flow condition		Submerged vegetation Submergence: 2.1–7.5	Emergent vegetation	Submerged Solid surface	Submerged Solid surface	Submerged Solid surface	Submerged Solid surface
Total number of experiments		149	77	168	119	119	98
Q [l/s]		5–70	5–35	5–70	5–70	5–70	5–70
h [cm]		3.1–11.2	1.2–14.3	1.0–9.5	1.1–7.1	1.3–7.5	0.9–8.0
Re		2.48×10^4–3.31×10^5	2.75×10^4–1.76×10^5	2.78×10^4 – 3.75×10^5	2.65×10^4 – 3.64×10^5	2.63×10^4 – 3.60×10^5	2.92×10^4 – 3.74×10^5
S [%]	1	X	X	X	X	X	X
	2	X	X	X			
	3	X	X	X			
	4	X	X	X			
	5	X	X	X	X	X	X
	10	X	X	X	X	X	X
	15	X	X	X	X	X	X
	20	X	X	X	X	X	X
	25	X	X	X	X	X	
	30	X	X	X	X	X	X
	35	X	X	X	X	X	
	40	X		X	X	X	X

2.4 Results and Discussion

For the analysis of experiments, Darcy–Weisbach's friction factor f was used because it is the only dimensionless resistance coefficient and valid for all states of flow (Abrahams et al., 1994; Huthoff and Augustijn, 2006). With the results of the measured discharge, water depth and slope and given boundary conditions of the experimental flume, all parameters are available to calculate f with Equation (2-1) and k_N of each experiment with calculated f and Equation (2-2). Figure 2-3 summarizes the data of all types of bed roughness in this study with slopes from 1% to 20%. For this first overview, no distinction is made between solid or vegetation bed roughness, and for every experiment, coefficient k_N is considered as bed roughness to show the range of values. For further analyses, the friction factor f or coefficient k_N is used, depending on the surface. The plot depicts the dependence of water depth on roughness k_N. With a split y-axis, the range of data points for low k_N values can be

better recognized. For submerged vegetation (artificial grass), roughness decreases with increasing water depth and submergence. In contrast, for emergent vegetation (wheat), roughness increases with increasing water depth. These results of change in roughness depending on submergence are plausible regarding results from the literature for vegetation in the channel (Nepf, 2012) and for overland flow (Abrahams et al., 1990, 1994). Solid surfaces (cement-based coating, asphaltic emulsion, exposed aggregate concrete and aluminum) show a much smoother roughness with a reasonable constant roughness coefficient k_N.

By conducting experiments with 1% (independent of bed roughness), discharge losses were noticed at the inlet of the experimental flume. These losses could not be completely avoided, and quantity could only be approximated. Therefore, the measured discharge for all experimental data of slopes = 1% was reduced by 10%. In addition to the investigation of water depth, the second part of this experimental study was to investigate if and how roughness is influenced by bottom slope. For each bed roughness, a range of different slopes was used as the experimental setup. A list of slope configurations for each experiment is contained in Table 2-1.

2.4.1 Consideration of Roughness for Submerged Vegetation

2.4.1.1 Analyses and Evaluation of Experimental Results

Figure 2-3 shows that submerged vegetation, in this study artificial grass, leads to a rougher surface with decreasing water depths. Thus, roughness decreases with higher submergence. Previous studies have investigated (artificial) grass with different blade heights and slopes. A comparison of data from this study with data from previous studies is illustrated in Figure 2-4. All data are shown in terms of relative submergence (h/h_{veg}). The experiments of Ruiz Rodriguez and Trost (2017) and Oberle et al. (2021) with artificial grass are comparable to the surface used in this study. Accordingly, the data points largely agree with the measurements of this study. Scheres et al. (2020) observed a smoother surface for a “species-poor grass-dominated mixture” with a vegetation coverage of 82%. The friction factor for these experiments deviates widely from the results of this study. Here, friction factors are constant for all submergence ratios, and in total, values are lower. Experiments by Wilson and Horritt (2002) were carried out in a flume with a bottom slope of 1% and grass blades of 7 cm height. A curve of friction factors for different submergence is given, although data points show lower friction factors for a given submergence than data from the literature. In a study by Karantounias (1972), he used a grass mat with blades, which were 8 cm long and bent to the ground. Unfortunately, the height of the vegetation layer was not reported, but one photo was presented. For comparison in Figure 2-4, a height of 1 cm was assumed to calculate submergence. With this assumption, the results of this study also fit the results

of the present study. By increasing the assumed vegetation height, the data points slide to the left. For all data, friction factors are highest for minimum submergence. Reports by Nepf (2012) and Abrahams et al. (1990, 1994) and the results of wheat in this study indicate that the curve changes with a submergence of 1 (change from submerged to emergent). Hence, the maximum roughness is reached with submerged vegetation (submergence = 1). With this knowledge, an assumption of a vegetation height of 1 cm for experiments by Karantounias seems plausible because a submergence of 1 is not exceeded.

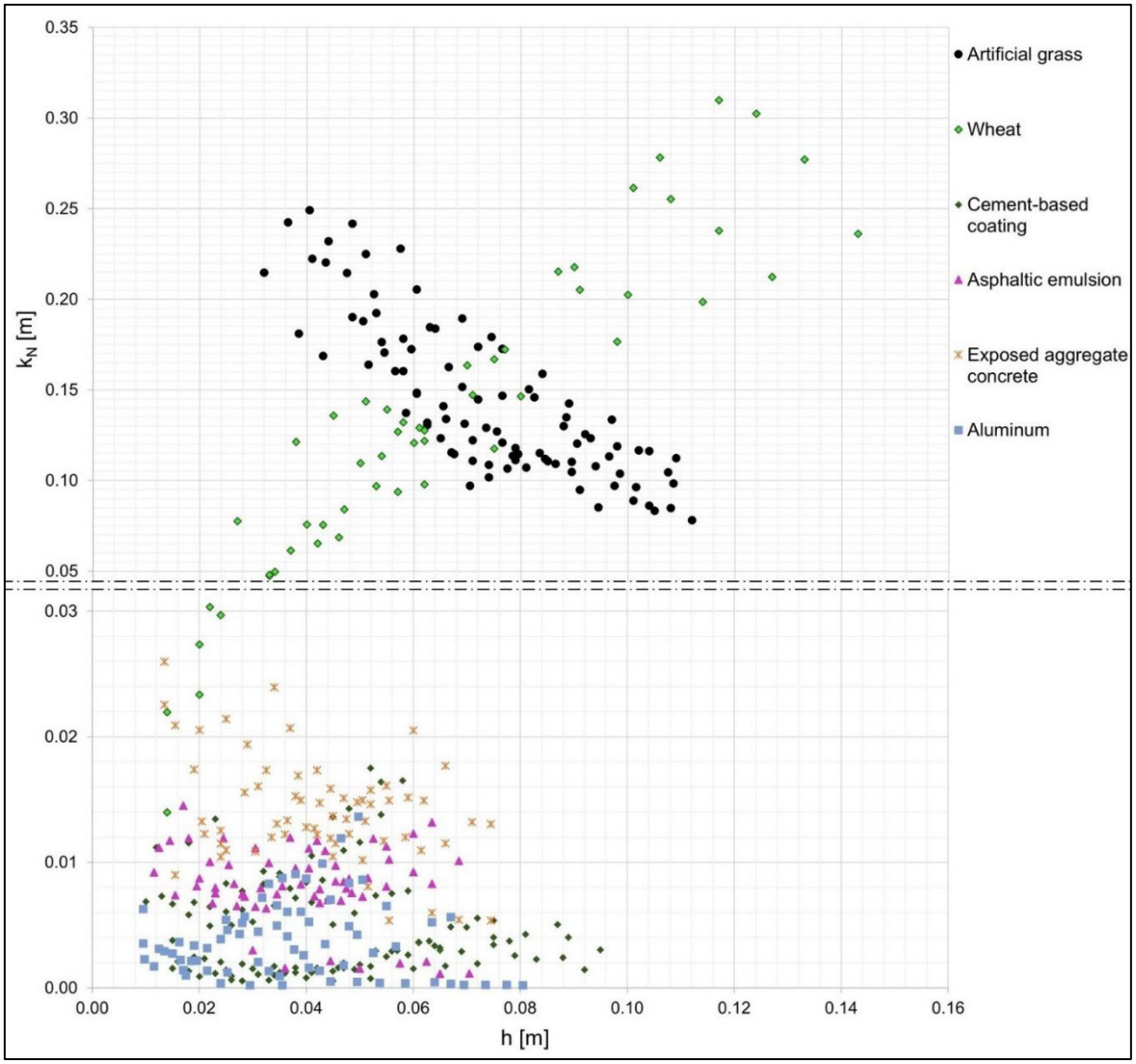

Figure 2-3: Relationship between water depth h and equivalent sand–grain roughness kN for different bed roughnesses. Ordinate was split to better show data points with low kN.

According to Augustijn et al. (2008), Gualtieri et al. (2018) and Huthoff et al. (2007), roughness approaches a constant value when water depth is much higher than vegetation height. In the mentioned literature, a submergence higher than 5 is stated. The results of the present study indicate constant roughness from a submergence higher than 6 or 7.

Apart from Scheres et al. (2020), all experimental data of submerged vegetation from the literature show a similar dependence of submergence on roughness. This result is also mentioned by Scheres et al. (2020), who state that, contrary to other data from the literature, the friction factor of their study seems independent of submergence. In the comparison shown in Figure 2-4, the shape of the functions and submergence deviate because of different vegetation properties (density, shape, …). For a given submergence, data from Wilson and Horritt (2002) show lower resistance than the compared data. Against the submergence ratios for constant hydraulic resistance stated by Augustijn et al. (2008), Gualtieri et al. (2018) and Huthoff et al. (2007), data from Wilson and Horritt (2002) seem to reach a constant value from a submergence of 3. This phenomenon, which does not fit with other literature data, is also mentioned by Wilson and Horritt themselves. One possible explanation is the flexibility of 7 cm high grass compared to heights of 1 or 2 cm.

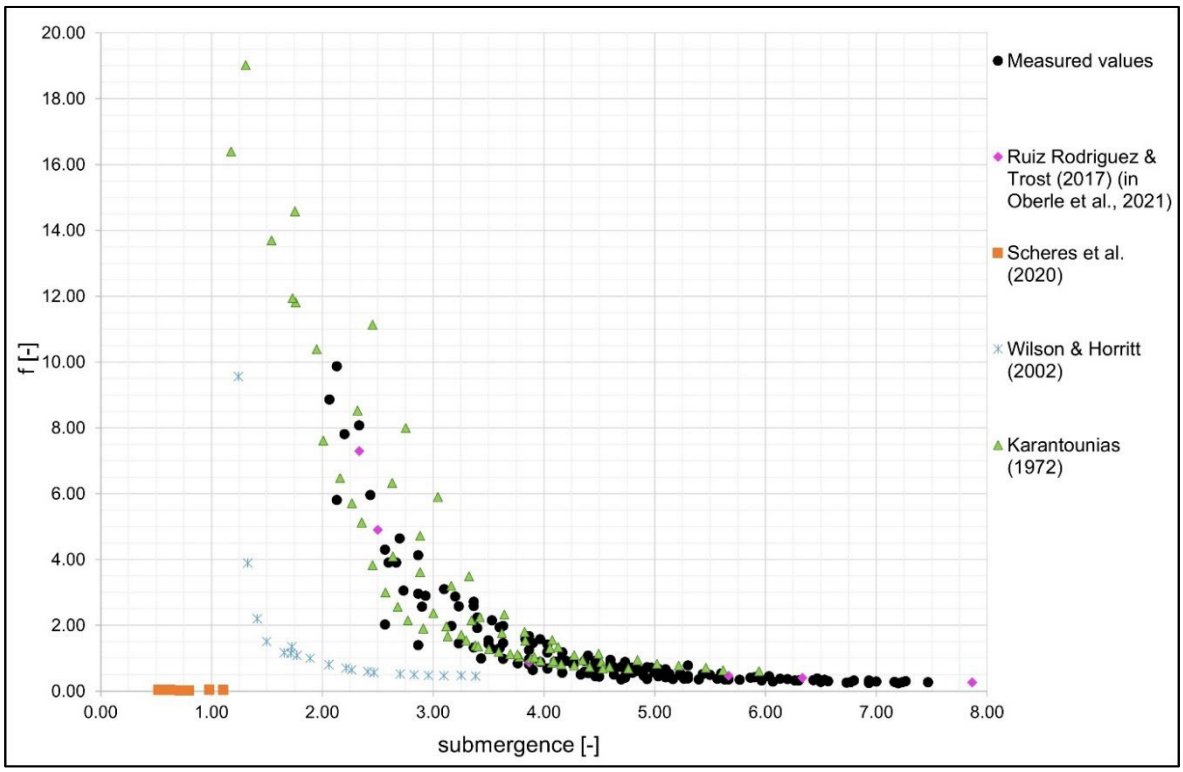

Figure 2-4: Relationship between relative submergence (h/h_{veg}) and friction factor f. Measured values of this study (black dots) are compared to data from the literature.

Figure 2-4 shows that the dependence of water depth and roughness for submerged vegetation is known in the literature and thus, these data validate our experiments. In addition to the water depth, the dependence of the bottom slope was investigated. These results are shown and discussed at the end of Section 2.4.1, subsection Novel Approach.

To reproduce measured values with a model, different approaches that consider vegetational properties are available.

2.4.1.2 Existing Models

There are several experiments and analyses to consider submerged vegetation, mentioned in the Background section. With vegetation properties of artificial grass used in the present study, approaches lead to the following constant k_N values: Gualtieri et al. (2018): 0.205 m; Huthoff (2012): 0.017 m; Schröder (1990): several meters. The k_N value from the approach by Schröder (1990) strongly deviates from the experimental results of this study, whereas values from the approaches by Gualtieri et al. (2018) and Huthoff (2012) reproduce the mean values of the experimental data (see Figure 2-3 and Figure 2-5a). However, the k_N value resulting from the approach by Gualtieri et al. (2018) should be valid for submergence ≥5 when hydraulic resistance reaches a constant value. In this study, a constant value of k_N = 0.1 m is reached for high submergence (see Figure 2-5a).

According to the approach by Ferro and Guida (2022), by choosing the right calibration parameter (0.21 for artificial grass in this study; selected according to the lowest RMSE), measurements fit quite perfectly with this approach because the “measured” friction factor is calculated with the Darcy-Weisbach equation. However, by using water depth and flow velocity in this equation, an initial value problem appears.

Different approaches suggested in the literature, and data from the literature were compared to the experimental data from this study. In Figure 2-5, water depth is plotted against k_N (Figure 2-5a) and submergence against f (Figure 2-5b) for different approaches in comparison to the experimental data. In Figure 2-5a, experimental data are shown separately for each slope condition, and in Figure 2-5b, data from this study are shown as black point clouds for better clarity compared to other data. Both plots show a constant k_N, f values obtained with a constant k_N (gray, dashed line), as suggested in the literature, and k_N/f values obtained with a constant k_S (black, dotted line), as it is state of the art in 2D models (LfU, 2018). All k_S values are transformed to f with a combination of the Gauckler–Manning–Strickler equation and Darcy–Weisbach equation (Equation (2-5)) in the following paragraph); conversion of f to k_N and backward is carried out with Equation (2-2). Constant k_N and constant k_S were chosen as values for high submergence, as these values are listed in the literature for channel flow (see paragraph “Vegetation Resistance”) and therefore fit high water depth. For that, the values of k_N = 100 mm and k_S = 25 $m^{1/3}/s$ represent these conditions. Mean values for k_N and k_S could fit the experimental data better as a whole, but over- and underestimate specific ranges of values. The influence of water depth for k_S in Figure 2-5a and for k_N in Figure 2-5b arises from the factor of hydraulic radius R_H in both transformation equations. The plot depicts that a constant k_N as well as a constant k_S merely applies with experiments with high water depths (submergence >6 to 7), although constant k_N values can represent the quality of the curve progression in Figure 2-5b. In Figure 2-5b, it can

be seen that data from Scheres et al. (2020) fit with a constant k_S and data from Wilson and Horritt (2002) fit with a constant k_N. Furthermore, Wilson and Horritt conducted experiments with grass blades of 7 cm. If these blades bend, submergence rises, and the curve of data points from Wilson and Horritt approximates the data curve from this study. Properties, especially the density of vegetation, deviate in each experiment, so different values for hydraulic resistance are reasonable.

In the literature, the dependence of vegetation bed roughness and water depth has been reported. However, the friction factor f always depends on the water depth because of the factor R_H in Equation (2-2). Nevertheless, an additional dependence of k_N and water depth is shown in Figure 2-5a. According to these findings, a novel approach for k_N depending on water depth is introduced.

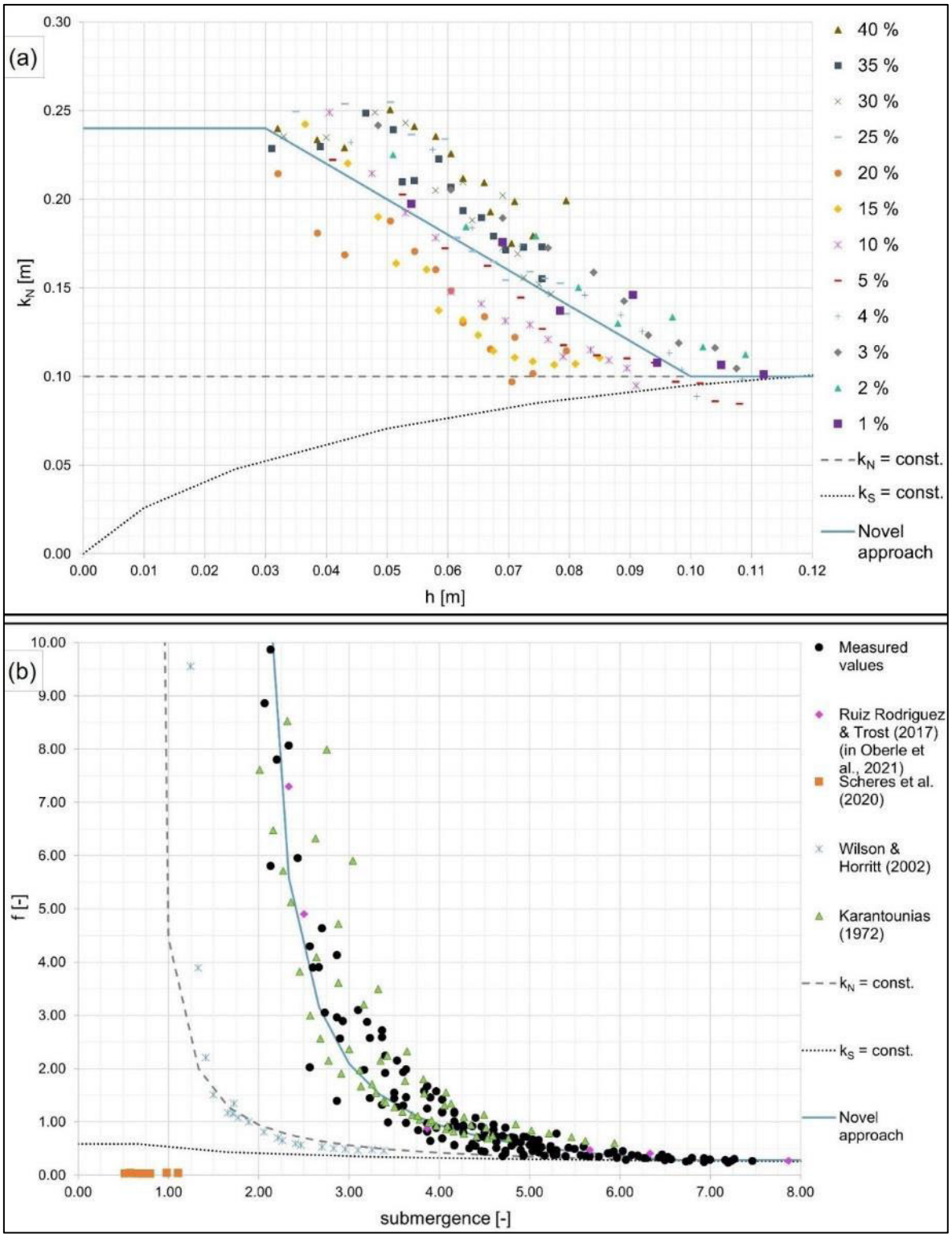

Figure 2-5: Relationship between water depth or submergence and roughness parameters: (a) water depth h against equivalent sand–grain roughness k_N with courses of the novel approach (Equation (2-4)), a constant k_N and a constant k_S in comparison to measured values of this study (dots, separately for each slope condition) and (b) submergence against friction factor f with courses of the novel approach (Equation (2-4)), a constant k_N and a constant k_S in comparison to measured values of this study (black dots) and data from the literature.

2.4.1.3 Novel Approach

As shown in Figure 2-5a, roughness coefficient k_N is dependent on water depth. This dependence can be described with a linear approach (Figure 2-5, blue, solid line) in Equation (2-4).

Equation (2-4) for k_N consists of three parts: (a) a part for submergence ≤1, (b) a part for high submergence and (c) a part for the intermediate area. For submergence ≤1 ($h \leq h_{veg}$), the conditions change to emergent, and the hydraulic response is different. To simplify the novel approach, the roughness coefficient k_N for $h \leq h_{veg}$ is assumed to be constant ($k_{N\text{-}S1}$). For water depths with high submergence ($h >> h_{veg}$ or submergence ≥5), a constant value (k_N) can be assumed as well (Augustijn et al., 2008; Barbero et al., 2022; Huthoff et al., 2007). For the intermediate area, k_N will be changed approximately linearly between $k_{N\text{-}S1}$ and k_N. This valid range of values is constrained by the minimum k_N for high submergence and the maximum $k_{N\text{-}S1}$ for low submergence. The change in roughness for $1 < h/h_{veg} < 5$ to 7 depends on the gradient $\Delta k_N / \Delta$ submergence and therefore on the water depth.

$$k_{N,CORR} = \begin{cases} k_{N-S1} & for\ \frac{h}{h_{veg}} \leq 1 \\ k_{N-S1} - \frac{k_{N-S1} - k_N}{c-1} * \left(\frac{h}{h_{veg}} - 1\right) & for\ 1 < \frac{h}{h_{veg}} < c \\ k_N & for\ \frac{h}{h_{veg}} \geq c \end{cases} \quad (2\text{-}4)$$

Here, c is the coefficient for high submergence in a value range of 5 and 7 (Huang et al., 2015; Zeiger and Hubbart, 2021).

The experimental setup of this study was limited to a minimum discharge of 5 L per second, which led to a water depth >3 cm. With a vegetation height of 1.5 cm, a submergence of 1 could not be reached. Due to the lack of knowledge in this range of values, a constant k_N for water depths <3 cm was assumed for all the following analyses (as shown in Figure 2-5a, blue line).

In addition to the evaluation of the appropriate course with water depth vs. k_N and submergence vs. f (Figure 2-5), a comparison of the predicted velocity to the measured velocity (calculated with measured discharge and water depth) for all approaches is shown in Figure 2-6a–c. For k_S = 25 $m^{1/3}/s$ = constant (a) and k_N = 0.1 m = constant (b), approaches approximate measured values for high velocities and therefore for high water depths. For data with high bottom slopes, the approaches fit less well. The root mean square error (RMSE) of flow velocity v is 0.463 for k_N = constant and 0.604 for k_S = constant. Altogether, both

approaches lead to velocities that are too high. In the right column of Figure 2-6d–f, the plot Reynolds number Re against friction factor f indicates the same trend. Accordingly, both approaches cause friction factors that are too small for the predicted scenario (dashed lines). For the novel approach (bottom row), the velocity fits well for small values; for higher velocities, the values scatter (Figure 2-6c). The RMSE of velocity v is 0.138 for all measurements and 0.094 for v < 1 m/s. The friction factor f can be predicted more precisely than with constant approaches (Figure 2-6f). Here, an RMSE of 0.57 can be reached for all measurements.

Apart from the influence of water depth on roughness, the bottom slope was investigated. For artificial grass, slopes from 1% to 40% were set. Comparisons of roughness (f/k_N) with water depth or submergence do not show clear dependence. From Figure 2-5a, it can be assumed that roughness increases with decreasing slope for a given water depth. However, some slopes deviate, e.g., 1% and 25% to 40%. The plot of Re vs. f (Figure 2-6f) shows that the friction factor can be predicted adequately with k_N depending on the water depth, and an additional dependence on the bottom slope is not necessary. As described in the "Modeling Extreme Events" section, considering roughness is an important input and calibration factor for 2D models to calculate water depth and flow velocity and thus to simulate the intensity and temporal course of flood waves at certain points of interest. Therefore, consideration of the correct roughness coefficient is essential. In the following, approaches k_S = constant, k_N = constant and the novel approach were used in a flash flood simulation to evaluate their effects in a real catchment area

2.4.1.4 Implementation in a 2D Model

As one objective of this study is the usage and influence of roughness in simulations, the consideration of roughness in the HydroAS model (Hydrotec, Aachen, Germany), which is standard software for flood simulation in Germany and neighboring countries, should be introduced.

HydroAS is a two-dimensional hydrodynamic numerical model for simulations of channel flows and flash floods. In contrast to 1D calculations, which include merely the flow velocity and acceleration in the flow direction (x-direction), two-dimensional models calculate the upstream-downstream and transverse direction of the stream (x- and y-direction). The fundamental principle of this model is the utilization of shallow water equations (Hydrotec, 2021).

The simulations of the HydroAS models are influenced by roughness coefficients for every compiled land usage. Modelers can input the value as Strickler roughness k_S, either as a constant value or a value depending on the water depth. The programming code of the

model converts the Strickler roughness coefficient k_S into the friction factor f by merging the Gauckler–Manning–Strickler equation and Darcy–Weisbach equation into the following equation (Hydrotec, 2021):

$$f = 6.34 \frac{2g}{{k_S}^2 * {D_H}^{1/3}} \tag{2-5}$$

In this case, D_H represents the hydraulic diameter, with $D_H = 4 \times R_H$. According to Hydrotec (2021), the factor R_H can be replaced by water depth for 2D shallow water equations.

By using approaches for submerged vegetation with the Darcy–Weisbach equation, as presented in the previous paragraph (Figure 2-6), water depth is the only factor used to calculate k_N and derive the friction factor f and flow velocity. Thus, appropriate discharge for water depth and velocity is not considered. However, in 2D modeling, discharge or precipitation are initial parameters for simulations. To estimate the influence of this condition, the experimental flume was rebuilt as a 2D model, approaches were applied, and discharge from experiments was used as the initial condition. In Figure 2-7, measured flow velocities are compared to velocities from manually calculated approaches (a–c) and to velocities from simulations (d–f). Figure 2-7a–c are extracts from Figure 2-6a–c. For this comparison, exemplary slopes of 3%, 5%, 15% and 40% were used. This selection represents the total range of values for scattering.

By using a 2D model with roughness approaches and given discharge from measurements, flow velocity is calculated more accurately than manually calculated velocities, and scattering can be reduced. As a result, RMSE improves. For selected data (3, 5, 15 and 40%), RMSE for v predicted (manually) is 0.61 compared to 0.30 for the 2D model with k_S = constant; with k_N = constant 0.47 against 0.19 and with novel approach, 0.16 against 0.06. Experimental runs with slopes of 40% and low discharge do not bring plausible results with the 2D model and are therefore excluded from Figure 2-7. Water depth and flow velocity seem unstable. The reason for this is the usage of shallow water equations in 2D simulations. As presented in the introduction of the HydroAS model, only the x- and y-directions are considered for simulation, and the z-direction is not calculated. For very high slopes, such as 40% in experimental runs, conditions of high slopes and low water depth could result in resilient simulation values. However, the analysis of slopes with SRTM1 data (shuttle radar topography mission) shows a share of less than 2% for slopes of 40% and higher for the area of Germany. Consequently, a combination of the mentioned conditions is rare.

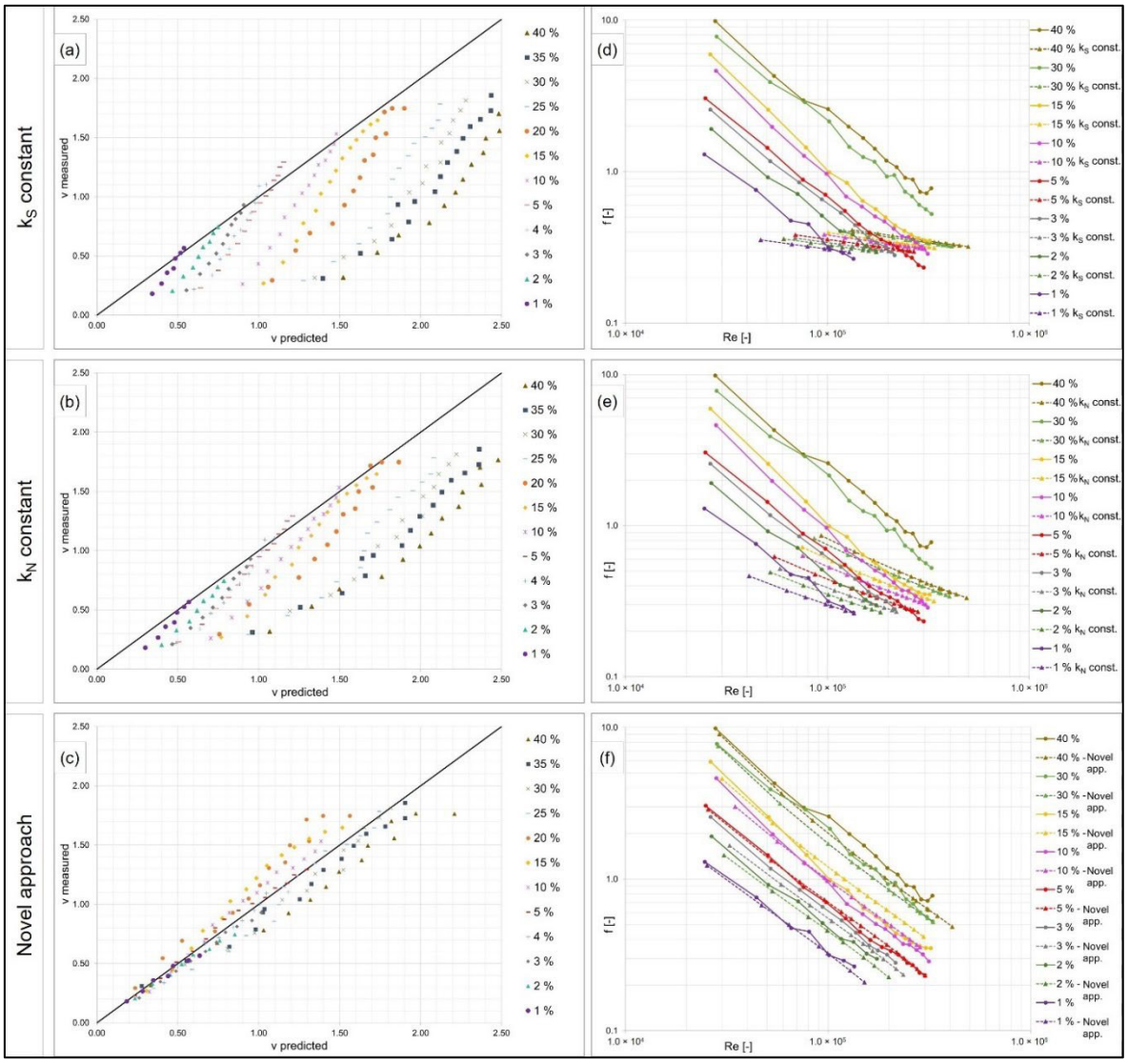

Figure 2-6: Comparison of approaches kS = constant, kN = constant and novel approach for quality assurance. (a–c): Comparison of predicted velocity and measured velocity. (d–f): Comparison of Reynolds number Re and friction factor f (logarithmic) for measurements (continuous lines) and predictions (dashed lines).

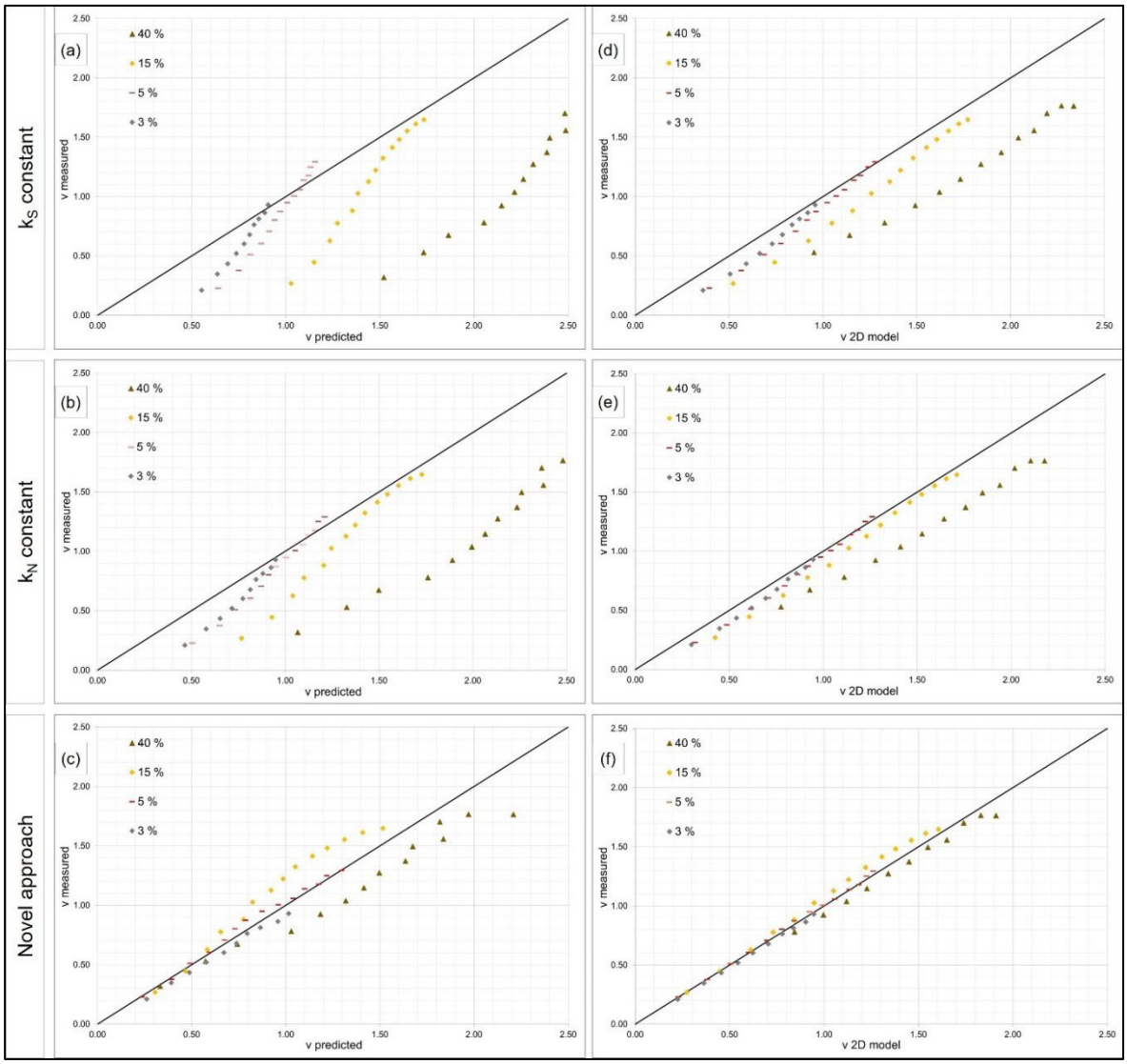

Figure 2-7: Comparison of approaches k_S = constant, k_N = constant and novel approach, manually calculated and implemented in 2D model. (a–c): Comparison of predicted velocity and measured velocity for 3%, 5%, 15%, and 40%. (d–f): Comparison of velocity from the 2D model and measured velocity for 3%, 5%, 15%, and 40%.

By simulating the experimental flume and comparing the results of the simulated and measured flow velocities, the plausibility check shows improvement compared to the manual calculation. To evaluate the effect of different approaches in a real catchment area, a 2D model was built with a DEM (Figure 2-8a).

The model used for the following enquiry comprises an area of 1.1 km^2, and the elevation varies from 288.13 m to 371.61 m above sea level. In the model, there is no deviation in different land uses, so grassland approaches were applied for the entire model. This method was selected to avoid interactions with different roughness values and other processes. Hence, the discharge curve only results from different grassland approaches to evaluate their effects. Precipitation was considered with an intensity of 60 mm/h for a duration of one

hour, and initial losses were taken into account at 2.5 mm. For all scenarios, the total runoff volume is equal.

With the described model, four simulations with different roughness approaches for grassland were carried out:

- An approach with a constant k_S of 25 $m^{1/3}/s$ was applied. This is a plausible value for 2D flooding models (Aigner and Bollrich, 2015; Chow, 1959).
- An approach with a constant k_N of 100 mm was applied. A constant k_N is proposed by Gualtieri et al. (2018), Huthoff (2012), and Schröder (1990).
- The novel approach of this study (Equation (2-4)) with k_N as a function of water depth was applied.
- The approach of Ferro and Guida (2022) with friction factor f as a function of slope, Reynolds number and Froude number was applied. Here, the calibration factor was 0.21, which fits best to the measured values of high water depth in this study.

At the main outlet of the model, different discharge curves are reached. Figure 2-8b illustrates all scenarios mentioned above. Simulation with k_S = constant leads to the earliest and highest discharge peak. The approach with k_N = constant results in a similar curve but shows translational motion. Due to a higher friction factor for k_N = constant, which is presented in Figure 2-6, overland flow slows down, and a delayed discharge is plausible. By using the novel approach with even higher roughness, translation and retention effects are clearly visible in the discharge curve. For the roughness approach by Ferro and Guida (2022), the 2D model has to use water depth and velocity to calculate roughness in every time step. However, these variables should be calculated in the model with existing default roughness. Consequently, the discharge curve shows strong oscillation, and the model seems unstable. Discharge approximates the shown curves and becomes more stable due to the limitation of different equation parameters, such as Re and Fr. Nevertheless, the range of limitations is difficult to define.

A higher friction value for constant k_S and k_N would lead to an intensified retention and translation of the discharge curve. However, these values over- or underestimate specific areas in the catchment. The accuracy of the hydrograph does not ensure the correct determination of the hydraulics in the entire model (Cea et al., 2014). Therefore, the correct approach for friction is essential for obtaining precise results at each point in the model.

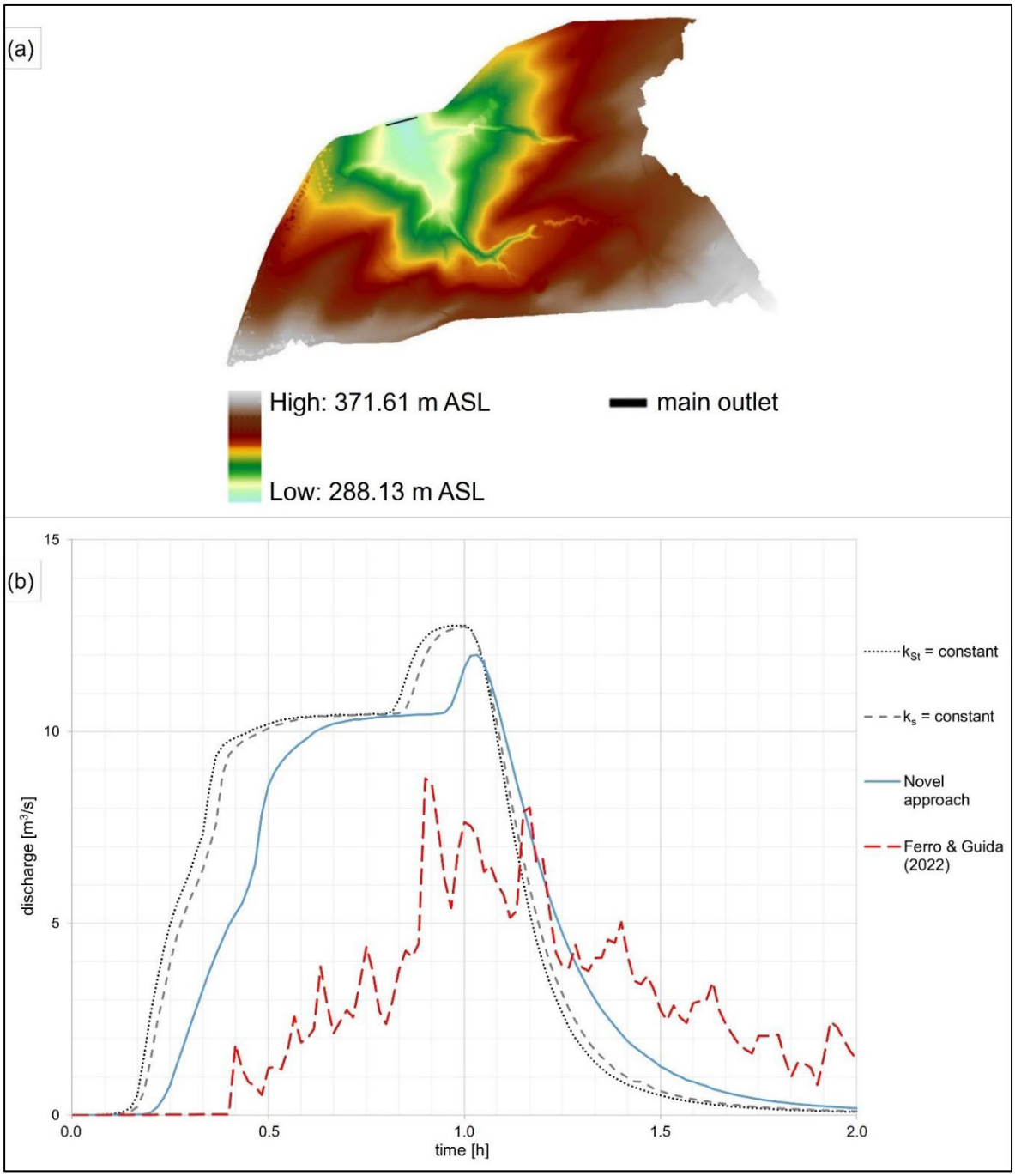

Figure 2-8: Model area and 2D results: (a) DEM of the model and location of the main outlet, (b) hydrograph for different scenarios at the main outlet.

2.4.2 Consideration of Roughness for Emergent Vegetation

For experiments with emergent vegetation, wheat boxes were constructed. They contain wheat stalks that are 0.5 m high and therefore tower above water depth for each experiment. Each box consists of a bottom layer of Styrodur and a mixture of masonry mortal and tile adhesive to fix wheat stalks. The mortal–adhesive mixture is the same material and therefore has the same surface as the solid surface “cement-based coating” in the “Consideration of Roughness for Solid Surfaces” section.

For the analysis of roughness, total friction must be considered for the bottom layer of the cement-based coating (f') and further for the vegetation layer of wheat stalks (f''), as described in the "Vegetational Resistance" section. To calculate friction, the results of the experiments with cement-based coating are suitable considering the bottom friction f'. Wheat stalks are considered with a separate vegetation approach for f" (Equation (2-3)). The sum of both roughness parts leads to the total resistance f.

The vegetation approach (Equation (2-3)) considers two parameters that depend on specific vegetational properties. The first is the drag coefficient C_D, which is an empirically determined value. In this study, the shape of a cylinder is assumed for wheat stalks, and therefore, a value for C_D of 1.2 is selected (Aigner and Bollrich, 2015). The second parameter is the specific frontal area of the vegetation in the x-direction. Due to the experimental setup of this study, a mean diameter of wheat stalks of 3.7 mm and a density of vegetation of 500 pieces/m² were used for calculation.

To compare the vegetation approach and data from experiments, the experimental results must be adjusted. For each experiment, a total f can be derived from the measured discharge, water depth and slope with the Darcy-Weisbach equation (Equation (2-1)). Part of the bottom resistance f' was calculated with Equation (2-2) in combination with a constant k_N derived from experiments with a cement-based coating. Here, the approach was simplified by an assumption of k_N = 0.006 m as a uniform value for each experiment. Scattering of results from experiments with cement-based coating was not considered. However, the influence of the bottom friction f' is almost insignificant because the values for k_N vary from 2.3 mm to 10.2 mm (see section "Consideration of Roughness for Solid Surfaces") and therefore f' varies from 0.05 to 0.1. However, f" varies from 0.1 to 0.8 (Figure 2-9). Part of the vegetational resistance f" was calculated by subtracting f and f'.

Figure 2-9 shows the share of f" for the measured data of wheat in comparison to the vegetation approach (Equation (2-3)) from the literature. For data points with slopes from 1% to 15%, the friction factor f" increases with increasing submergence. According to Nepf (2012) and Abrahams et al. (1990, 1994), this behavior is plausible for emergent vegetation. In contrast, the data points of high bottom slopes (20–35%) vary widely. To reproduce the measured values, a vegetation approach was used. For slopes up to 15%, the curve of this approach lies in the mean range of data scatter. For low submergence with values <0.10, the vegetational approach represents the measured data well. Here, the RMSE of f" is 0.045. The higher the submergence is, the higher the scattering. For all data of slopes 1–15%, RMSE is 0.112. Data scatters for high velocities and water depth. This is possibly caused by measurement errors due to turbulence. For slopes >15%, the data points do not

show an increase in f" with an increase in submergence. Scattering is strong and results in a total RMSE for f" of 0.488.

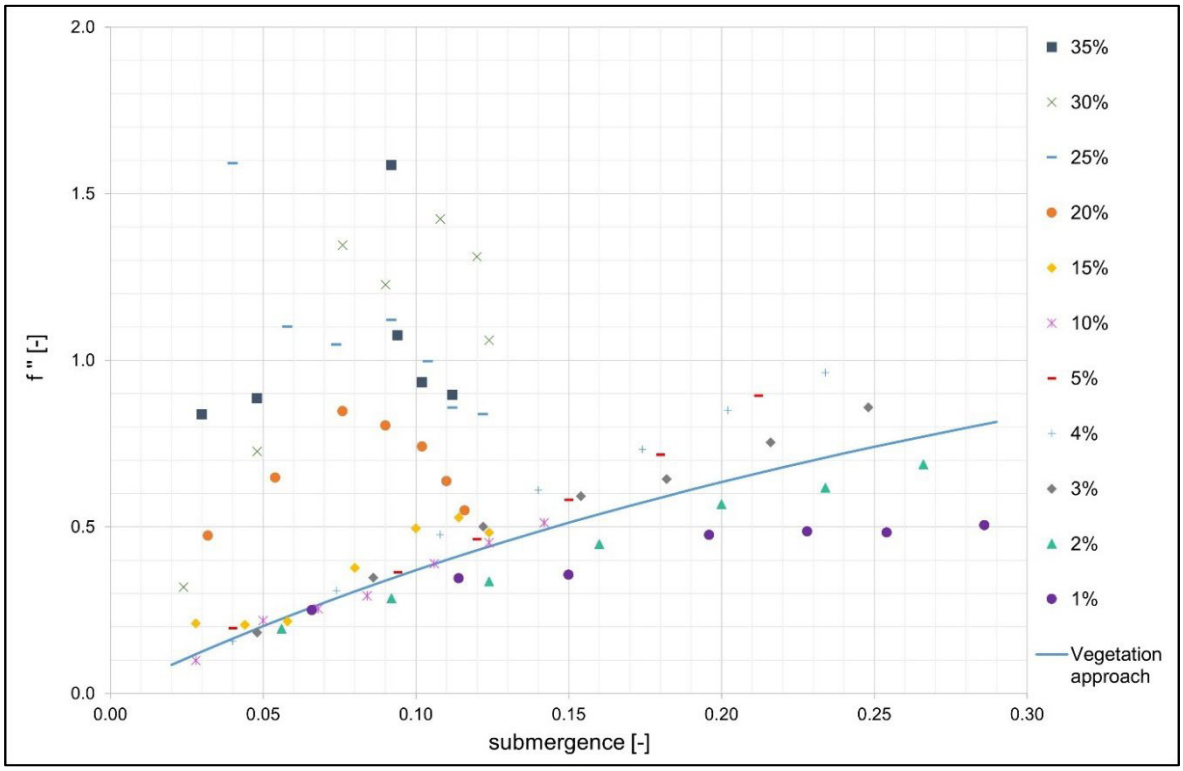

Figure 2-9: Relationship between submergence (h/h_{veg}) and friction factor f" for measured values of experiments with wheat (dots) in comparison to the vegetation approach (blue, solid line, Equation (2-3).

By examining all results regarding slope, no clear dependence can be established. For slopes from 1% to 5%, for a given submergence, the friction factor increases with slope. However, slopes of 10% and 15% do not continue this trend. In total, for experiments of this study with slopes up to 15%, a mean value can be reproduced with a vegetation approach and can be used for the consideration of emergent vegetation in model-based simulations.

2.4.3 Consideration of Roughness for Solid Surfaces

For the category “solid surfaces”, cement-based coating, asphaltic emulsion, exposed aggregate concrete and aluminum were used. Figure 2-10 shows four plots, one for each material used. Here, water depth is plotted against sand–grain roughness k_N to describe bed roughness. In all plots, a similar phenomenon can be perceived. For data of slopes up to 15/20%, the sand-grain roughness k_N is an almost constant value for all water depths. This suggests that the roughness coefficient k_N does not depend on the water depth. Compared to a condition of constant k_N for $h >> h_{veg}$ for submerged vegetation, in this case, water depth is much higher than roughness height k_N and therefore, it could be seen as a very high submergence. Against this background, constant k_N values seem plausible. For

higher slopes, k_N scatters or increases with increasing water depth. Similar to the experimental data of the wheat, scattering increases with both bottom slope and water depth. The range of values for the derived k_N are listed in Table 2-2. Here, the mean values for different slope conditions are presented.

Table 2-2: Derived, mean k_N values from experiments of this study and literature references.

Surface	Range of Mean k_N Values (For S = 2%–S = 20%)	Literature (Albert, 2020)
Cement-based coating (Figure 2-10a)	2.3–10.3 mm (for slope = 1%: k_N = 1.4 mm)	Concrete, smooth: k_N = 1–6 mm
Asphaltic emulsion (Figure 2-10b)	8.3–9.7 mm (for slope = 1%: k_N = 2.3 mm)	Asphaltic concrete or mastic asphalt: k_N = 1.5–2.2 mm
Exposed aggregate concrete (Figure 2-10c)	12.4–18.4 mm (for slope = 1%: k_N = 8.3 mm)	Concrete smooth–rough: k_N = 1–20 mm
Aluminum (Figure 2-10d)	1.3–4.6 mm (for slope = 1%: k_N = 0.4 mm)	Steel: k_N = 0.04–0.1 mm

The derived k_N values of this study are higher than the orders of magnitude listed in the literature. By comparing measured data with data from the literature, it is noticeable that values from the literature often fit within the range of data with slope = 1%. Two explanations are possible: (a) despite the assumption of 90% discharge (see paragraph “Outline”), some data with 1% slope scatter and deviate from the expected curve; perhaps even more discharge was lost, or (b) data from the literature fit with data of 1% slope because literature values are derived from channel conditions with low slopes. Overall, it could be seen that for a given water depth, k_N rises with slope. However, this conclusion is weakened by considering scatter due to measurement inaccuracies. By changing the measured water depth by ± 3 mm, k_N varies widely by −39 to −60% or rather +53 to +100% (for slopes up to 20%). For comparison of plots shown for submerged vegetation, here, a plot of Re and friction factor (logarithmic display) shows negatively sloping functions with low slopes. This result seems reasonable to what has been reported in the literature (Abrahams et al., 1990, 1994).

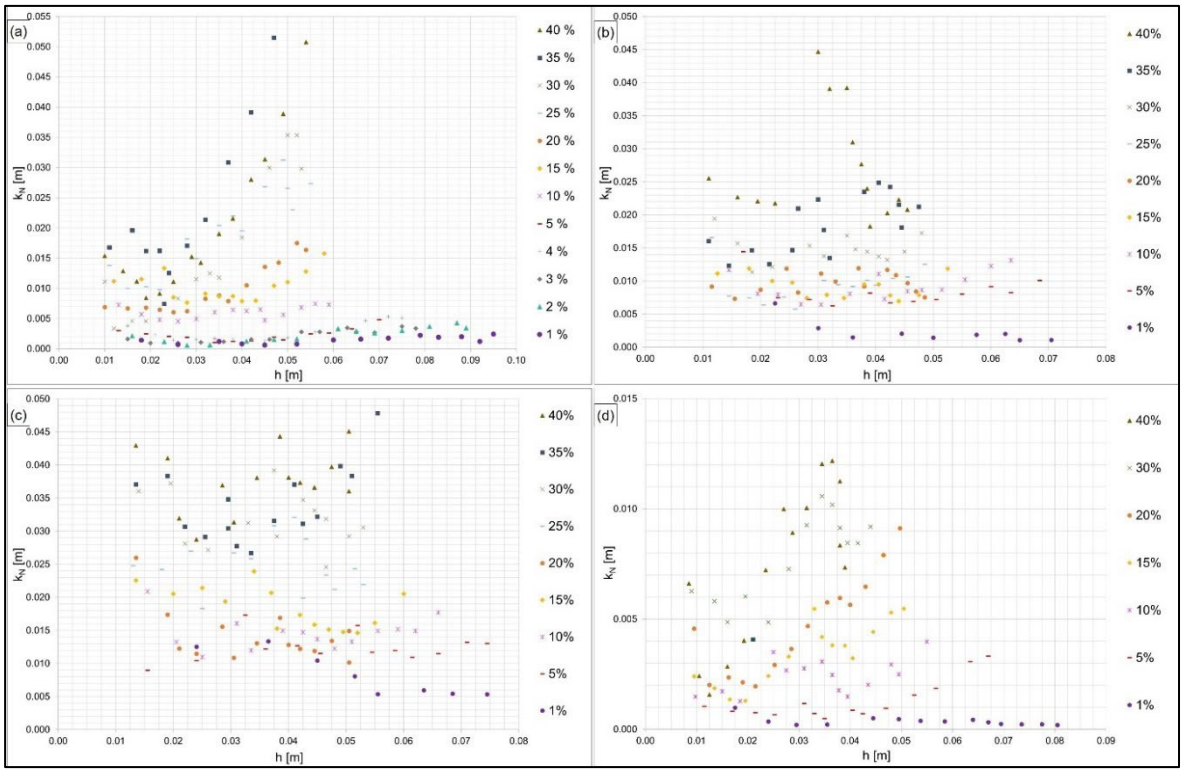

Figure 2-10: Relationship between water depth h and equivalent sand–grain roughness k_N for measured values of (a) cement-based coating, (b) asphalt emulsion, (c) exposed aggregate concrete, and (d) aluminum.

2.5 Conclusions

In this study, laboratory experiments with submerged and emergent vegetation as well as solid surfaces were carried out. As a result of these measurements, different roughness coefficients were derived and analyzed to estimate the influence of water depth and slope on roughness.

For submerged vegetation (artificial grass), the influence of water depth on roughness shows a decrease in roughness with an increase in submergence. The opposite result was observed for emergent vegetation (wheat). Here, a rising submergence leads to a higher roughness. Both results are plausible regarding results from the literature. Due to the submergence of roughness structures, such as vegetation, roughness increases until a submergence of 1, and therefore, its highest roughness is reached. For higher submergence, roughness decreases to a constant value. Analyses of solid surfaces show no dependence of water depth on roughness k_N. However, by calculating the friction factor f with the Prandtl–Colebrook equation and a constant k_N, the water depth is an influencing factor. Investigations regarding the influence of the bottom slope on roughness show uniform results. In a plot of water depth and roughness k_N, the influence of slope could be seen for some data points. Due to scattering, this trend is vague for high slopes and high water depths. However, when considering the friction factor f, the influence disappears or is only slightly visible.

Comparing the results of solid surfaces with results from the literature, constant k_N values are reasonable, although the measurements of this study lead, in total, to a slightly higher roughness than presented in the literature. The results of emergent vegetation show that the existing vegetation approach depicts the mean curve for measured values. Scattering rises with increasing water depth and slope. In contrast, the consideration of submerged vegetation is not fully applicable to existing approaches. Consequently, a novel approach appropriate for measured data has been introduced to consider water depth-related roughness. Simulations of an RoG model with different approaches clearly show visible changes in discharge curves. The decision of the roughness approach to correctly calculate water depth and flow velocity has a very high impact on the catchment response. Thus, this response depends on the consideration of the correct roughness value at each point in the entire catchment. To evaluate the quality and decision about the most reasonable approach, real measurements of water level gauges at several points in the catchment area are necessary. For the best model performance, a simple approach is recommended. Calibrated RoG models can be used to simulate specific precipitations and investigate precautions for real flash floods.

The bed roughness investigated in this study was always based on specific surfaces. Other surface structures or vegetational properties lead to different values and approaches. For the vegetation approach of emergent vegetation, properties are considered. For the usage of the proposed, novel approach, the factor $\Delta k_N / \Delta$ submergence should be derived by vegetation properties with data from this study and data from the literature. Thus, further research is needed.

In general, one challenge for modeling flash floods is the knowledge about land use. For given information about, for example, arable land, used roughness is always just a scenario. The surface can be bare soil, or in contrast, fields of wheat, with different stalk heights, depending on the culture and season. Differences in roughness can be immense. At the moment, no increase in roughness with increasing water depth for emergent vegetation is considered in the guidelines (LUBW, 2020). With this approach, wheat fields, as an example of emergent vegetation, could slow overland flow more than currently assumed.

Data Availability Statement

All experimental data of this study are provided at a data repository (doi.org/10.6084/m9.figshare.17142440). The software HydroAS is commercially available from Hydrotec GmbH, Aachen, Germany (2021b). The simulation model is available as part of a previous project of flash flood simulations in the municipality of Eppelborn.

Limitations

Even though laboratory experiments show, in general, scale invariances to overland flow (Ferguson, 2021a), laboratory experiments offer the possibility of using one bed roughness with different slope settings. In on-site setups, it is nearly impossible to perform experiments with the same bed roughness on different slope sections with slopes ranging from 1% to 40%. During the performance of laboratory experiments, especially for setups with low slopes, some water was leaked after the flow measurement. Although the junction between the reservoir and flume was sealed with foil and duct tape, some loss of flow cannot be ruled out. For slopes = 1%, discharge was adapted to 90% of the measured value.

3 Accuracy of Recording Linear Erosion using an Unmanned Aerial Vehicle (UAV)

Soil erosion is an ongoing environmental problem. To address this issue, calibrated erosion models are used to forecast areas vulnerable to erosion and to determine appropriate preventive measures. Model calibrations are based on erosion data recorded using different techniques such as photogrammetry from an unmanned aerial vehicle (UAV). In the following study, the accuracy of the DJI P4 RTK UAV data was estimated for cropland boundary conditions. Ground heights of tilled and untilled arable land and standing water surfaces were determined using aerial surveys and compared to terrestrial surveys conducted on site. The results revealed that untilled soils can be accurately detected using a UAV, whereas the detection error rates of tilled soils were 2–3 folds higher. Additionally, the width and height of linear erosion tracks were measured and compared using aerial surveys and manual on-site measurements. The erosion width of the linear tracks was accurately recorded using a UAV whereas the erosion depth was underestimated by the digital elevation model (DEM) generated from UAV data.

Rebecca Hinsberger and Alpaslan Yörük

PLoS One, 2025, 20(9): e0329286
DOI: 10.1371/journal.pone.0329286

3.1 Introduction

Erosion of agricultural land is an ongoing and highly discussed research topic. The collection of erosion data is important to calibrate and validate erosion models and to estimate the influence of erosion events on the environment (Malinowski et al., 2022; Pineux et al., 2017). To derive the spatial distribution and the volumetric quantity of erosion, erosion can be measured with direct contact techniques or with indirect non-contact techniques (Báčová et al., 2018; Di Stefano et al., 2019c). The direct method uses tools such as a metric ruler or rill meter. Especially in the early stages of erosion measuring, studies used mechanical profile meters to measure rill and gully cross-sections (Casalí et al., 1999, 2006). These tools are time-consuming due to intensive field work and expensive due to personnel costs (Khanal et al., 2020). According to Báčová et al. (2018), the major disadvantage is the deformation of the soil surface during measurements and the limited resolution. The indirect method uses tools such as terrestrial laser scanners or photogrammetric methods that lead to fast data acquisition (Báčová et al., 2018). These methods require specific environmental and boundary conditions, such as weather and surface conditions. To evaluate the accuracy of these indirect methods, direct measurements were used for comparison in previous studies (Khanal et al., 2020; Pourali et al., 2014; Soininen et al., 2024). In addition, terrestrial laser data was compared to photogrammetric data (Castillo et al., 2012; Glendell et al., 2017; Gómez-Gutiérrez et al., 2014; Kaiser et al., 2014) and the studies assume that photogrammetry is less costly but produces similar results in terms of accuracy.

Accuracy investigations of photogrammetry using UAVs were conducted in several studies. For the UAV ‘DJI P4 RTK’ used in this study, DJI (2021) stated that the photogrammetry of the UAV can record surfaces with a vertical variance of ±1.5 cm (+1 ppm) and a horizontal variance of ±1 cm (+1 ppm). To achieve these values, optimal satellite configurations and optimal reception of real-time correction data are required (Przybilla et al., 2020). For the accuracy of the UAV data, studies indicate variances of 2–3 cm for asphalt and grassland (Przybilla et al., 2020), observed vertical variances of 2 cm and horizontal variances of 1.2 cm on a solid surface (DroneDeploy et al., 2019), and suggested maximum vertical and horizontal variances of 4–5 cm for a façade (Taddia et al., 2020). To improve accuracy, some studies have focused on the usage of ground control points (GCP) (Forlani et al., 2018; Martínez-Carricondo et al., 2018; Štroner et al., 2020). These are linked in UAV images for additional georeferencing. Štroner et al. (2020) indicate that horizontal measurements are adequate, but vertical variances are insufficient without GCP. Consequently, a combination of RTK (real-time kinematic) and GCPs provides the best results (Štroner et al., 2020). Martínez-Carricondo et al. (2018) suggest one GCP at each edge of the investigation area to minimize altitude errors. For the evaluation of the errors, the root mean

square error (RMSE) and the mean absolute error (MAE) are widely used statistical values. The RMSE is better for (normal) Gaussian errors and the MAE for Laplacian errors (Hodson, 2022). However, it is common to present both values and leave it up to the reader to choose which error value to use.

UAV-based photogrammetry presents a balance of resolution and efficiency and, consequently, a good compromise between field measurements and satellite-based remote sensing (Liu et al., 2016; D'Oleire-Oltmanns et al., 2012). The photogrammetric method results in digital elevation models (DEM) and orthophotos with a high resolution of a few centimeters (Liu et al., 2016) and provides a good opportunity to measure soil surface changes (Eltner et al., 2014).

Erosion structures have been investigated using different indirect methods, such as specifically designed kites (Giménez et al., 2009), fixed-wing aircrafts (D'Oleire-Oltmanns et al., 2012; Peter et al., 2014), and UAVs (Di Stefano et al., 2019; Eltner et al., 2014). These observation data were used to detect and monitor (gully) erosion (Liu et al., 2016; Maugnard et al., 2014; Zhang et al., 2015). Giménez et al. (2009) recorded different gully geomorphology and pointed out that the shadow of gullies negatively influences photogrammetric methods. Another study reported inaccuracies due to vegetation, water, and small-scale textures (Cook, 2017). A study on the Chinese Loess Plateau (Liu et al., 2016) indicated the influence of different terrain characteristics on the accuracy of the UAV data.

This study focuses on evaluating the accuracy of the DEM derived from photogrammetric data collected by the DJI P4 RTK UAV for erosion surface conditions, specifically bare soil of croplands and linear erosion tracks. In order to apply the observed erosion quantity data in erosion model calibration or validation, it is crucial to estimate the errors present in the observational data. The surface structure is particularly important for this estimation (Liu et al., 2016), so the focus was on erosion surface conditions, such as bare soil with tilled and untilled surfaces. Both tilled and untilled surfaces are potentially present in the case of an erosion event. The use of UAV-based photogrammetry was considered suitable due to its capability to generate high-resolution DEMs necessary for studying soil microrelief. Aerial surveys were conducted on three bare soil fields with tilled and untilled soils as well as in an area with standing water and steep slopes. The latter test was used to assess how remaining water from a previous heavy precipitation event might affect the accuracy of erosion extent estimated by photogrammetry. The quality of these surveys was validated by comparing them to terrestrial measurements, as previously done in other studies (Khanal et al., 2020; Pourali et al., 2014; Soininen et al., 2024). The high geospatial accuracy of the selected UAV made it ideal for these comparisons.

Furthermore, the study aimed to examine the accuracy of linear erosion width and depth in UAV-based DEMs. Croplands spanning several hectares with erosion tracks were recorded using the UAV and the erosion tracks were measured using the direct method. By comparing the UAV-derived measurements of linear erosion tracks to those obtained with a metric ruler, the study assessed the accuracy of the UAV-generated DEM for erosion tracks, in particular. The objective of this part of the study was to investigate the accuracy and usability of the DJI P4 RTK for erosion investigations and identify potential uncertainties in erosion recording.

3.2 Materials and Methods

In this study, the accuracy of a UAV-generated DEM was investigated for tilled and untilled soil, as well as linear erosion tracks. Direct measurements were used as a benchmark. All investigated fields are located in southwestern Germany, in the federal state of Saarland. Two measurement series were conducted: i) To analyze the accuracy of the UAV-generated DEM due to tillage and water, four investigation areas were selected. These croplands were known by municipalities to experience erosion and are marked as Fields A–D in Figure 3-1; ii) To analyze linear erosion, six fields were selected. These fields were affected by real erosion events occurring over a period of two years and are marked as Fields 1–8 in Figure 3-1. Field 5 and 7 were excluded from this study because no manual measurements were conducted on these fields.

Prior to the surveys, permissions for the investigations were obtained from the tenant of each individual field.

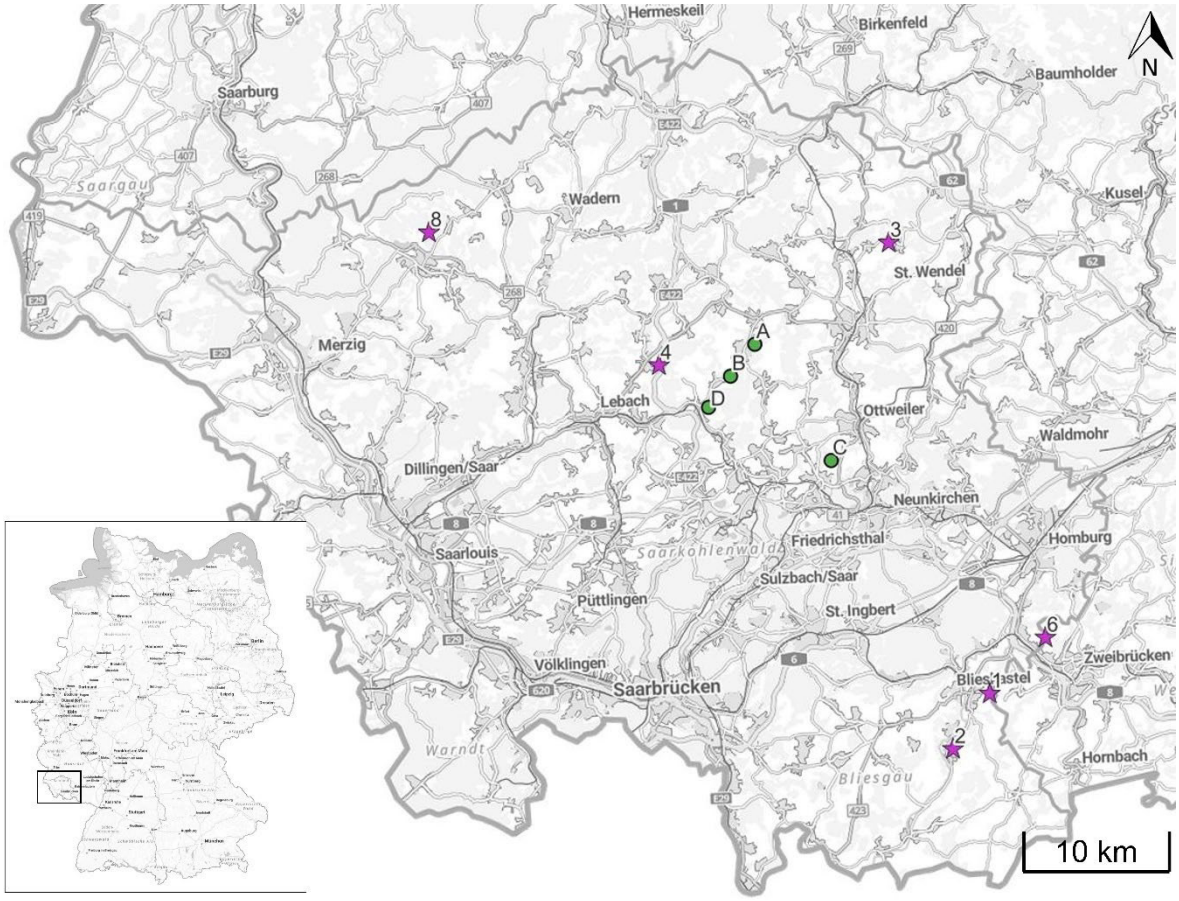

Figure 3-1: Overview of investigation areas. All areas are located in southwestern Germany, in the federal state of Saarland. Fields marked with green dots and labeled A–D are used for the investigations of different tillage and water surfaces (Section 3.2.2); Fields marked with purple stars and numbered 1–8 are used for linear erosion measurements (Section 3.2.3). Basemap: Reprinted from BKG under a CC BY license, with permission from BKG, original copyright 2025. © GeoBasis-DE/ BKG (2025) CC BY 4.0.

3.2.1 General Evaluation Method

The UAV used in this study was a DJI Phantom 4 with real time kinematic (P4 RTK). The UAV is equipped with a built-in camera (1-inch CMOS sensor, effective pixel of 20 M, 24 mm wide-angle lens) and an RTK system for improved geospatial data (DJI, 2021). The positioning precision was further enhanced by using a combination of the UAV and DJI D-RTK 2 mobile station. The output coordinate system for all aerial surveys was WGS84 with ellipsoidal heights. Since terrestrial surveys were conducted in the DHDN 3, Gauss-Kruger Zone 2 coordinate system (EPSG: 31466), the aerial surveys were transformed to this coordinate system and the German height system, DHHN2016.

All aerial surveys in this study were conducted in 2D mode, where images are recorded perpendicular to the ground. For the study on the water surface (Section 3.2.2), an additional survey in 3D mode was conducted. In 3D (multi-oriented) mode, the UAV initially records images in 2D mode and then takes additional images by rotating the camera gimbal by 30°. These additional images are recorded from four sides of the investigation area.

In the post-processing of the aerial surveys, the structure from motion (SfM) technique using Agisoft Metashape Professional software (Agisoft LLC, St. Petersburg, Russia) (Agisoft, n.d.) was used. The photos taken by the UAV were aligned, and a dense cloud was built. From this dense cloud, a digital elevation model (DEM; referred to as UAV DEM) and an orthoimage were generated. The software settings were configured based on Agisoft's specifications, matching those used in previous studies (Štroner et al., 2020), and are presented in Table 3-1.

Table 3-1: Agisoft Metashape software settings used for the generation of the UAV DEM and orthoimages.

Setting	Value
Align Photos	
Accuracy	High
Key point limit	40,000
Tie point limit	8,000
Optimize Camera Alignment	Fit f, cx, cy, k1-4, p1-2
Build Dense Cloud	
Quality	High
Depth filtering	Aggressive
Build DEM	
Projection	Geographic
Source data	Depth maps
Quality	High
Interpolation	Enabled
Build Orthomosaic	
Surface	DEM
Blending mode	Mosaic (enable hole filling)

3.2.2 UAV Accuracy due to Tillage and Water Surfaces

To estimate the accuracy of elevation measurements using the UAV, aerial (indirect method) and terrestrial (direct method) surveys were carried out at different investigation fields. Elevation measurements were compared and analyzed to evaluate the UAV DEM accuracy. Three croplands with bare soil (Fields A–C in Figure 3-1 and Figure 3-2A–C) and one flood control reservoir with standing water (Field D in Figure 3-1 and Figure 3-2D) were selected for the study.

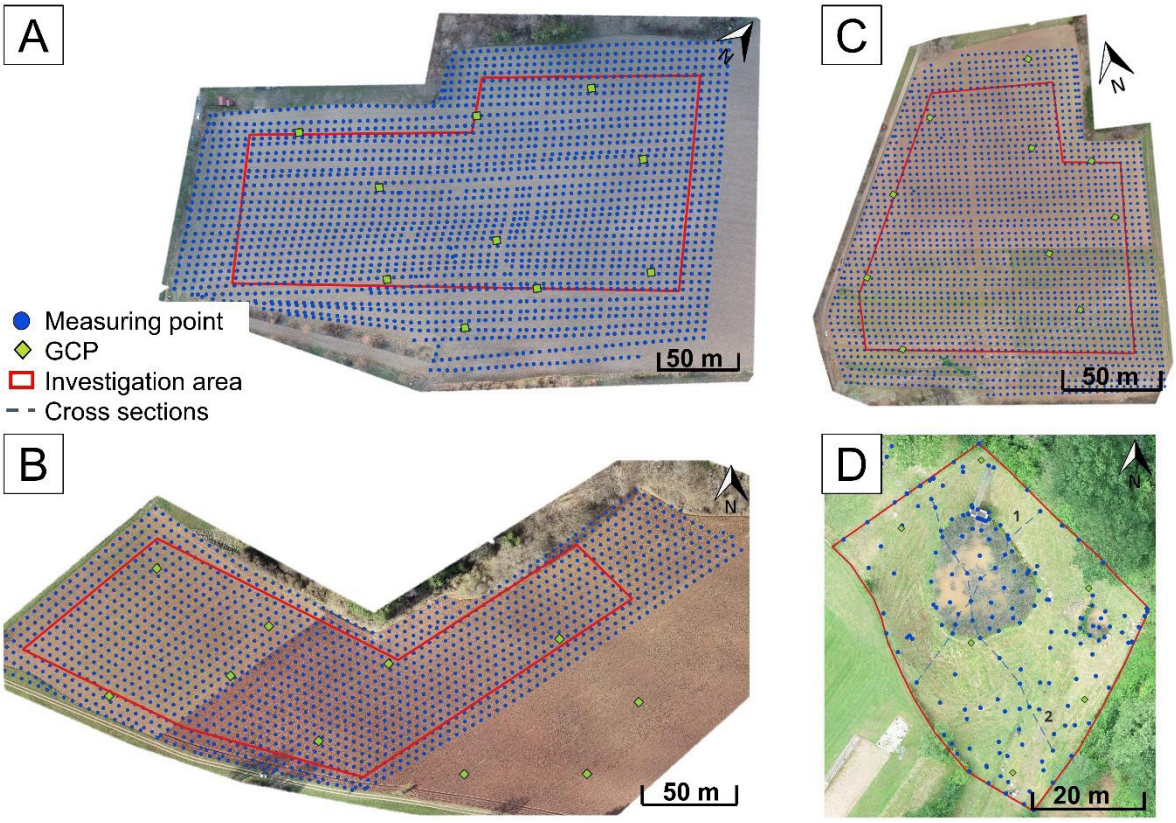

Figure 3-2: Investigation areas for the analysis of the influence of tillage and water surfaces. Investigated croplands (A, B, and C) and flood protection system (D) marked with the respective investigation area (red outline). Terrestrial measured points are marked as blue dots and the cross sections in Field D as blue dashed lines. Ground control points (GCP) used for the positioning of the UAV are marked as green diamonds. The orthophotos that serve as background map are the results of the aerial surveys.

All fields were investigated in the spring. Field A was tilled (Figure 3-2A), Field B was half tilled/half untilled (Figure 3-2B), and Field C was completely untilled (Figure 3-2C). Vegetation was absent, except for a thin moss layer on parts of Field C. The fields ranged from 3 to 5 hectares in size, with steep slopes, in average between 12 and 18.5%.

To reduce errors caused by vegetation in neighboring areas, the perimeter of all investigated fields was buffered inside (outlined in red in Figure 3-2A–C).

An important quality factor for aerial surveys is reproducibility. Thus, the UAV investigations on cropland were performed twice consecutively in each field to examine reproducibility. Both flights were carried out in the 2D mode, with consistent settings and the usage of an RTK-fix throughout the entire flight. Further analyses, independent of reproducibility, were conducted using the data from the second aerial survey.

Additionally, 2–3 GCPs per hectare (marked with green diamonds in Figure 3-2) were recorded using the Global Navigation Satellite System (GNSS) receiver ‘Trimble R6’. This receiver achieved standard deviations of 1.4 cm in position in preliminary tests. According to literature (see Section 3.1), these GCPs can enhance UAV accuracy. To confirm this and

analyze the impact, the post-processing of the aerial survey was conducted with GCPs to enhance accuracy in one analysis and without GCPs in another analysis.

Parallel to the aerial survey, all fields were surveyed terrestrially with the total station ‘Trimble S7’ approximately in a 5 m grid. In Figure 3-2, these terrestrial survey points are marked by blue dots in each investigation field and serve as a reference.

To verify the UAV DEM accuracy, the survey points from the total station were compared with corresponding points in the UAV DEM, with a total of 3470 points (1619 and 1851 points for untilled and tilled soil, respectively). Elevation data from the UAV DEM was extracted at the total station survey points using the point sampling tool in the geo-information system QGIS (QGIS, n.d.). This method was also used in literature (Khanal et al., 2020) and, therefore, used for all comparisons of point and DEM elevations.

The flood control reservoir area (Figure 3-2D) has an extension of 0.2 ha. The surface consists of grassland with varying slopes, as well as stagnant and turbid water areas. The grass was cut the day before the surveys to minimize vegetation interference. Some vegetation in the water areas was not removed, resulting in localized measurement errors in this area. Similar to the investigations on arable land, aerial and terrestrial surveys were conducted concurrently. UAV flights were conducted in both 2D and 3D modes. The data collected was used to compare the different flight modes. For this terrestrial survey, the total station ‘Trimble M3’ was used to measure points across the entire area at significant locations, around the water level, and at the ground of the water reservoir. Two cross-sections (indicated by blue dashed lines in Figure 3-2D) at the steep slope and water area of the reservoir were used to compare the terrestrial and aerial measurements in 2D and 3D modes.

Details of all study areas and flight metrics are provided in Table 3-2.

Table 3-2: Details of study areas and flight metrics for Fields A–D.

Field	A	B	C	D	
Mode	2D	2D	2D	2D	3D
DEM extent [ha]	10.35	12.58	8.5	3.57	5.57
Investigated area [ha]	1.92	3.09	3.05	0.2	
Investigated measuring points	893	1308	1269	182	
Flight date	19 March, 2021	02 March, 2021	22 March, 2021	25 June, 2021	
Flight height [m]	50	50	50	50	
Number of pictures	300	311	228	168	399
Overlapping [%]					
Horizontal	70	70	70	70	70
Vertical	80	80	80	80	80
Speed [m/s]	3.9	3.0	3.9	3.9	3.9
Obtained resolution UAV DEM [cm/px]	3.3	3.8	3.6	4.1	4.7

3.2.3 Analysis of Linear Erosion Measurements

Measurements of eroded croplands are crucial for achieving the main objective of using erosion data from natural events for model calibration. In this study, six eroded croplands without vegetation were investigated over a period of two years.

Aerial surveys were conducted using the DJI P4 RTK. The survey and photogrammetry processes in Agisoft Metashape Professional resulted in the generation of a DEM and orthoimage of the investigated area (see Section 3.2.1). Both grids have a resolution of a few centimeters that allows the clear visibility of linear erosion on both the orthoimage and the DEM (Figure 3-3).

Groove depth and width are essential measurements for accurately calculating erosion volume. To ensure quality control of these measurements, manual on-site measurements using a measuring stick were compared to the depth and width of grooves in the UAV DEM and orthoimage. The measuring points were located in six fields, with Field 1 being a potato field with bare soil and Fields 2, 3, 4, 6, and 8 being cornfields with bare soil or sparse vegetation. In total, 48 and 44 points for groove depth and width, respectively, were recorded. The precise location of the measuring points is essential due to the partly immense heterogeneity in different parts of the grooves. Thus, the positions of the on-site measurements were recorded using the GNSS receiver ‘Trimble R6’. As mentioned before, an accuracy of ≤1.4 cm of the position was possible. With the RTK system of the UAV, this point can be accurately represented in the UAV DEM with erosion. The groove width and depth were determined from cross sections in the DEM at the measuring points of the manual measurements.

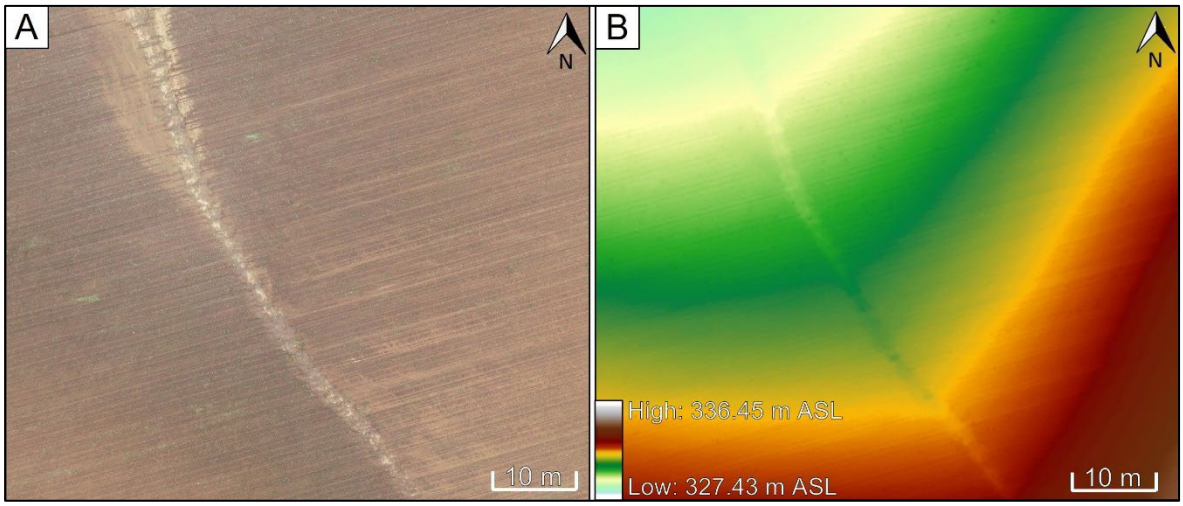

Figure 3-3: Recorded linear erosion track on Field 8. The erosion track is clearly visible on the orthoimage (A) and the DEM (B) generated using photogrammetric UAV data.

3.3 Results and Discussion

3.3.1 UAV-generated DEM Accuracy due to Tillage and Water Surfaces

The analysis of investigations on arable land with bare soil (Fields A–C) produced results regarding the i) reproducibility of UAV flights, ii) accuracy of the UAV DEM with and without GCPs, and iii) influence of tillage. Investigations of standing water in Field D produced results regarding iv) accuracy of recorded water surfaces and vegetation, and v) accuracy of photogrammetry in 2D and 3D modes.

Reproducibility

For each of the investigation areas A–C, two consecutive flights were conducted and the photos from the UAV were used to create two DEMs without the use of GCPs. In Field A, the elevations in the DEM from the second flight are lower than those from the first flight. In Field C, the opposite is true, while in Field B, there are clusters where the elevations from either the first or second flight are higher. There is no discernible pattern, and tillage does not seem to have any influence. A comparison of all DEM grid cells (Field A: 21,044,504; Field B: 16,774,663; Field C: 20,115,771) shows a RMSE of 0.96 cm indicating a low scattering effect. Additional statistical values are available in Table 3-3, under the ‘reproducibility’ row. This error could potentially occur in all flights.

Accuracy with and without GCPs

To analyze the influence of GCPs on the accuracy of the DEM, post-processing of the second aerial survey was conducted with and without GCPs. For the DEM without GCPs, the same DEM used for the reproducibility analysis was used. A new DEM was processed for the DEM with GCPs. At the locations of the terrestrial survey points, both the UAV with and without GCPs were scanned for their elevations and compared to the directly measured

terrestrial elevations. The results indicate that the DEM with GCPs aligns better with manual measurements compared to the DEM without GCPs. For untilled and tilled soil, the RMSE improved from 4.99 cm to 1.91 cm and from 7.52 cm to 4.63 cm, respectively. Additional statistical values are available in Table 3-3, under the 'Accuracy UAV DEM' rows. The negative mean value suggests that the elevations in the generated DEM tend to be higher than the directly measured elevations. Measurements with GCPs demonstrated the best performance in these investigations and were used for further analysis. This result is consistent with findings from previous studies (Martínez-Carricondo et al., 2018; Štroner et al., 2020). In a study by Liu et al. (2016), vertical RMSE values of 24.5 cm and 33.9 cm were observed for different locations using a microdrone md4−1000 and GCPs, which are higher than the values in this study. However, the mean values are 2 cm and 3 cm and show less deviation compared to the RMSE. The errors indicate that the mean value is similar and the values show a higher scatter in the study of Liu et al. (2016). The discrepancies may be attributed to the UAV used, study area, and flight height. In another study (Martínez-Carricondo et al., 2018), the influence of the amount and distribution of GCPs was investigated using an octocopter. For a comparable stratified distribution with 2 GCPs/ha, they obtained a vertical RMSE of 4.3 cm. This value aligns with the results of this study. By using the DJI P4 RTK UAV that was also used in this study, Štroner et al. (2020) observed mean deviations of −1.8 cm and standard deviations of 2.8 cm for vertical checkpoints in a rural area, further confirming the results of this study. The consideration of GCPs is very time-consuming (Liu et al., 2016), both for recording and marking the GCPs in the UAV photos. However, GCPs are important to consider when evaluating the accuracy of the UAV DEM.

The influence of tillage is analyzed in the following section.

Table 3-3: Statistics of vertical error values for different accuracy analyses. Min = Minimum, Max = Maximum, Mean = Mean value, MAE = Mean Absolute Error, RMSE = Root Mean Square Error (all values in meter).

	Min	Max	Mean	MAE	RMSE
Reproducibility (Flight 1 – Flight 2, without GCP)	-0.7704	0.2346	0.0015	0.0119	0.0096
Accuracy UAV DEM					
Untilled – with GCP	-0.0664	0.0461	-0.0074	0.0145	0.0191
Untilled – without GCP	-1.1847	0.0325	-0.0161	0.0224	0.0499
Tilled – with GCP	-0.3367	0.0875	-0.0358	0.0390	0.0463
Tilled – without GCP	-0.2315	0.0540	-0.0645	0.0655	0.0752
Accuracy DEM1 (reg. authorities)					
Untilled	-0.4660	0.0940	-0.0785	0.0818	0.0980
Tilled	-0.2400	0.1080	-0.0587	0.0662	0.0817

Influence of tillage

Significant differences in accuracy were determined for measurements on tilled and untilled soils, indicating that the accuracy of UAV DEMs depends on tillage (Table 3-3, under the 'Accuracy UAV DEM' row). Figure 3-4A shows the differences between terrestrial survey elevations and UAV DEM elevations (with GCPs). The average absolute errors (MAE) were 1.45 cm and 3.90 cm, while the root mean square error (RMSE) values, indicating scattering, were 1.91 cm and 4.63 cm for untilled and tilled soils, respectively. For even and more solid surfaces, deviations suggested in the literature (see Introduction) were confirmed. The results are consistent with Khanal et al. (2020), who used a DJI P4 (without RTK) and indicated varying accuracy for road and non-road surfaces, with a RMSE of 4.4 cm on even road surfaces and 19.7 cm on other areas. Uneven, soft soil surfaces led to lower quality results. These differences could be attributed to shades of field grooves, as observed in a previous study (Giménez et al., 2009), and modifications in soft soil during manual total station measurements in the field. This modification can affect aerial surveys and lead to errors between aerial and terrestrial surveys. This main disadvantage of the direct method (Castillo et al., 2012) could not be avoided. For accurately recording erosion on bare soil, better results can be expected when erosion tracks occur on untilled and even soil surfaces.

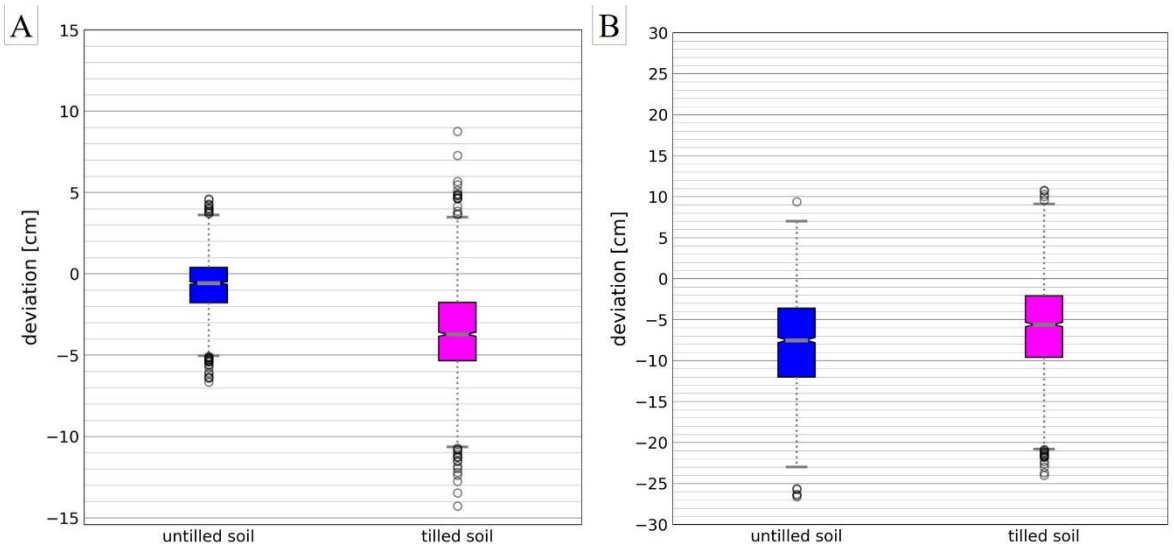

Figure 3-4: Calculated difference between terrestrial survey elevations and pursuant elevations from (A) UAV DEMs and (B) 1 m DEM provided by reg. authorities. There is a separate analysis for untilled (blue) and tilled (pink) soils. Negative values represent DEM elevations that are higher than terrestrial elevations.

Furthermore, comparisons of survey points with pursuant points from a 1 m grid DEM provided by regional authorities were conducted (Table 3-3, under the 'Accuracy DEM1, reg. authorities' row, and Figure 3-4B). The 1 m DEM is often the only data available as a basis for modeling. This DEM was situated predominantly higher than the terrestrial survey points. In total, the differences between terrestrial survey points and the 1 m DEM are higher than

the differences between terrestrial survey points and UAV DEM. One reason is the lower resolution of the 1 m DEM. This raster cannot display specific points or centimeter resolutions. Another important reason is the temporal gap between recording operations in 2016 for the 1 m DEM and March 2021 for Fields A–C. The tillage of arable land had less influence on accuracy differences from the 1 m DEM compared to the UAV DEM. Comparisons correspond better for tilled soil than untilled soil, but caps and fliers in the boxplots are similar (Figure 3-4B). Differences of up to 20 cm were observed, consistent with the accuracy statement of the regional authority (LVGL, 2019).

Accuracy of water surfaces and vegetation

During the aerial survey of the flood control reservoir, the river water was stagnant, dark, and turbid. Comparisons of aerial and terrestrial survey points revealed that the UAV surveys of turbid water only captured the water surface. Vegetation on banks and foreland could cause measurement errors because only the surface of the vegetation was recorded. Figure 3-5 shows two examples of cross sections in the flood control reservoir. The position of the cross sections is shown in Figure 3-2D. Both cross sections show terrestrial survey points (black) and the water level height (blue line) on the day of the investigation. Aerial surveys in 2D (purple, dashed line) and 3D mode (orange line) are shown as well. In the middle of the water surface, aerial survey elevations align with the water surface. However, at the edges of the water surface, aerial survey elevations are influenced by vegetation. In the transition zone between the water and the bank, grass that could not be mowed resulted in measurement inaccuracies. These inaccuracies, caused by vegetation and water, are consistent with the results of previous studies (Cook, 2017).

In the context of erosion measurement, water surfaces, resulting from a precipitation event, can lead to errors. Depending on the water depth in erosion tracks, the erosion depth can be underestimated, because water surfaces are recorded during the aerial survey. As this circumstance can be a disadvantage of the method, it is recommended to conduct an aerial survey for the erosion record one day after the event to avoid any water residues. According to DWA (2020), a maximum of 3 days should not be exceeded.

Accuracy 2D and 3D UAV mode

For flat and lightly vegetated surfaces, the measurements of flights in 2D and 3D modes aligned well (Figure 3-5). There were no significant differences in slope changes observed in either mode. However, dense vegetation in the water area resulted in different elevations in 2D and 3D mode measurements. In the 3D mode, measurements often displayed enveloping lines for the tallest vegetation, while the 2D mode showed fluctuations in vegetation heights. This discrepancy can be attributed to the number of images and different camera

angles in the 3D mode. Therefore, the 2D mode is only suitable for soil surfaces lacking vegetation. The comparability of results between 2D and 3D modes is an advantage, as aerial surveys in 2D mode are less time-consuming for recording and post-processing when using GCPs.

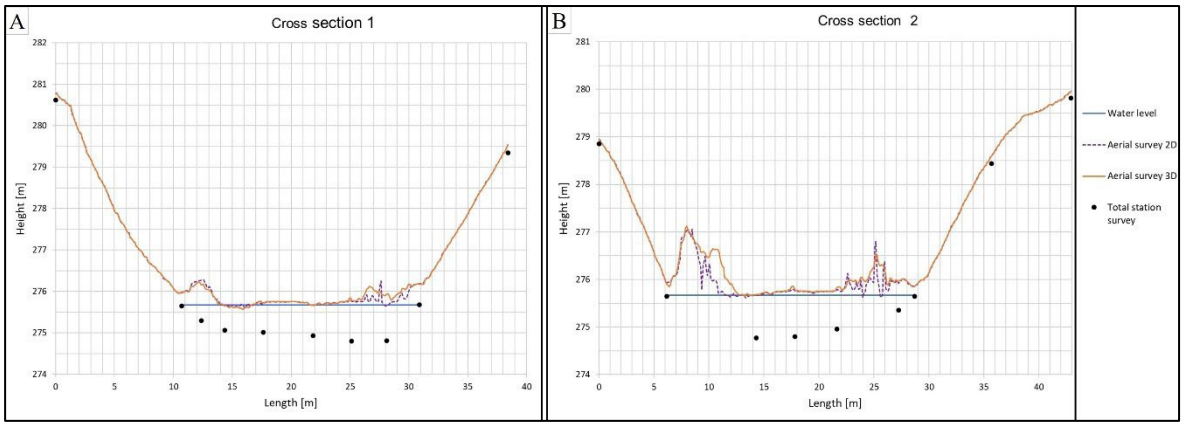

Figure 3-5: Comparison of measurements at cross sections in Field D. Measurements with the UAV in 2D mode are shown with a purple, dashed line, 3D mode with an orange line, and terrestrial survey points with black dots. Blue lines indicate the water level on the day of the surveys.

The investigations and analyses conducted showed that using the DJI P4 RTK represents a good option for investigating arable land with centimeter accuracy. However, potential errors arising from water and vegetation must be excluded. Erosion typically occurs on bare soils without any vegetation to protect them from rainfall. Therefore, the negative influence of vegetation on accuracy may often be neglected. For bare and untilled soils, as they may occur during heavy precipitation periods, the study reveals an average absolute deviation of 1.5 cm. For a 20 m long and 1 m wide gully, this equates to an erosion volume of ± 0.3 m³ of soil and a mass of 390 kg (assuming a density of 1,300 kg/m³).

3.3.2 Analysis of Linear Erosion Measurements

For the quality assessment of erosion tracks, erosion fields were surveyed using the UAV one or two days after the heavy precipitation event. The groove width and depth were measured in the generated UAV DEM and manually with a measuring stick. Figure 3-6 shows a comparison of groove width (A) and depth (B) measurements obtained from the UAV DEM and the measuring stick (manual). The groove width is often easily recognizable in orthoimages and aligns well with manual measurements. Deviations in Field 3 occur because groove boundaries were washed out at the foot of the slope and partly covered with sediment. Thus, clear boundaries are difficult to define on the orthoimage. The manual rill width measurements range from 17 to 350 cm. In total, the indirect measurements correspond well for the rill width, with an RMSE of 10.8 cm for rills that are up to 350 cm wide. Additional statistical values are available in Table 3-4. The manual rill depth measurements range from 4 to 20 cm. A comparison of depth measurements shows that the UAV DEM underestimates

groove depth with an RMSE of 2.13 cm for rills up to 20 cm (Table 3-4). However, Field 1 shows several measuring points that overestimated the groove depth. A possible reason for this discrepancy is the instability of the surface caused by furrows in the potato field. Measuring points on other fields also overestimated groove depth when the groove was washed out at the foot of the slope. In this case, the derivation depends on the individual. The narrower the groove, the greater the likelihood that the measuring points of the DEM would underestimate the groove depth. This could be caused by the shadowing of the groove (Giménez et al., 2009). Additionally, the reflection of gullies can be affected by their deep location and small terrain openness (Liu et al., 2016). Aerial surveys have produced lower depth values, leading to an underestimation of the total groove depth and erosion volume, ultimately resulting in a minimum volume.

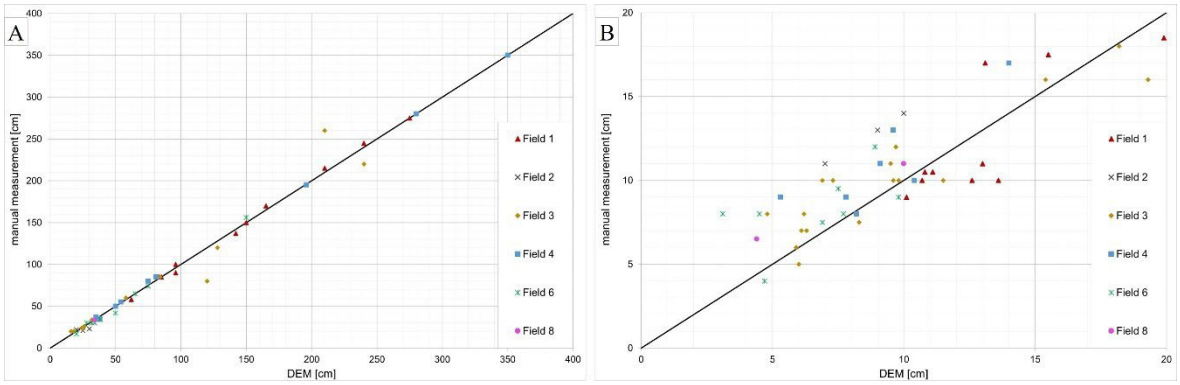

Figure 3-6: Comparison of DEM and manual measurements for (A) groove width and (B) groove depth.

Table 3-4: Statistics for the difference between UAV and manual measurements of groove width and depth. Min = Minimum, Max = Maximum, Mean = Mean value, MAE = Mean Absolute Error, RMSE = Root Mean Square Error (all values in meter).

	Min	Max	Mean	MAE	RMSE
Rill width	-0.50	0.40	0.0037	0.0521	0.1083
Rill depth	-0.0490	0.0360	-0.0074	0.0170	0.0213

3.4 Conclusions

In this study, accuracy investigations were conducted using the DJI Phantom 4 RTK UAV. The results showed centimeter accuracy of the UAV-generated DEM for even surfaces and less accurate measurements for tilled soils. As erosion often occurs due to poor vegetation on arable land, vegetation does not adversely affect aerial measurements. Thus, aerial surveys of erosion using a UAV and photogrammetry are a useful method. For erosion measurements, the lack of shadowing and even surfaces without harrowed and plowed soil are

advantageous. Comparisons of groove measurements showed that DEMs derived from recordings using a UAV reproduced groove width well. However, groove depth was underestimated compared to on-site direct measurements.

Collecting and recording natural erosion provides a foundation for the calibration of erosion models. With these models, appropriate simulations can be achieved to obtain information on areas at risk of erosion, which can be the basis for implementing countermeasures.

Data Availability Statement

Datasets (DEMs, orthoimages, and terrestrial surveys) generated during this study are provided in a data repository at the following DOI: doi.org/10.6084/m9.figshare.27325518.

Limitations

There are limitations in the application of UAVs for recording arable land that must be taken into account. UAV positions may have been adversely affected by wind gusts in some measurements. In addition, erosion often occurs during heavy precipitation. Recording erosion tracks is weather-dependent and can only be performed once the precipitation has stopped. It cannot be ruled out that changes in the fields were made between the erosion event and the measurements. The consideration of GCPs is very time-consuming (Liu et al., 2016); both for recording and marking the GCPs in the UAV photos. Linear erosion can be affected by shadowing (Giménez et al., 2009), deep location, and small terrain openness (Liu et al., 2016) (see Section 3.3.2). This study also demonstrated the impact of water and vegetation surfaces on aerial survey outcomes (see Section 3.3.1).

4 Analysis of Heavy Precipitation-Induced Rill Erosion

Erosion is an ongoing environmental problem that leads to soil loss and damages ecosystems downstream of agriculture. Increasingly frequent heavy precipitation causes single erosion events with potentially high erosion rates owing to gully erosion. In this study, analyses of croplands affected by heavy precipitation and linear erosion indicate that erosion occurs only on sparsely vegetated fields with land cover ≤ 25 % and that slope gradient and length are significant factors for the occurrence of linear erosion tracks. Existing erosion models are not calibrated to the conditions of heavy precipitation and linear erosion, namely high precipitation intensities and long and steep croplands. In the following study, natural linear erosion was analyzed using an unmanned aerial vehicle and erosion volumes were determined for 32 rills and gullies of different sizes. Comparisons with the RUSLE2 and EROSION-3D model values showed an underestimation of linear erosion in both models. Therefore, calibration data for erosion models used for heavy precipitation conditions must be adapted. The data obtained in this study meet the required criteria.

Rebecca Hinsberger

Environmental Earth Sciences, 2024, 83:354
DOI: 10.1007/s12665-024-11671-6

4.1 Introduction

Terrestrial ecosystems and especially soils are the fundamental basis for life on earth and are a resource for high-priority protection. However, the continuous increase in the world population has led to the intensified use of soil for arable land and, consequently, competition for use between food, fodder, and energy production or nature preservation. The process that damages soil is erosion. The Intergovernmental Panel on Climate Change (IPCC) Special Report (2021) indicated that erosion is a significant factor in land degradation and desertification. In this study, water-induced soil erosion in conjunction with heavy precipitation was investigated.

Previously, erosion models were developed to forecast soil losses. Existing soil erosion models can be divided into empirical, conceptual, and process-oriented or physically based models, developed for different central issues, depending on the nature and characteristics of the model and the intended application (Andualem et al., 2023). Models such as the well-known Universal Soil Loss Equation (USLE) (Wischmeyer and Smith, 1978) are useful for simulating long-term erosion, whereas the Water Erosion Prediction Project (WEPP) (Laflen et al., 1991) and the European Soil Erosion Model (EUROSEM) (Morgan et al., 1998a) are suitable for single events. Simple empirical models, such as the USLE, have a small number of input parameters that are relatively easy to obtain. This contrasts with models such as EUROSEM, which are based on a large amount of input information. However, data acquisition is difficult. Detailed lists of existing erosion models for different aims have been provided in review articles (e.g., Andualem et al., 2023; Borelli et al., 2021; Michael, 2000).

Thus far, many of the existing erosion models have been based on experimental studies to calculate the erosion quantity. Two main types of erosion can be distinguished: sheet and linear erosion. Sheet erosion occurs over the entire surface of arable land, where the soil is evenly eroded as thin sheets. Linear erosion is characterized by linear shapes, such as grooves (rills) or deeper and wider gullies. These shapes are formed by the friction of water in the resulting flow paths. To detect sheet erosion, time series were observed by Cândido et al. (2020) and Pineux et al. (2017), whereas Eltner et al. (2014) and Kou et al. (2020) recorded multi-temporal soil surface changes. Linear erosion can be identified visually (as opposed to sheet erosion) and has been investigated using different indirect methods, such as specifically designed kites (Giménez et al., 2009), fixed-wing aircraft (D'Oleire-Oltmanns et al., 2012; Peter et al., 2014), and quadrocopters (Di Stefano et al., 2019c). Some studies have conducted laboratory erosion experiments at the plot scale (Aksoy et al., 2013; Di Stefano et al., 2017; Tackmann, 2010), whereas others have conducted field investigations (Bruno et al., 2008; Carollo et al., 2015; Wirtz et al., 2010, 2012). Furthermore, studies have investigated the erosion caused by natural rainfall (Bruno et al., 2008; Carollo et al., 2015),

rainfall simulators (Aksoy et al., 2013; Polyakov et al., 2018; Römkens et al., 2001; Zhang et al., 2021), and overland flow (Di Stefano et al., 2017). In addition to the mere recording of erosion, post-processing the detection of erosion shapes and assessing erosion volumes are important steps in producing useful data for erosion model calibration and validation. In terms of detecting the spatial extent of erosion rills, Malinowski et al. (2022) developed an automatic recognition and mapping of erosion rills at the field scale. In terms of volumetric assessments, previous studies have dealt with the reconstruction of the original surface (pre-erosion). D'Oleire-Oltmanns et al. (2012) and Peter et al. (2014) derived a 3D polygon from rill edges, whereas Báčová et al. (2018) presented an algorithm and Python implementation for automatic volume calculations in a geo-information system (GIS). In recent decades, several studies have focused on the continuous development and forecasting of erosion (Boardman and Favis-Mortlock, 1998; Borselli et al., 2021; Bryan, 1990; Morgan and Nearing, 2011).

However, a large portion of the total eroded material is affected by a few heavy precipitation events (Parkin et al., 2008), causing damage also downstream the eroded field. These extreme events are expected to increase in frequency and intensity owing to climate change (IPCC, 2021). Heavy precipitation often leads to linear erosion, such as rills and gullies. Several studies have investigated the quantity and spread of erosion and sedimentation in test plots using rainfall simulators (Aksoy et al., 2013; Polyakov et al., 2018; Römkens et al., 2001; Zhang et al., 2021). However, laboratory and in-situ test plots are often limited in size. Linear erosion requires space to develop from precipitation-induced overland flow. The decision for model usability is based on the data used for calibrating the erosion quantity (Malinowski et al., 2022; Pineux et al., 2017). Data for the USLE model contains test plots in various sizes, slopes and cropping which are compared with the unit plot that is 22.1 m in length, 1.87 m in width, and has a 9 % gradient (Carollo et al., 2024; Schwertmann et al., 1987; Wischmeyer and Smith, 1978). In the EROSION-3D (E3D) model, the test plots were 0.64 × 0.24 m for experiments to derive the erosion quantity (Schmidt, 1984; Schmidt, 1988) and 22 m long and 2 m or 4 m wide (USLE unit plots) for experiments to derive erosion resistance and correction factors (Michael et al., 1996, Michael, 2000). Besides including linear erosion conditions, the precipitation and discharge that leads to specific erosion forms are important factors. In existing calibration data, precipitation intensity often does not correspond to heavy precipitation events [intensity ≥15 mm/h (DWA, n.d.)] or are sometimes neglected in erosion meta data. Investigations of the USLE, for example, include various events in different years (Schwertmann et al., 1987; Wischmeyer and Smith, 1978), whereas E3D uses erosion quantities based on laboratory experiments with rainfall simulators with intensities up to 54 mm/h (Michael, 2000; Schmidt, 1988).

This study focused on linear erosion based on single heavy precipitation events at the hillslope scale. For croplands affected by heavy precipitation, framework conditions were analyzed to determine the significant factors for the occurrence of linear erosion. When linear erosion occurred, the surface structures were collected at the hillslope scale using an unmanned aerial vehicle (UAV) and manual field measurements, and the erosion volumes of the rills were quantified. The erosion quantities of these natural events were determined and compared with results obtained using existing erosion models. As the data requirement for the USLE family models is affordable and the models are one of the most commonly used erosion models (Borelli et al., 2021), the RUSLE2 model that is applicable for single days was used for comparison. In addition, E3D was selected for comparison because of the possibility of simulating single precipitation events and erosion quantity data based on heavy precipitation intensity.

4.2 Materials and Methods

Measurements of eroded croplands are important for addressing the overarching objective of using erosion quantities from natural events for model calibration. To achieve this objective, several steps are necessary: a) localization of erosion due to local heavy precipitation events, b) on-site recording of erosion, c) photogrammetric analysis of erosion to generate a digital elevation model (DEM) of arable land, and d) analysis of the DEM as a basis for quantifying erosion and delineating the spatial distribution of erosion tracks. For three years, heavy precipitation events that occurred in Saarland, Germany (federal state with 2,500 km²) and neighboring states, were investigated with respect to the occurrence and extent of erosion.

4.2.1 Localization of Erosion

The measurement of erosion due to natural precipitation (compared with rainfall simulators) requires the localization of heavy precipitation events. The German Meteorological Service (Deutscher Wetterdienst, DWD) defines precipitation as having at least 15 mm/h intensity as heavy precipitation. A challenge in this localization is the local limitation and occurrence of extreme events. One method of delimiting potential areas is to use radar data. The RY RADOLAN data from the DWD show precipitation intensities and have a temporal resolution of 5 minutes and a spatial resolution of 1 km² (DWD, 2004, 2017). These data are provided online shortly after their occurrence. To display precipitation intensities, the Flood Early Warning System (FEWS) software (Deltares, Delft, The Netherlands) (Deltares, n.d.) was used in this study. The areas affected by heavy precipitation were categorized based on land usage. A pre-selection of areas that are agriculturally used and affected by heavy precipitation has thus already been made. All these arable land areas were inspected on-site

for erosion one to two days after the event. The croplands were identified and visually inspected for signs of erosion (gullies, rills, sedimentation tracks). A total of 456 croplands affected by heavy precipitation were examined for erosion. For these fields, framework conditions (erosion type, land cover, amount of precipitation, slope length and gradient) were collected on-site and/or by analyzed geodata.

4.2.2 Linear Erosion Measurements

When linear erosion occurred, the cropland areas were recorded using a UAV. The approach of using UAVs for erosion recording was suggested by the German Association for Water, Wastewater, and Waste (DWA) (DWA, 2020) and has been performed in previous studies (see Introduction). In this study, croplands with linear erosion were investigated using the DJI Phantom 4 RTK (real-time kinematic) (P4RTK) UAV. Preliminary tests were conducted using the UAV to investigate accuracy. Comparisons of P4RTK with manual measurements using a measuring stick at linear erosion tracks show good correspondence for the rill width, with an Root Mean Square Error (RMSE) of 10.7 cm for rills that were up to 350 cm wide. For the rill depth, the erosion tracks in the UAV measurements were underestimated. Here, the RMSE was 2.11 cm for rills up to 20 cm. For the following study, errors in this range of values must be considered.

Aerial surveys were conducted one or two days after heavy precipitation events at the hillslope scale. Photographs taken by the UAV were aligned, and a dense point cloud was built before generating a DEM (hereinafter referred to as rill DEM) and an orthoimage with the structure from motion technique using the Agisoft Metashape Professional software (Agisoft LLC, St. Petersburg, Russia) (Agisoft LLC, n.d.). All UAV- and event-related information is listed in Table 4-1.

Table 4-1: Information on investigated areas and flight metrics for Fields 1–11.

Field	UAV mode	DEM extent [ha]	Flight date	Flight height [m]	Number of pictures	Overlapping [%] Horizontal/ Vertical	Speed [m/s]	Obtained resolution [cm/px]	Precipitation intensity [mm/h]	Geographical position (Lon/Lat)
1	2D	8.29	21 May, 2022	40	497	70/ 80	3.1	2.7	51.81	7.287492 / 49.235052
2	2D	8.24	23 June, 2021	50	230	70/ 80	3.9	3.2	19.1	7.251585 / 49.201051
3	2D	9.94	20 May, 2022	40	552	70/ 80	3.1	2.0	14.42 + 19.43	7.196362 / 49.517098
4	2D	7.37	20 May, 2022	40	312	70/ 80	3.1	3.0	11.60 + 19.37	6.976104 / 49.443117
5	2D	7.37	20 May, 2022	40	312	70/ 80	3.1	3.0	11.60 + 19.37	6.976587 / 49.442301
6	2D	2.58	21 May, 2022	40	120	70/ 80	3.1	2.0	53.05	7.342572 / 49.270588
7	2D	13.75	21 May, 2022	40	557	70/ 80	3.1	3.5	66.92	7.339650 / 49.267832
8	2D	37.30	05 June, 2021	70	449	70/ 80	4.5	4.1	46.19	6.757593 / 49.527604
9	2D	37.30	05 June, 2021	70	449	70/ 80	4.5	4.1	46.19	6.758614 / 49.525492
10	2D	14.07	23 May, 2023	50	614	70/ 80	3.9	2.8	28.59	6.846149 / 49.553545
11	2D	32.91	18 May, 2023	50	1,014	70/ 80	3.9	4.9	23.82	6.981664 / 49.390056

In addition, two undisturbed soil samples were taken in from each field at the day of the aerial survey using predefined cylinders. These soil samples were examined in laboratory tests in accordance with DIN 18125–2 (2020) to determine the bulk density of the croplands. Besides, a few months after the event, 5 disturbed soil samples per field were taken from the upper soil layer (0–20 cm). These samples were analyzed regarding particle size distribution using sieve and sedimentation analyses (DIN EN ISO 17892-4:2017-04). The soil types were derived from these results.

4.2.3 Analysis of Erosion Quantity

By recording the surface of fields affected by erosion, high-quality data were available for reporting the conditions after the erosion event. However, heavy precipitation occurs in limited areas and has short forecasting times. Consequently, prior measurements of the erosion areas and data on the situation before an erosion event are usually not available due to the research approach. A pre-erosion dataset similar to the original surface must be available to calculate the groove width, depth, and erosion quantity. One possible dataset is a DEM with a spatial resolution of 1 × 1 m, which is available from regional authorities. However, the accuracy of ±20 cm, stated by the regional authority (LVGL, 2019), is higher than most of the recorded rill depths, and the resolution of 1 m is much higher than most of the recorded rill widths. Another possibility is to create a pre-erosion dataset from the recorded high-resolution rill DEM data. In this study, a pre-erosion dataset was created using the volumetric loss measurement technique, which is a modified approach proposed by Peter et al. (2014). Erosion tracks were identified using the following steps. The rill DEM was converted to a mesh, which was modified with the Surface-water Modeling System (SMS) (Aquaveo LLC, Provo, UT, United States) (Aquaveo, n.d.). In this mesh, all points in the erosion area were deleted to generate a surface unaffected by erosion. The orthoimage and superelevation of the mesh helped identify the affected and unaffected field parts. Thereafter, the gap in the mesh was retriangulated with the SMS workflow “mesh node triangulation.” In this workflow, triangular elements were generated between the boundary nodes (Aquaveo, n.d.). Subsequently, the mesh was converted into a raster. The final product was a DEM with smoothed erosion areas, called a pre-erosion DEM. Figure 4-1a shows an example of a rill area in Field 6. Figure 4-1b and Figure 4-1c show one rill in the rill DEM and smoothed pre-erosion DEM, respectively. The differences between the rill and pre-erosion DEM were determined using a raster calculator (DEMs of difference). This process provided the groove depth at each grid point. Positive and negative values distinguished between erosion and sedimentation. The product of the erosion depth and raster resolution was the erosion volume.

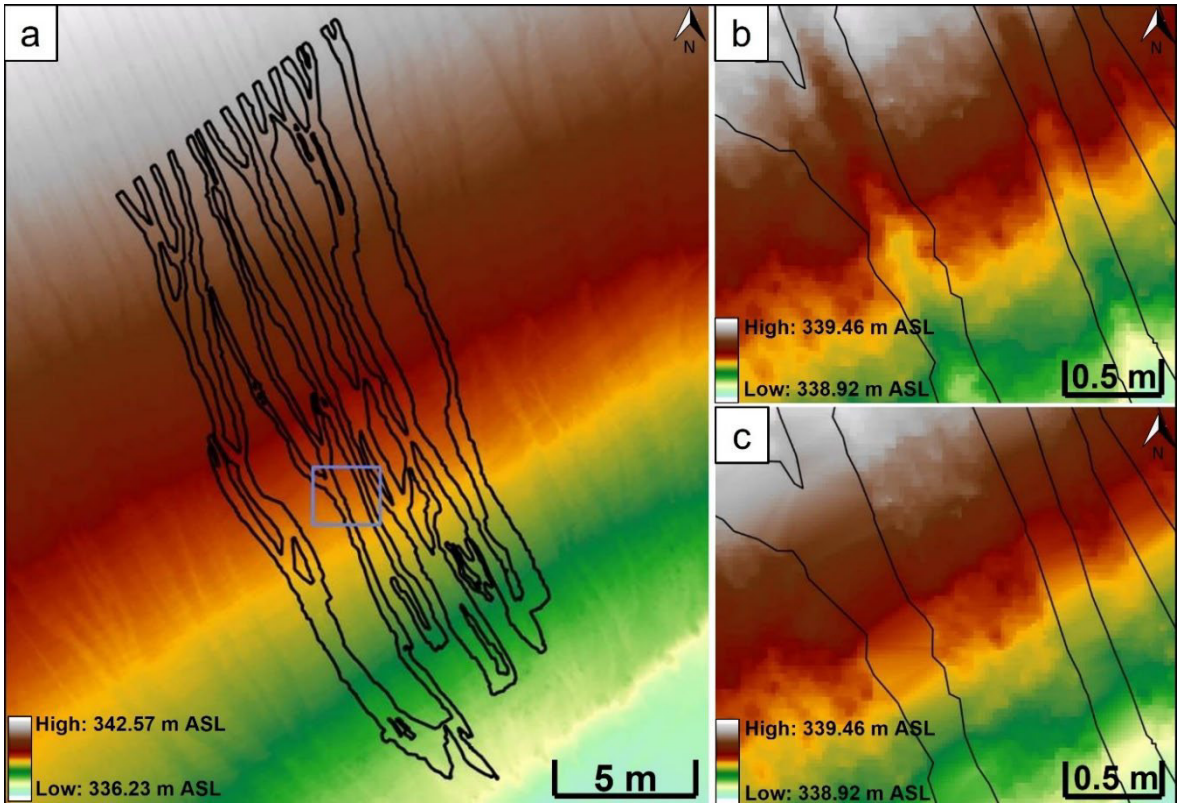

Figure 4-1: Example of the triangulation method used to create the pre-erosion surface. (a) Perimeter of Field 6, erosion area 2; details of (b) erosion area in the recorded rill DEM, and (c) pre-erosion surface with closed erosion area, obtained using the mesh node triangulation method.

A limitation of this approach is the assumption that the recorded heavy precipitation event is the only event that led to erosion between sowing and the UAV survey.

4.2.4 Erosion Models

For the comparison of the calculated natural erosion data of this study with existing models, the detachment share of the empirical model RUSLE2 was used as well as the more physically based model E3D (GeoGnostics, Berlin, Germany) (GeoGnostics, n.d., b).

The RUSLE2 calculates the rill and interrill (sheet) erosion based on five basic factors of the USLE that are assumed for the day of the event: rainfall erosivity factor R, soil erodibility factor K, topographic factors (slope gradient S and length L), crop cover and management factor C, and protection factor P (Wischmeyer and Smith, 1978). In this study, rainfall erosivity factor R was derived from YW-RADKLIM radar data provided by the German Meteorological Service (DWD) for a specific event (Winterrath et al., 2018). These data have spatial and temporal resolutions of 1 × 1 km² and 5 min, respectively and show quasi gauge-adjusted five-minute precipitation rates in Germany. For the calculation of the RUSLE2, the R factor was calculated using the EI30 index, the product of the kinetic energy, E, and the maximum precipitation intensity over 30 minutes, I30 (DIN 19708 2017). Here, E is the sum of all periods with a constant intensity. The soil erodibility (K factor) was derived from the

soil type. The soil types of the soil samples taken in this study, were compared with the soil types of a soil map [scale: 1:5,000 (LVGL n.d.)]. The derived K factors were the same for 50 % of the samples and differed by 0.05 for the other half of the soil samples. As soil analyses were not carried out for all fields, the soil type from the map was used to derive the K factor for reasons of comparability. Both the R and K factors are calculated according to the equations of DIN 19708 (2017), as these are suitable for German conditions. The L and S factor were calculated according to the User's Reference Guide of the RUSLE2 (USDA 2008). Here, the ratio of rill and interrill erosion β was considered by using the slope and land cover that were determined and analyzed in Section 4.2.1. The ration of rill and interrill erodibility K_r/K_i and the rill to interrill ratio for prior land use c_{pr}/c_{pi} were derived from the Science documentation of the RUSLE2 (USDA, 2013). As not all information were available for the latter parameters, worst case parameters were used. As the fields show, in general, a uniform topography, a differentiated analysis of hillslope segments was not carried out. The C factor is considered as 1-covering factor and the P factor was neglected.

For the comparison with the natural erosion data of this study, only the rill share of the RUSLE2 was considered. The amount of RUSLE 2 rill erosion is calculated as difference between the results of RUSLE2 equation for rill and interrill erosion (described above) and the corresponding interrill erosion only. The interrill erosion is calculated according to the science documentation of the RUSLE2 (USDA, 2013, equ. 2.11).

For the simulation using E3D, the precipitation load was taken into account by the time series of the precipitation intensity based on the YW data of the DWD. The soil characteristics were derived from the soil type using the guideline by Michael et al. (1996). In the model, various parameter, such as the critical momentum flux, are derived from the soil input information. The topography was considered by the DEM. As the minimum resolution for the input data was 1 × 1 m, the DEM available from the regional authorities was used.

4.3 Results and Discussion

All croplands investigated in this study were analyzed to determine the factors that are most important for the occurrence of linear erosion tracks due to heavy precipitation. For fields where linear erosion was detected, the erosion volume was quantified and then compared with the results of the RUSLE2 and E3D model applications. For fields where no linear erosion or sedimentation tracks could be detected, the amount of erosion was considered irrelevant.

4.3.1 Influencing Factors of Erosion

In this study, 456 croplands were investigated after different heavy precipitation events. All fields vary in their locations and, consequently, in their framework conditions (e.g., slope

length, gradient, or land cover). Among these fields, 141 were not covered or were covered very little, and 315 were fully covered with different agricultural crops, for example, different types of grain or grassland. Of these 141 bare-soil fields, visible linear and/or sheet erosion occurred in 20 (see Section 4.2.1). As a result, erosion occurred only in vegetation-free, sparsely covered fields. In one vegetation-covered field, only small erosion tracks from previous events (overgrown rills) were detected.

For all fields, framework conditions such as slope length, gradient, land cover, and precipitation were analyzed. However, not all data were available for one event. Therefore, 30 fields were excluded and 426 fields were used for subsequent analyses. All fields were classified according to the erosion type to determine which factors were relevant and when erosion started. The fields were divided into “linear erosion with partly occurring sheet erosion” (n =15), “exclusively sheet erosion” (n =5), and “no erosion” (n =406). Figure 4-2 shows four box plots, including the influence of different factors on erosion types.

A comparison of the erosion types with respect to land cover (Figure 4-2a) showed that linear and/or sheet erosion occurred only in sparsely covered fields. No erosion could be detected on fields with a cover ≥25 %. This threshold corresponds to values reported by Armand et al. (2009). They stated that land cover >30 % reduces soil crusting and, consequently, overland flow as well as erosion. For the 406 fields that were assigned to the “no erosion” group, 75 % showed a land cover of 100 % and 25 % did not show full cover. For these 25 %, other impact factors were the decisive as to why no erosion had taken place. The analysis of the LS factor (Figure 4-2b) indicated small differences for all erosion types. The interquartile range was lower for the “no erosion” type than the range for linear and sheet erosion. However, the overall span and number of outliers were higher for fields with no erosion. This result indicates an even distribution of the LS factor for all 426 investigated fields. By aggregating LS and land cover, land cover was transferred to the C factor by considering the share of uncovered soil (1−land cover). As the land cover for “no erosion” fields tended to 100 %, the LSC factor for this group was very low (Figure 4-2c). Considering the precipitation with the R factor, the linear and sheet erosion fields showed a high value range (Figure 4-2d). For “no erosion” type fields, there was still a high number of outliers with values as high as those of the linear and sheet erosion fields. However, values that seemed very high for the “no erosion” category can be explained by one dominant factor, e.g., very high precipitation intensity or a very high slope gradient. All the factors influenced the different erosion categories. Land cover, in particular, exerted a strong influence on the “no erosion” fields. No difference was apparent between linear and sheet erosion.

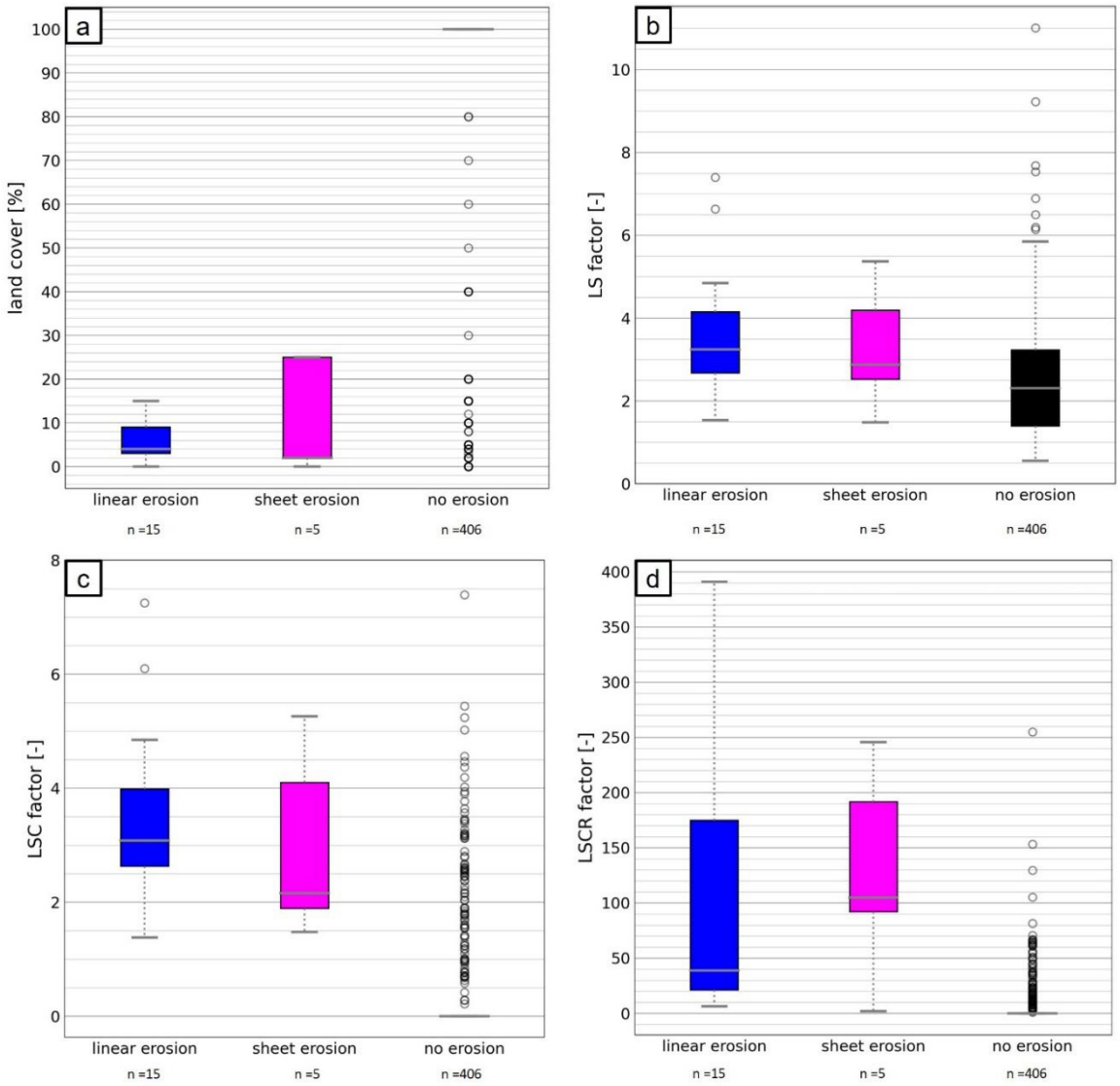

Figure 4-2: Comparison of (a) share of land cover, (b) LS factor, (c) LSC factor, and (d) LSCR factor influencing linear erosion, sheet erosion, and no erosion fields. The boxplots display the interquartile range (boxes), the median (horizontal gray lines), the 25th and 75th percentiles (horizontal gray lines), and outliers (circles).

4.3.2 Analysis of Erosion Quantity

Of the 426 investigated croplands, 15 fields exhibited linear erosion tracks with different rill and gully types. Some fields showed many small rills (a few centimeters wide and deep), whereas others showed only one gully in the thalweg (several decimeters wide and deep). The retriangulation method presented in the Materials and Methods section was used to create the pre-eroded surface. Because the method retriangulates the unaffected surface areas, it is only suitable for surfaces with low microrelief. Thus, aerial surveys and analyses of erosion quantity were conducted for 7 cornfields, where 33 rills were analyzed. The spread of the rills ranged from 10 m² to 580 m².

With the retriangulation method, a pre-erosion surface was created, and with the DEMs of difference method, the erosion depth was calculated at each grid point. As the differences in the DEMs are only located at the rill, all grid points should show negative values, which indicate erosion. Positive values indicate errors. For 97 % of the investigated rills, the error was less than 4 %, resulting in a standard deviation of 1.13 %. One rill showed an error of approximately 30 %. This rill was wide and shallow and contained vehicle lanes. Therefore, this rill was excluded from further analysis. Overall, no dependence of the error on the rill width, erosive slope length, or gradient was identified. Gully depth and bulk density were used to calculate the erosion volume of each rill. Information regarding the rills and catchment areas is presented in Table 4-2.

For each of the 32 analyzed rills, the mean rill width, LS factor for the rill catchment area, and precipitation volume for the rill catchment area were calculated. Comparisons of these factors with erosion quantity always showed an increase in each factor with an increase in erosion quantity.

The preliminary accuracy tests in this study (see Materials and Methods section) showed that the erosion rill depth resulting from UAV recordings underestimates the existing rill depth. Thus, the erosion rates listed in Table 4-2 indicate the minimum of the expected erosion, which may be up to 20 % higher.

Forecasting erosion using erosion models can be effective for developing measures to protect human lives, infrastructure, and valuable soils. In the following sections, two erosion models are used to calculate the erosion quantities of events recorded in this study: the well-known RUSLE2 as an empirical but easy-to-use model and E3D as a physically based erosion model that includes simplified flow accumulation processes.

Table 4-2: Results of erosion analyses.

Reference Field no.	Area no.	Max. erosion depth [m]	Erosion area [m²]	Bulk density [kg/m³]	Erosion volume [m³]	Error [%]	Rill catch-ment area [ha]	Average slope (rill catch-ment area) [%]	Average length (rill catch-ment area) [m]	Erosion rate [t/ha]
3	1	0.181	578.99	1,190	23.970	1.18	0.601	10.95	185	47.461
	2	0.148	184.18	1,190	5.174	1.99	0.341	10.97	160	18.056
	3	0.136	128.91	1,190	3.236	1.42	0.138	10.66	151	27.905
	4	0.097	24.45	1,190	0.519	0.96	0.071	9.22	66	8.699
	5	0.189	20.39	1,190	0.699	0.72	0.043	13.11	46	19.344
	6	0.152	23.04	1,190	0.791	0.76	0.093	10.95	121	10.121
	7	0.195	16.39	1,190	0.673	0.30	0.041	11.78	112	19.533
4	1	0.410	236.90	1,120	10.680	0.78	0.111	16.51	93	107.762
	2	0.185	239.87	1,120	7.302	1.68	0.126	16.13	100	64.907
	3	0.115	61.77	1,120	1.318	2.43	0.065	16.62	79	22.710
	4	0.129	63.60	1,120	1.289	1.86	0.088	16.20	90	16.405
	5	0.127	167.04	1,120	4.026	1.19	0.180	16.07	88	25.051
5	1	0.145	48.26	1,120	0.987	2.23	0.051	9.68	73	21.675
	2	0.810	9.39	1,120	0.141	3.55	0.147	11.64	73	1.074
6	1	0.130	96.01	1,200	2.563	2.30	0.218	10.91	118	14.108
	2	0.120	85.57	1,200	2.070	2.32	0.076	14.43	118	32.684
	3	0.124	113.2	1,200	2.675	3.55	0.165	12.68	135	19.455
	4	0.157	61.72	1,200	1.384	2.82	0.102	12.03	130	16.282
	5	0.118	35.32	1,200	0.938	1.60	0.051	14.84	73	22.071
	6	0.137	92.51	1,200	2.776	1.01	0.142	12.34	115	23.459
	7	0.124	17.96	1,200	0.509	0.79	0.056	13.84	94	10.907
7	1	0.089	32.75	1,420	0.416	3.61	0.028	14.28	31	21.097
	2	0.105	148.31	1,420	1.826	1.75	0.183	14.72	44	14.169
	3	0.156	80.94	1,420	1.552	0.64	0.050	13.60	59	44.077
	4	0.096	50.80	1,420	1.366	0.88	0.047	14.18	73	41.271
	5	0.109	79.97	1,420	2.214	1.04	0.061	12.55	108	51.539
	6	0.383	448.49	1,420	12.418	2.65	0.095	11.21	193	185.616
	7	0.175	267.89	1,420	10.481	1.10	0.411	11.47	245	36.212
	8	0.262	352.72	1,420	9.487	1.45	0.205	11.60	222	65.715
	9	0.116	99.93	1,420	2.503	1.12	0.241	11.84	235	14.748
	10	0.456	148.31	1,420	4.078	1.64	0.167	11.98	218	34.675
8	1	0.294	230.84	1,310	12.143	1.25	0.818	8.87	175	19.447

4.3.3 Comparison using Existing Erosion Models

Recent review articles (Andualem et al., 2023; Borelli et al., 2021) have shown that many erosion and sedimentation models are available worldwide. According to Batista et al. (2019), such models are not scarce. However, the knowledge and testing of transferability in different application cases and areas still require further research. For comparison with data from this study (Section 4.3.2), the RUSLE2 and E3D models were applied to selected fields.

4.3.3.1 RUSLE2 model at the rill catchment area scale

To compare the RUSLE2 with the rill erosion data of this study, the RUSLE2 was applied to all rill catchment areas. For this analysis, the RUSLE2 was applied to a single event (R factor) for comparability reasons. The erosion quantity in this study represents only linear erosion and neglects sheet erosion owing to the quantification method (Section 4.2.3). Therefore, the RUSLE2 model was applied to calculate sheet and rill erosion (standard) and only to sheet erosion (interrill area). The difference between both values leads to the rill erosion share of the RUSLE2 that was compared to the linear erosion of this study. The share of interrill and rill erosion is 15 to 42 % and 58 to 85 % respectively. In most cases, the share of rill erosion is around 80 %.

The comparison of RUSLE2 rill erosion and the natural rill erosion is shown in Figure 4-3a. Each symbol type represents one field and each data point one rill. It appears that the quality of RUSLE2 model values depends on the field. The erosion rate of the natural events was higher than the calculated rate using RUSLE2 for most rills. The percentage difference ranged from -75 % to +934 % and the root mean square error (RMSE) is 38.26. An analysis of the rill characteristics shows that the rill expansion is decisive for the differences. The larger and more pronounced the rill, the higher the deviation compared to the RUSLE2. The higher the number and the smaller the rills, the lower the deviation. Hence, strong erosion leads to a higher error of RUSLE2, because larger rill systems are formed. For small rills, a correlation between the measured erosion and the erosion calculated using the RUSLE2 was apparent (Figure 4-3a, Field 5) or RUSLE2 slightly overestimated the rill erosion (Figure 4-3a, Field 6). This may have been because many small rills showed a similar amount of erosion or the erosion type recorded by the calibration data of the RUSLE2. In particular, the analysis showed that the recorded erosion that best matched the RUSLE2 erosion had a small LS factor compared to other data points. Therefore, LS is a significant factor in linear erosion. Erosion rates obtained using the RUSLE2 strongly underestimated the linear erosion quantities because linear erosion was not considered. This can be largely attributed to the test plots, where linear erosion tracks could not develop out of the surface flow. By considering the LS factor in the RUSLE2 to be a power, the erosion of the natural event

approximated the RUSLE2 values better (Figure 4-3b). With this modification, the percentage difference improves to a range from -75 % to +345 %. Here, a RMSE of 33.78 can be reached. Calculating the RUSLE2 with factor $(LS)^x$ does not represent an equation for linear erosion quantities. Rather, this demonstrates the strong influence of LS. However, the accuracy of this approach is limited as the USLE family models are not suitable for large rill and gully erosion.

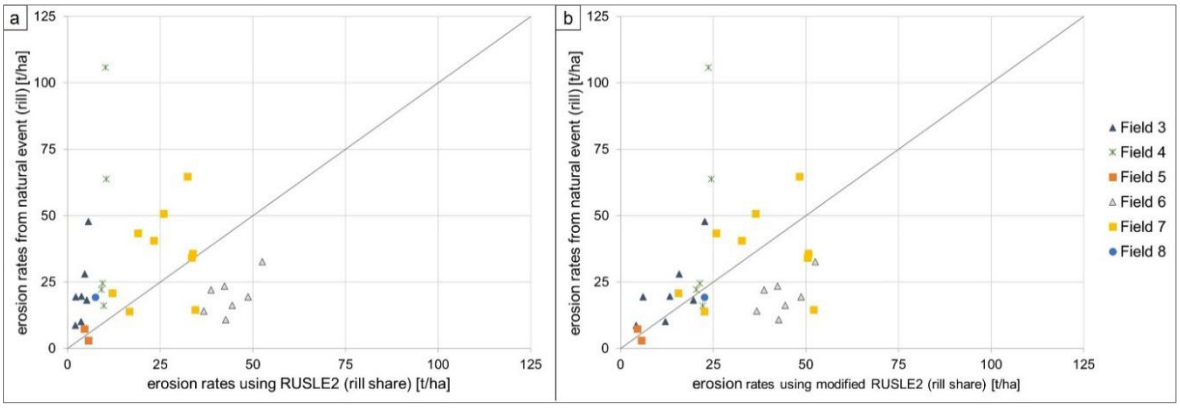

Figure 4-3: Comparison of erosion rates from RUSLE2 rill erosion and erosion rates of linear erosion from the natural event (a), and the same graph with considered $(LS)^x$ in RUSLE2 equation for rill and interrill erosion (b). Here, x is 2 for Field 3, 1.5 for Field 4, 1 for Field 5, 1 for Field 6, 1.25 for Field 7, and 2 for Field 8. Each data point represents one rill. Different colors and forms of the points represent different fields. The graphs shown are limited to 125 t/ha, although one data point has a higher value in each graph. The gray line indicates the 1:1 line.

In contrast, the K factor has a low influence on the amount of erosion calculated using the RUSLE2. For the rill catchment areas, the K factor ranged from 0.25 to 0.35. One outlier shows a value of 0.15. The minor influence of the factor becomes clear when K factors of 0.25 to 0.35 are replaced by a constant of 0.3. This modification alters the soil erosion using RUSLE2 by -17 % to +17 %.

The quantity of erosion depends on many different factors such as the volume and intensity of precipitation, slope length and gradient, soil, and vegetation cover. The combination of these factors depends on the site, crop and management choices of farmers, and natural events. Furthermore, the discharge of a flash flood, which accumulates at different velocities along the flow path, is significant for the dynamic forces on the soil and depends on specific surfaces. These surface conditions, including the gradient, often vary within the field, resulting in inaccurate considerations with empirical factors. Considering the flow accumulation and total flow, depending on the surface model, these restrictions are reduced. This approach was used in the erosion simulations using E3D software.

4.3.3.2 RUSLE2 and E3D at the rill catchment area scale

For this analysis, erosion quantities for single rills calculated using RUSLE2, E3D and results of this study were compared. The E3D and RUSLE2 models were applied to natural heavy precipitation events on three hillslopes recorded in this study. For E3D, the erosion quantity of the whole field, shown in Figure 4-4 was calculated. For RUSLE2, the calculation for the rill catchment area remains unchanged compared to Section 4.3.3.1. All erosion fields showed different rill types: Field 4: two large rills; Field 7: a large field with many small and shallow rills and a single large rill (without thalweg); Field 8: one rill in the thalweg.

The simulation results for the three fields using E3D are shown in Figure 4-4. The sediment budget showed pink erosion and green sedimentation. Sheet erosion was clearly visible in all fields. In addition, more or less pronounced linear erosion tracks were observed. In particular, in Field 8, as shown in Figure 4-4c, one rill in the thalweg of the field is visible. The position of the rill matched that of the natural event. Fields 4 and 7 show only small rills. In addition, these rills match the rills of recorded events. However, specifically in Field 7, many rills were not considered in the modeling results. For all visible rills, the erosion quantity of E3D was analyzed, and the RUSLE2 was applied to these rill catchments. The spatial distribution of the rills cannot be determined using the manual calculations of the RUSLE2. For the RUSLE 2, the values in Table 4-3 are in accordance with the values shown in Figure 4-3a (change of the unit). The resulting erosion quantities are presented in Table 4-3.

Figure 4-4: Simulation results of sediment budget obtained using E3D for Field 4 (a), Field 7 (b), and Field 8 (c).

The calculated erosion quantities of the natural events were always higher than those calculated using E3D or RUSLE2. Notably, the E3D reflects only a fraction of the recorded natural erosion, whereas the RUSLE2 simulates a higher share. However, it must be considered that E3D outputs the net erosion, while RUSLE2 outputs the gross erosion (without considering sedimentation). As the recording of the natural events in this study occurred after the event, the recorded natural erosion was also net erosion. Furthermore, Schmidt (1996) and von Werner (1995) claim that the E3D model calculates the detachment of linear erosion but no spatial or temporal initiation of rill erosion is available in the model. Thus, the application is limited to sheet erosion.

Table 4-3: Linear erosion of rills in E3D and RUSLE2 models compared to calculated rill masses of this study.

Field no.	Area no.	Rill type	Measure-ment natural event [t]	E3D [t]	Share of E3D in natural erosion [%]	RUSLE2 rill share [t]	Share of RUSLE2 (rill) in natural erosion [%]
4	1	One big rill (slight thalweg in DEM)	**11.962**	0.022	0.18	1.14	9.53
7	6	One big rill (no visible thalweg in DEM)	**17.634**	1.350	7.66	11.71	66.35
7	8	One big rill (slight thalweg in DEM)	**13.472**	0.565	4.19	7.81	57.97
8	1	One big rill (thalweg in DEM)	**15.907**	4.336	27.26	6.11	38.41

4.4 Conclusions

In the present study, 456 croplands were investigated over three years after heavy precipitation events in Saarland, Germany, and neighboring states. Analyses of field conditions showed that erosion occurred only in fields with bare soil or sparse vegetation. No erosion was detected in fields with a cover greater than 25 %. Heavy precipitation-induced linear erosion was recorded using a UAV. The spatial distributions of the linear erosion tracks and erosion quantities were derived from aerial survey data. These data are appropriate for providing information on erosion quantities and rates based on heavy precipitation events and pronounced linear erosion at the hillslope scale. The measured erosion rates ranged from 1 t/ha to 185 t/ha. Comparisons of the empirically based erosion data of this study with the E3D and RUSLE2 model values indicate that the erosion of natural events does not fit the erosion quantities obtained using existing models (RUSLE2 and E3D). The model applications underestimated naturally occurring erosion tracks. The spatial distribution of the linear erosion tracks was considered in E3D for erosion that occurred in the thalweg. Overall, linear erosion was not sufficiently reproduced by the applied erosion models. In most existing models, the erosion data used for calibration are limited to test plots that do not reflect the LS factors of a hillslope. In this study, it was shown that LS was the most significant factor for the occurrence of linear erosion rather than sheet erosion. However, it was also shown that the parameter that considers soil properties (K factor) does not influence the erosion significantly. To correctly simulate the linear erosion caused by heavy precipitation, reliable calibration data based on these conditions must be considered. The data

collected in this study are appropriate for this purpose. Further research is required to calibrate erosion models using data that is appropriate for heavy precipitation-induced erosion and, therefore, for linear erosion. Furthermore, existing models (e.g., E3D) consider overland flow using simplified approaches (hydrological modeling using GIS). However, the current state-of-the-art simulation of heavy precipitation events, such as pluvial flash floods, is a two-dimensional (2D) hydrodynamic numerical model. Using 2D models of flash floods to simulate erosion will improve our knowledge of the attacking forces of water, thereby increasing the accuracy of heavy precipitation-induced erosion modeling.

Data Availability Statement

The datasets (DEMs and orthoimages) generated during this study are provided in a data repository (https://doi.org/10.6084/m9.figshare.24592338.v1).

5 Application of a 2D Hydrodynamic Numerical Model for Heavy Precipitation-Induced Soil Erosion

Soil erosion, particularly when intensified by heavy precipitation, is a natural process and a persistent challenge in agricultural management. To date, this problem has been addressed using existing erosion models. However, these models often rely on simplified hydraulic approaches, whereas two-dimensional (2D) hydrodynamic numerical models are state-of-the-art for overland flow simulations. In the following study, the combination of a 2D model and a soil erosion approach allowed for a more precise consideration of the hydraulics. The Govers approach was used with the 2D HydroAS model and evaluated using experimental plot data and naturally occurring field-scale erosion data, sourced from the literature. Results indicate that the combined model simulated sheet erosion and produced reasonable estimates for small rills using the Govers transport capacity approach. However, larger rills require calibration of this method. Additionally, the resolution of the digital elevation model (0.25 m) used as the basis for the simulation was of great importance to avoid overestimating smaller rills. Sensitivity analysis revealed that these smaller rills were particularly influenced by the input grain diameter and surface roughness. Comparisons with other erosion models underscore that incorporating an improved hydraulic approach and adapting the topography at each simulation time step enhances estimation of the spatial distribution and quantity of erosion of the rills. Knowledge about the occurrence and quantification of rill erosion can help planners develop geoecological solutions for flooding and erosion.

Rebecca Hinsberger and Alpaslan Yörük

Environmental Processes, 2025
Accepted for publication

DOI: 10.1007/s40710-025-00797-9

5.1 Introduction

Heavy precipitation events with increasing rainfall erosivity occur frequently, leading to flash floods that adversely affect human settlements and infrastructure (IPCC, 2021; Nunes and Nearing, 2011). Beyond the risk of water damage, soil loss can cause on-site and off-site damage. According to Parkin et al. (2008), a few heavy precipitation events account for the majority of erosion. Flash floods are defined as overland flow with shallow water depths and steep slopes. On these slopes, there is high sediment concentration resulting from soil erosion (Dugan et al., 2024; Govers, 1990; Semwal et al., 2017).

Several models are currently available to simulate overland flow and erosion. These range from empirical models, such as the Universal Soil Loss Equation (USLE) (Wischmeier and Smith, 1978), to process-oriented models like the Water Erosion Prediction Project (WEPP) (Laflen et al., 1991), the European Soil Erosion Model (EUROSEM) (Morgan et al., 1998a), the Areal Nonpoint Source Watershed Environment Response Simulation (ANSWERS) (Beasley et al., 1980), and the Limburg Soil Erosion Model (LISEM) (De Roo et al., 1994). Reviews of the existing models have been reported in previous studies (Andualem et al., 2023; Borelli et al., 2021). Sediment transport capacity (TC) is a key component for describing the potential of water flow to transport detached materials. However, interpretations of the TC concept may vary. In models like WEPP and EUROSEM, detachment is constrained by the TC and the current sediment load. According to Wainwright et al. (2015), this approach lacks justification and may be unsuitable. Alternative approaches, such as the Meyer-Peter-Müller (MPM) approach (Meyer-Peter and Müller, 1948), represent the actual bedload transport rate (Wainwright et al., 2015). Furthermore, contrasting perspectives regarding the use of capacity (equilibrium) and non-capacity (non-equilibrium) approaches exist (Biswas et al., 2021, Hu et al., 2025). However, since this study focused on bedload, a capacity-based approach was adopted. Different TC approaches have been applied into existing erosion models. Empirical approaches developed from stream data, such as MPM, Ackers-White (Ackers and White, 1973), Engelund-Hansen (Engelund and Hansen, 1967), and Yalin (Yalin, 1963), are widely used in the context of rivers. Although these were developed for stream erosion conditions with low slopes and water depths of several decimeters, some models have applied them to soil erosion. For example, WEPP uses a simplified Yalin approach to calculate TC. In contrast, EUROSEM uses the Govers (1990) approach, which is based on experimental data on overland flow conditions, with steep slopes up to 21%, and shallow water depths.

Because the accuracy of erosion simulations depends on the hydraulic simulation precision, proper consideration and calibration of hydraulics are essential (Morgan et al., 1998b; Smith

et al., 1999). However, existing soil erosion models continue to use simplified hydraulic approaches to calculate water forces acting on the soil (Huang et al., 2022).

In addition to erosion models, hydraulic models have also been used to simulate floods and flash floods (Al-Fugara et al., 2023; Hu and Song, 2018; Huang et al., 2015; Liang et al., 2016). These vary in accuracy and detail. For example, HEC-RAS (U.S. Army Corps of Engineers, CA, USA) employ a one-dimensional (1D) energy equation, whereas HydroAS (Hydrotec, Aachen, Germany) solves complete shallow–water equations, including turbulence and acceleration terms. As the level of accuracy affects computational efficiency, previous studies have explored the acceleration of two-dimensional (2D) models using the LTS method or GPU acceleration (Hu et al., 2019; Wu et al., 2023). Other studies have focused on the combined modeling of 2D hydraulics and sediment transport during floods. Huang et al. (2022) investigated the impact of sediment on the simulated peak discharge. Existing hydraulic models, such as HydroAS GS/ST (Hydrotec, 2025b) and Iber+ (Costabile et al., 2024; García-Feal et al., 2018), support river erosion modeling in combination with hydraulic simulations. Past research has mainly focused on sediment in fluvial flows. Studies on the combination of 2D hydraulics and soil erosion caused by pluvial flows remain scarce. Jia et al. (2023) demonstrated the advantage of a 2D hydraulic approach for simulating soil erosion by comparing observed and simulated data. However, they did not compare these results with existing models that considered simplified hydraulics.

This study focuses on arable land erosion and flash floods that occur as overland flows, unified in one model. In existing soil erosion models, simplified hydraulics are considered, which underestimate rill erosion (Hinsberger, 2024).

The core hypothesis is that a detailed hydraulic approach—through a 2D hydrodynamic numerical model that solves complete shallow water equations—is essential for soil erosion modeling. Such models are currently state-of-the-art for flash flood simulations in Germany. This study aims to simulate soil erosion from a single heavy precipitation event. This was achieved by using a 2D approach, which dynamically updated the topography of the model according to progressive erosion and sedimentation. The TC approach of Govers (1990) was implemented for the required conditions and evaluated using laboratory and plot experiments under heavy precipitation framework conditions. The experiments were chosen to be partially outside Govers' validity range, in order to investigate their influence and provide insight into the applicability and limitations of this approach. Accordingly, a suitable approach for simulating the soil erosion caused by heavy precipitation should be identified. To calibrate the field-scale event data, a sensitivity analysis was performed on different parameters and one influential parameter was selected. Observed natural erosion data from

the literature were compared with the simulated results of the combined approach, and existing models demonstrated the improved performance of the combined 2D hydraulic and erosion model. Using a soil erosion model with advanced hydraulics, rill erosion can be accurately simulated in terms of quantitative variation and spatial distribution. Comparing the simulation results of the model used in this study with those of existing models that use simplified hydraulics, demonstrates the benefits of utilizing 2D hydraulics, particularly in the generation of rills. Knowledge of these rills, which contribute significantly to soil erosion, is valuable for erosion management.

5.2 Materials and Methods

In this study, a combination of a soil erosion approach and a 2D hydrodynamic numerical model was used. The HydroAS model, which is suitable for 2D hydraulic simulations, was selected to represent hydraulic processes (Section 5.2.1). The Govers approach was selected and confirmed as the TC approach to represent soil erosion because of its suitability for overland flow conditions (Section 5.2.2). This approach was implemented within the HydroAS model and applied to experimental plots and field data from the literature (Sections 5.2.3 and 5.2.4).

5.2.1 Selection of 2D Model

The 2D HydroAS model, which is widely used in Germany for flood and flash flood simulations, was selected for this study (Huber et al., 2021; Lavoie and Mahdi, 2017; Yörük and Sacher, 2014). To simulate surface runoff, HydroAS solves the complete shallow-water equations and includes the acceleration term, thereby meeting the requirements of this study for accurately simulating erosion driven by overland flow and flash floods. The model can simulate both discharge and rain-on-grid conditions. Infiltration can be considered through sink terms at each mesh node. In this study, heavy precipitation events occurring in early summer were simulated, under the assumption that the soil was dry, water-repellent, and silted due to splash erosion (see Section 5.2.4). As a result, soil processes are negligible, effective precipitation is used as an input parameter for the simulations, and infiltration is excluded. The runoff simulation (both overland and channel flows) was based on Equations (5-1)–(5-5). Approaches to the roughness, viscosity, and other details can be found in the HydroAS Model Manual (Hydrotec, 2025a).

$$\frac{\partial \mathbf{w}}{\partial t} + \frac{\partial \mathbf{f}}{\partial x} + \frac{\partial \mathbf{g}}{\partial y} + \mathbf{s} = 0 \tag{5-1}$$

with

$$\mathbf{w} = \begin{bmatrix} H \\ uh \\ \mathrm{v}h \end{bmatrix} \tag{5-2}$$

$$\mathbf{f} = \begin{bmatrix} uh \\ u^2h + 0.5gh^2 - \nu h\dfrac{\partial u}{\partial x} \\ uvh - \nu h\dfrac{\partial \mathrm{v}}{\partial x} \end{bmatrix} \tag{5-3}$$

$$\mathbf{g} = \begin{bmatrix} \mathrm{v}h \\ uvh - \nu h\dfrac{\partial u}{\partial y} \\ \mathrm{v}^2h + 0.5gh^2 - \nu h\dfrac{\partial \mathrm{v}}{\partial y} \end{bmatrix} \tag{5-4}$$

$$\mathbf{s} = \begin{bmatrix} 0 \\ gh(I_{Rx} - I_{Sx}) \\ gh(I_{Ry} - I_{Sy}) \end{bmatrix} \tag{5-5}$$

where t is the time [s], and x and y represent the streamwise and transverse directions [m], respectively. H is the water level above a reference level [m]; h is the water depth [m]; u and v are components of the flow velocity in x and y directions [m s^{-1}], respectively; g is gravitational acceleration [m s^{-2}]; and Greek letter nu (ν) is the viscosity. The source term s contains the friction slope I_R and bed slope I_S.

5

5.2.2 Governing Erosion Equations

As noted in the Introduction, the HydroAS model can simulate river erosion using its add-on module, GS, which simulates the total sediment load. At each mesh node, the model calculates the driving forces acting on the soil based on hydraulic parameters. Depending on the selected sediment transport equation, such as MPM or Ackers-White, the TC represents the actual transport rate, and sediment is transported to the following mesh node, where the calculation is repeated. In the existing program, it is possible to specify different particle sizes to consider the layer management. This study used the median grain diameter as a uniform particle size. Soil exchange with the surface (detachment or sedimentation), which leads to changes in topography, was calculated using the Exner equation (Hydrotec, 2025b):

$$\left(1 - n_p\right)\rho_s \frac{\partial Z}{\partial t} + S = 0 \tag{5-6}$$

where n_p is the porosity of the sediment, ρ_s is sediment density [kg m^{-3}], Z the bed elevation [m], t is the time [s], and S is the balance of sedimentation and erosion [kg m^{-2} s^{-1}]. The soil mass S_e for erosion was calculated as the product of the sink velocity w_s [m s^{-1}], the TC approach, and sediment density ρ_s [kg m^{-3}]:

$$S_e = w_s \, TC \, \rho_s \tag{5-7}$$

Mass conservation was maintained, as soil mass S was redistributed only among neighboring mesh nodes. However, soil masses can either increase or decrease at the model boundaries. To represent TC, the MPM, Ackers-White, and Engelund-Hansen approaches are pre-integrated into HydroAS GS as the bedload transport rate. In this study, the Govers approach was implemented and is defined as:

$$TC_{Govers} = c * (\omega - \omega_{crit})^d \tag{5-8}$$

where *c* and *d* are parameters dependent on grain diameter. The unit stream power *ω* [kg m² s^{-3}] is the mathematical product of the slope and the mean flow velocity. The critical unit stream power has a threshold value of 0.004 m/s (Govers, 1990). Here, TC_{Govers} also serves as the bedload transport rate. The combined simulation using HydroAS and the Govers approach is referred to as *HydroAS GS–Govers*. In the HydroAS GS–Govers model, no distinction was made between rill and interrill erosion. Rill formation was driven purely by hydraulics.

Initially, the MPM, Ackers-White, and Engelund-Hansen approaches were evaluated for their suitability for soil erosion modeling and compared to the Govers approach (Section 5.3.1).

5.2.3 Application of the HydroAS GS–Govers Model on Experimental Plots

To evaluate the HydroAS GS–Govers model for soil erosion under heavy precipitation, experimental data were used to compare simulation results with measured observations. These experiments provided clear and traceable boundary conditions and were used as the first validation of the model. The framework conditions of the experimental data were assumed to represent rainfall as heavy precipitation (≥15 mm/h according to DWD, n.d.) and slope gradients that fit the overland flow conditions. Therefore, a minimum gradient of 5 % was determined. Three experimental studies were selected: Quan et al. (2020), Scherer et al. (2012), and Kilinc and Richardson (1973).

Kilinc and Richardson (1973) conducted flume experiments with various slope gradients, rainfall intensities, and one soil type (Table 5-1). Six runs were selected for this study and named according to their original identifiers (Kil I-IV, Kil IX and Kil X). The 2D model was constructed as a rectangular mesh with 12 elements across the flume width and an aspect ratio of 1:2, following Hydrotec (2025c) guidelines, which suggests a ratio of 1:2 to 1:3. The model was calibrated using runoff and flow velocity values reported by Kilinc and Richardson (1973), with adjustments for surface roughness and rainfall intensity.

Quan et al. (2020) conducted laboratory rainfall experiments on two soils (*AS* from the Ansai Agricultural Experiment Station, and *SD* from the Suide Soil and Water Conservation Experiment Station), with a rainfall intensity of 60 mm/h over one hour and flume gradients of 5°, 10°, 15°, and 20° (Table 5-1). Although gradients of 15° and 20° exceeded the validity range of the Govers approach (slope <0.21; see Section 5.3.1), simulations were still performed. To simulate these experiments, a 2D model was built containing eight elements across the flume width, with an aspect ratio of 1:2. Simulations were named according to soil type and gradient (AS5°–AS20°, SD5°–SD20°). Quan et al. (2020) provided the grain size distribution used to derive d_{50} and measured the total runoff. However, no discharge or flow velocity was provided. Therefore, the amount of rainfall in the simulation was adjusted using a discharge coefficient to determine the indicated total runoff. These coefficients ranged from 0.18 to 0.32 and were used to calibrate the models. The roughness coefficient was not reported in the study; therefore, Manning's n was assumed to be 0.033, based on values stated by Kilinc and Richardson (1973), Scherer et al. (2012), and other studies (e.g., LUBW, 2020).

Table 5-1: Experimental conditions/information and data input / parametrization for the 2D model of plot models.

	Kilinc and Richardson (1973)	**Quan et al. (2020)**	**Scherer et al. (2012)**
Name	Kil I-IV, IX, X	AS5°–AS20° SD5°–SD20°	S33–34 S36-37 S40-41
Plot: L × W [m]	4.88 × 1.52	5 × 1	12 × 2
Slope [%]	5.7 15	8.75 – 36.4	14.7 – 17.8
Rainfall intensity [mm/h]	31.75 – 116.84	60	50.4 – 64.8
Rainfall duration [min]	60	60	68 – 75
Simulation duration [min]	70	70	120
Simulation time interval [min]	1	1	1
Roughness coefficient (Mannings's n)	0.033	0.033*	0.02 – 0.04
Median grain diameter (d_{50})	0.35	0.04 – 0.044	0.0216 – 0.0245**
Bulk density [kg/m³]	1500	1300 – 1350	1670*

* Values are assumptions; **Values derived by Gerlinger (1997)

Scherer et al. (2012) reported the field studies conducted in various loess soil areas in Germany by Gerlinger (1997), with 58 experiments on rainfall amount, intensity, and slope. Six experiments were selected (Table 5-1) to reflect heavy precipitation and erosion conditions in early summer with bare soil, with rainfall intensities of 50.4–64.8 mm/h over 68–75 min, and slopes of 14.7–17.8 %. The experiments were grouped into three pairs of plots, and each pair was used to examine the reproducibility and variability of similarly spaced plots (Gerlinger, 1997). The 2D model contained eight elements across the flume width, with an

aspect ratio of 1:3. The simulations were named according to their original experimental numbers (S33–34: pair 1; S36–37: pair 2; S40–S41: pair 3). Despite rainfall data, no flow data was available. Therefore, the rainfall was not reduced by any factor in the simulation. Calibration was not performed for the hydraulics. Roughness coefficients used were reported by Scherer et al. (2012). The d_{50} value was derived from the grain-size distribution provided by Gerlinger (1997).

All experimental data were sourced from the literature. Missing values were plausibly estimated. All the values used are presented in Table 5-1.

All flumes or plots described were designed as 2D models based on the framework conditions outlined in the literature and were simulated using the HydroAS GS–Govers model. In all simulations, the median diameter (d_{50}) was the only fraction used to calculate TC_{Govers}. The simulated sediment transport rates at the flume outlets were compared with the values observed from the literature.

5.2.4 Application of the HydroAS GS–Govers Model for Field Scale Event Data

Owing to the limitations of laboratory and small-scale field experiments in capturing the full extent of rill erosion, further evaluation of the model was conducted. The model was applied to natural erosion events that occurred in croplands following heavy precipitation.

For this application, three fields presented by Hinsberger (2024) were selected: Fields #4, #7, and #8, where natural erosion was detected and analyzed. These fields were selected because Hinsberger (2024) provided rill erosion estimations and simulation results using the RUSLE2 (Revised USLE 2) and EROSION-3D soil erosion models, which were discussed in this study. The data from Hinsberger (2024) included: i) orthophotos for the comparison of rill distribution, ii) measured erosion quantities from rills, iii) RUSLE2 total erosion, and iv) EROSION-3D simulation results. The results of the RUSLE2 and EROSION-3D (E3D) models used in this study are presented in Table 5-2.

Table 5-2: Results of measurements, RUSLE2 and EROSION-3D (E3D) models from Hinsberger (2024) used in this study. When no results were provided, - is shown in the Table.

	Total erosion [t/ha]		**Rill erosion [t]**		
	RUSLE2	**E3D**	**measured**	**RUSLE2**	**E3D**
#4	13.14	0.30			
Rill #4.1			11.75	1.14	0.02
Rill #4.2			8.03	1.32	-
#7	65.15	10.45			
Rill #7.6			17.39	11.71	1.35
Rill #7.7			14.67	6.93	-
Rill #7.8			13.28	7.81	0.57
Rill #7.10			5.71	5.76	-
#8	12.32	4.84			
Rill #8			15.79	6.11	4.34

For the simulation, precipitation rates were derived from YW radar data provided by the German Meteorological Service (Deutscher Wetterdienst DWD). As Hinsberger (2024) did not specify any effective precipitation or discharge data, the total precipitation was assumed for the simulations. In Europe, this neglect of infiltration is partially justified, as heavy precipitation often occurs in early summer, when soils are dried out and silted. As recorded rill erosion occurred in June (Hinsberger, 2024), these assumptions were supported.

Digital elevation models (DEM) provided by Hinsberger (2024) served as the simulation basis. Pre-erosion DEMs with centimeter-level resolutions were resampled to grid sizes of 0.25 m (DEM0.25) and 1 m (DEM1). Therefore, the model was built as a mesh using square elements of 0.25 × 0.25 m and 1 × 1 m.

Different calibration parameters for the models are possible, including surface roughness, grain diameter, and a factor for the transport capacity ($k \times TC_{Govers}$). A sensitivity analysis of the surface roughness parameter (Manning's n) and median grain diameter (d_{50}) was conducted. Manning's n was selected as a parameter to examine the influence on runoff, as it is state-of-the-art in flood modeling (e.g., Ferguson, 2021b). Grain size was selected because it is the only input parameter in the Govers equation suitable for sensitivity analysis. Both parameters were reduced and increased for each simulation. Manning's n was adjusted to a plausible range for the surface roughness for croplands (Aigner and Bollrich, 2015; Chow, 1959). Although studies have indicated that Manning's n is higher for overland flow (Sanz-Ramos et al., 2021) and that roughness depends on shallow-water depth (Hinsberger et al., 2022), this sensitivity analysis was reduced to the essential influence of roughness. Grain diameter was adjusted in a range of ± 30–40%. As a change in the grain diameter leads to a change in the surface roughness, this relationship was disregarded. Simulations were conducted using the original TC_{Govers} (Eq. (5-8)). As TC_{Govers} is the most uncertain calibration parameter, the models were calibrated to the measured rill quantities from the literature using a factor named 'Cali' (Table 5-3). Calibration was conducted for DEM1, which was more commonly available.

Table 5-3 presents an overview of the simulations and corresponding framework conditions. The simulation names consist of the DEM basis (1 m or 0.25 m grid) and the adapted parameter for the sensitivity analysis. The experiments were conducted in Fields #4, #7, and #8. Experiments Exp. DEM1 and Exp. DEM1 (Cali) were used for comparison with the measured data and results from RUSLE2 and E3D. Other simulations were used for sensitivity analysis. Table 5-4 presents basic information on field and event data and hydrodynamic model parameterization.

In many models, such as WEPP and EUROSEM, the erosion calculation is separated into interrill and rill shares or raindrop-induced and overland flow erosion (as in E3D). As the

contribution of splash erosion is less impactful than that of the rill share (Govers and Poesen, 1988), the splash erosion share was neglected.

The simulation results, including a modified topography (see Section 5.2.2), can be converted into a DEM with the same resolution as the input of the simulation. The difference between the original surface height (DEM0.25 or DEM1) and surface height at the final time step produces the erosion depth at each grid point, which can be converted to erosion quantities using bulk density. In addition, predefined cross sections provide information on the sediment load for each time step.

Table 5-3: Overview of simulations and sensitivity parameters for the fields #4, #7, and #8.

Experiment	**Manning's n [s/m$^{1/3}$]**			**Median grain diameter d_{50} [mm]**		
	#4	**#7**	**#8**	**#4**	**#7**	**#8**
Exp. DEM1	0.033	0.033	0.033	0.060	0.050	0.306
Exp. DEM1 (Cali)	0.033	0.033	0.033	0.060	0.050	0.306
Exp. DEM 0.25	0.033	0.033	0.033	0.060	0.050	0.306
Exp. DEM 1 n reduced	0.025	0.025	0.025	0.060	0.050	0.306
Exp. DEM 1 n increased	0.050	0.050	0.050	0.060	0.050	0.306
Exp. DEM 0.25 n reduced	0.025	0.025	0.025	0.060	0.050	0.306
Exp. DEM 0.25 n increased	0.050	0.050	0.050	0.060	0.050	0.306
Exp. DEM 1 d reduced	0.033	0.033	0.033	0.040	0.030	0.200
Exp. DEM 1 d increased	0.033	0.033	0.033	0.080	0.070	0.400
Exp. DEM 0.25 d reduced	0.033	0.033	0.033	0.040	0.030	0.200
Exp. DEM 0.25 d increased	0.033	0.033	0.033	0.080	0.070	0.400

Table 5-4: Experimental conditions/information and data input/parametrization for the 2D model of field-scale models.

Name	**#4**	**#7**	**#8**
Field extension [hectare]	1.10	6.61	4.37
Max. Rainfall intensity [mm/h]	20.35	48.23	33.01
Rainfall duration [min]	55	90	90
Simulation duration [min]	120	120	120
Time interval [min]	5	5	5
Roughness coefficient (Mannings's n)	0.033	0.033	0.033
Median grain diameter (d_{50})	0.060	0.053	0.306
Bulk density [kg/m³]	1120	1420	1300

5.3 Results and Discussion

This study employed the Govers approach as the TC approach for soil erosion modeling, in combination with the 2D HydroAS model. The model was applied to experimental plots and real-world field conditions. Section 5.3.1 evaluates the suitability of this approach by examining the validity ranges of different TC approaches. The simulation results of the HydroAS GS–Govers model for experimental flumes/plots and naturally occurring erosion are presented and analyzed in Sections 5.3.2 and 5.3.3, respectively.

5.3.1 Suitability of Govers (1990) Approach for Soil Erosion Modeling

Various TC approaches are available for erosion modeling. However, these approaches have been empirically calibrated from experiments using specific setups and soil properties. Therefore, each approach is only applicable to experiments within the specific validity range for which it was developed (Brazier et al., 2011). Figure 5-1 compares the validity ranges of the MPM, Ackers-White, Engelund-Hansen, and Govers TC approaches for the grain diameter and slope parameters. The MPM, Ackers-White, and Engelund-Hansen approaches have already been implemented into HydroAS GS, and the Govers approach is a part of the well-known EUROSEM (Morgan et al., 1998a) and LISEM (De Roo et al., 1994) models. The ranges for MPM, Ackers-White, and Engelund-Hansen were obtained from a compilation by BMLFUW and ÖWAV (2011), and the range for Govers was derived from Govers (1990). Notably, the slope parameter indicates different conditions: MPM, Ackers-White, and Engelund-Hansen showed validity for small slopes (<4 %) indicating river conditions and a wide range of grain diameters. In contrast, Govers exhibited validity for a wide range of slopes (<21 %), including overland flow conditions, and a more limited range of grain diameters.

In addition, Figure 5-1 shows the grain diameter and slope characteristics for the experimental plots and fields with naturally occurring erosion due to heavy precipitation. Due to the inclusion of the experiments used for the evaluation in this study, the validity range of Govers is significantly more appropriate than that of the comparative approaches. All experiments fall within Govers' validity range for slope. Regarding the grain diameter, the selected experiments were conducted outside Govers' approach. However, the experimental soil properties were similar to those used in the study by Govers (1990). In addition to the slope and grain diameter, the boundary conditions for erosion due to heavy precipitation events were of primary importance when selecting the experiments (see Section 5.2.3). This perception and selection of the approach agree with those of Wang et al. (2019a), who stated that the Govers approach was the best for cropland soil.

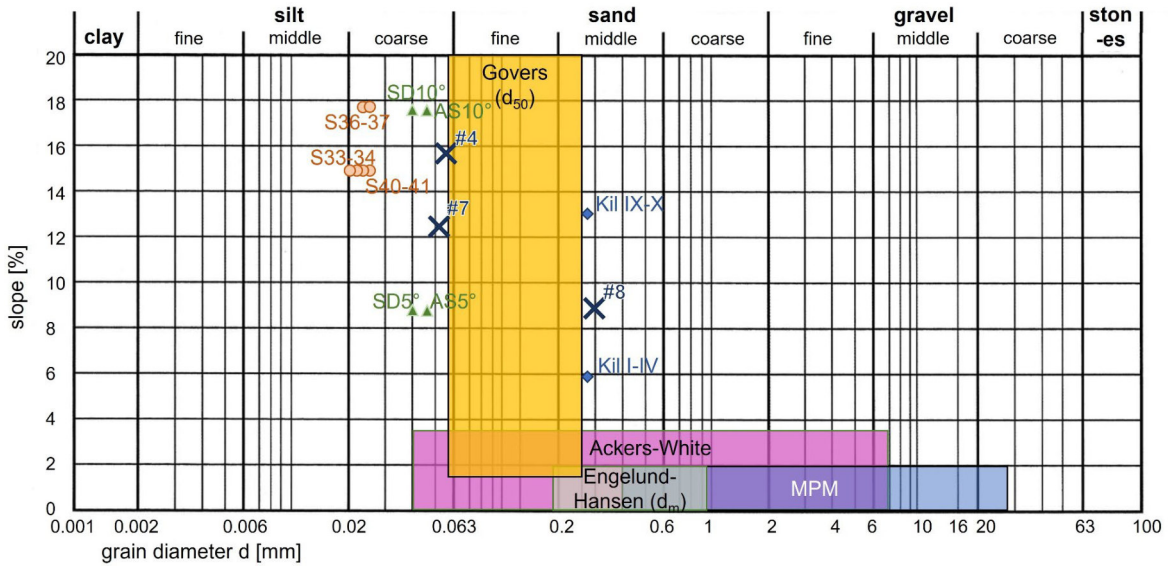

Figure 5-1: Validity range of different transport capacity approaches. For the grain diameter, the range of experimental sediments used are shown for Ackers-White and MPM, the range of the mean diameter (d_m) for Engelund-Hansen, and the range of the median diameter (d_{50}) for Govers. The x symbols, dots, triangles, and diamonds indicate the median grain size d_{50} and mean slope of investigations by Hinsberger (2024), Scherer et al. (2012), Quan et al. (2020), and Kilinc and Richardson (1973), respectively. Each symbol represents an erosion field or an experimental run.

5

5.3.2 Evaluation of the HydroAS GS–Govers Model for Experimental Plots

Data from Kilinc and Richardson (1973), Scherer et al. (2012), and Quan et al. (2020) were used to simulate rainfall in the experimental plots, using the HydroAS GS–Govers model. The framework conditions (median grain diameter and slope) are illustrated in Figure 5-1. The experiments conducted by Kilinc and Richardson, Scherer et al., and Quan et al. are highlighted by blue diamonds, orange dots, and green triangles, respectively. The figure indicates that the slope values fall within the validity range of the Govers approach. However, the median grain diameter d_{50} of the soil used by Kilinc and Richardson was coarser than that used by Govers, whereas the soils used by Scherer et al. and Quan et al. had finer median grain diameters.

The simulated results were compared with measurements from the literature to evaluate model suitability. To ensure comparability, as Scherer et al. (2012) and Quan et al. (2020) merely reported total detachment, the results of this study were adjusted by considering the total sediment that reached the outlet of the model during the simulation. The same procedure was followed for the results presented by Kilinc and Richardson. The observed data from the literature and the results of the HydroAS GS–Govers model are listed in Table 5-5.

Table 5-5: Total detachment [kg] presented or derived from the literature (Quan et al. 2020, Scherer et al. 2012, Kilinc and Richardson 1973) and HydroAS GS–Govers simulation results of experimental flumes/plots.

Experiment	Results from the literature	HydroAS GS–Govers
Quan et. al (2020)		
AS 5°	0.143	0
AS 10°	0.834	0.540
AS 15°	0.994	0.666
AS 20°	1.375	0.665
SD 5°	0.021	0.095
SD 10°	0.207	0.207
SD 15°	0.373	0.389
SD 20°	0.549	0.901
Kilinc and Richardson (1973)		
Kil I	0.776	0
Kil II	2.425	0
Kil III	5.222	0.014
Kil IV	11.980	0.029
Kil IX	5.129	0.029
Kil X	27.833	0.115
Scherer et al. (2012)		
S33	9.6	29.604
S34	14.7	35.171
S36	57.9	37.138
S37	22.9	39.543
S40	47.7	23.941
S41	31.0	32.996

The simulated results were compared with the measured data. Figure 5-2 compares the cumulative measured erosion (x-axis) with the cumulative simulated erosion (y-axis) for each experiment. Different erosion quantity ranges were included in the experiments.

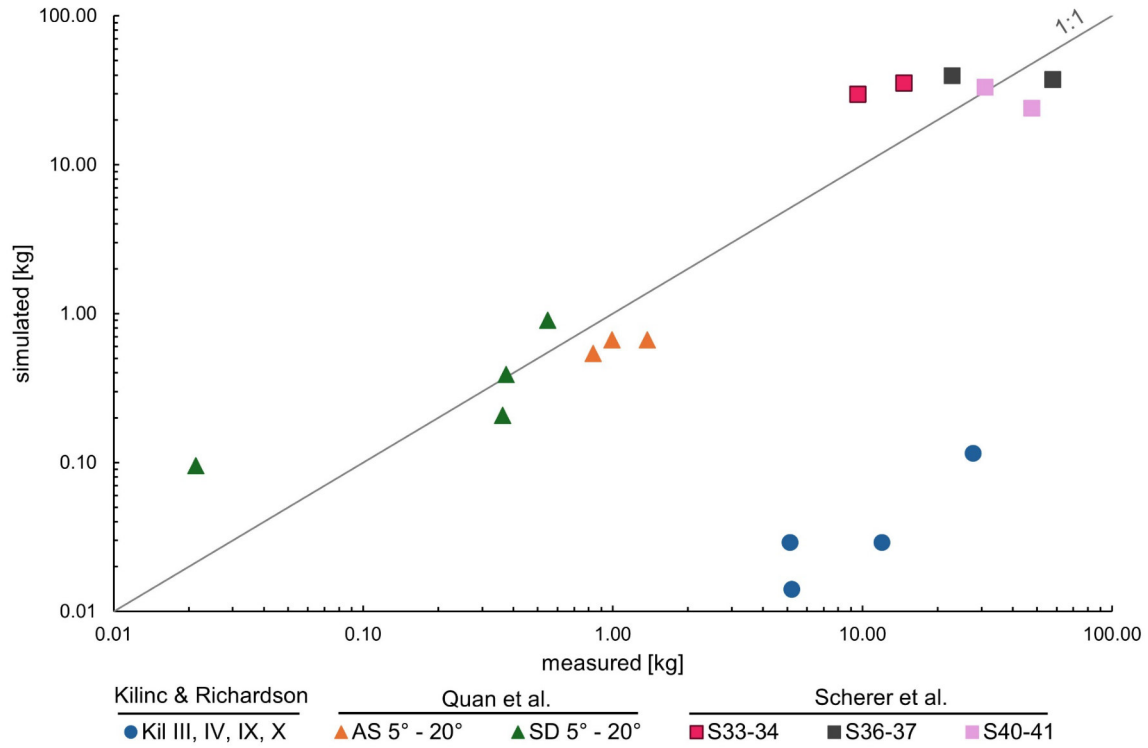

Figure 5-2: Comparison of simulated erosion [kg] using the 2D HydroAS GS–Govers model (ordinate) with respective measured erosion data from Kilinc and Richardson (1973) (blue dots), Quan et al. (2020) (orange and green triangles) and Scherer et al. (2012) (pink, grey and rose squares).

The simulation results for the experiments by Kilinc and Richardson indicated extremely low erosion rates. Experiments with low precipitation and discharge (Kil I and II) showed no erosion. Higher precipitation rates or steeper slopes (Kil III, IV, IX, and X) resulted in minimal erosion, with values approaching zero. This suggests that the threshold value for the critical unit stream power in the approach (0.004 m/s; see Eq. (5-8)), which is an empirically derived constant, was too high for these experimental conditions. As shown in Figure 5-1, the d_{50} values of the Kilinc and Richardson experiments were coarser than those of the Govers approach. Therefore, the threshold value must be adjusted to produce greater erosion in those conditions. Accordingly, the statistical values for the suitability of the model showed high deviation (Table 5-6).

Table 5-6: Statistics for the difference between the experimental results and the results of the HydroAS GS–Govers model. Mean = Mean value, MAE = Mean Absolute Error, RMSE = Root Mean Square Error (all values in kg).

	Kilinc and Richardson – HydroAS GS–Govers	**Quan et al. – HydroAS GS–Govers**	**Scherer et al. – HydroAS GS–Govers**
Mean	8.86	0.15	-2.43
MAE	8.86	0.26	17.27
RMSE	12.72	0.33	18.69

In the experiments of Quan et al., the observed and simulated values showed high agreement (Figure 5-2). Differences related to soil type (AS, orange; SD, green) were notable. The simulation results for SD soils (green triangles) were in high agreement with measured data, with an RMSE of 0.20. Notably, the experiment SD of 5° with the lowest erosion quantity showed strong agreement at the onset of sediment transport. In contrast, the AS simulations (orange triangles) consistently underestimated erosion measurements (RMSE = 0.42). Experiments SD 15° and 20° and AS 15° and 20° exhibited the highest erosion and fell outside the validity range of the Govers approach (see Section 5.2.3). The SD simulations overestimated erosion, while AS simulations underestimated it. Despite the limited number of simulations, these results suggest that the Govers approach can be applied to higher gradients than those shown in the validity range in Figure 5-1. Overall, the HydroAS GS–Govers results fit the measured erosion with an RMSE of 0.33, indicating good agreement.

Figure 5-2 also presents simulated and observed data from Scherer et al. (squares). Different colors indicate different experimental pairs, representing the reproducibility and variability of the adjacent plots. Pairs sometimes showed significant divergence. For S33–S34, the simulation matched the trend for both experiments: an overestimation of erosion. For S36–S37 and S40–S41, the simulated erosion for the pairs was similar; however, the measurements varied significantly. This suggests that although the scatter in the measured data is quite high, the simulation results indicate a plausible value, as one experiment overestimates and the other underestimates. These experiments fall within the slope validity range of the Govers approach but show smaller values for the grain diameter. However, the simulated results using HydroAS GS–Govers and the observed values showed good agreement (Table 5-6), suggesting the lower deviation of the grain diameter had limited influence on suitability.

In summary, the comparison between the validity range and the simulation of the laboratory and plot experiments showed that the Govers approach is suitable for simulating soil erosion caused by heavy precipitation. However, exceeding the valid grain diameter range (as in Kilinc and Richardson) had a strong influence on the erosion quantity, and the HydroAS GS–Govers model significantly underestimated the erosion. Interestingly, a smaller grain diameter than suggested influences the suitability of Govers' approach less (as in Scherer et al.). Therefore, exceeding the maximum grain diameter beyond the validity range should be avoided. Possibly, another TC approach for larger grain diameter could address this limitation. Exceeding the validity range of the slope (as in Quan et al.) did not adversely affect the simulation results.

As small plots do not represent the total influence of the catchment area (Brazier et al., 2011), and the relevance of the two-dimensional hydrodynamic numerical approach may

be limited under simple framework conditions, the HydroAS GS–Govers model was further tested on natural erosion fields.
The following section focuses on erosion at the field-scale based on measured data and simulation results from other soil erosion models.

5.3.3 Evaluation of the HydroAS GS–Govers Model for Naturally Occurring Erosion

To simulate erosion at the field scale using the HydroAS GS–Govers model, fields #4, #7, and #8 were investigated and analyzed by Hinsberger (2024). The framework conditions (median grain diameter and slope) for these fields are shown in Figure 5-1 and highlighted by black crosses. Slope conditions lie within the validity range of the Govers approach, whereas the grain diameter is finer for fields #4 and #7 and coarser for field #8.

For naturally occurring erosion at the field scale, a sensitivity analysis for Manning's n and the median grain diameter was first conducted (Section 5.3.3.1). Then, the total erosion rates, rill erosion quantities, and spatial distribution of the rills were compared with the measured data and results from the RUSLE2 and E3D models (Section 5.3.3.2 and 5.3.3.3).

5.3.3.1 Sensitivity Analysis and Calibration

A sensitivity analysis was conducted to assess the influence of selected input and possible calibration parameters.

Morgan et al. (1998b) stated that erosion depends heavily on hydraulic considerations. However, no hydrological measurements were available from Hinsberger (2024); therefore, the hydraulics could not be calibrated. Hence, surface roughness was selected as the sensitivity parameter because of its influence on flow velocity and, consequently, TC_{Govers}. Median grain diameter (d_{50}), the only soil parameter influencing TC_{Govers} (Eq. (5-8)), was selected as the second sensitivity parameter. The sensitivity analysis was conducted using DEMs with grid resolutions of 1 m and 0.25 m to investigate the influence of grid size. A summary of the simulations and their modifications is presented in Table 5-3.

The results of the sensitivity analysis are shown in Figure 5-3. The simulated erosion was set in relation to the measured value. A value of one (y-axis) represents perfect agreement, a value > 1 represents overestimation, and a value < 1 indicates underestimation. The figure shows three rills named #7.6, #7.10, and #8 (Figure 5-5). Rill #7.10 (green) represents a small rill, and #7.6 (dark yellow) and #8 (blue) represent large rills (Table 5-2). Triangles and crosses indicate the simulation bases using DEM1 and DEM0.25, respectively.

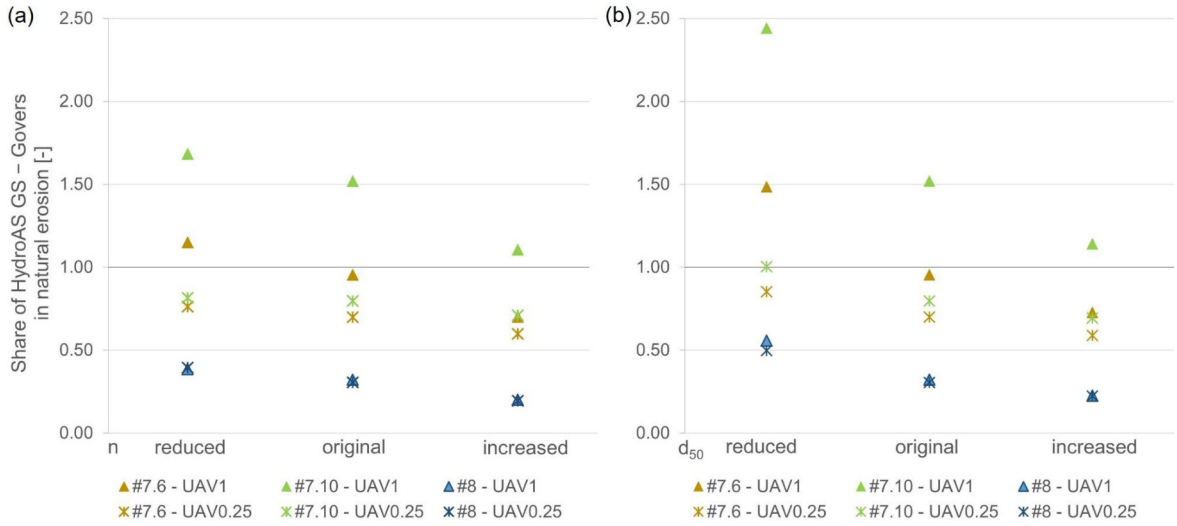

Figure 5-3: Sensitivity of Manning's n (a) and median grain diameter d_{50} (b) for selected rills based on simulated and measured rill erosion quantities.

To analyze the surface roughness, Manning's n was reduced and increased compared with the original assumption. A reduced n indicates a smoother surface and an increased n a rougher surface. As shown in Figure 5-3a, a reduced n value resulted in greater erosion, whereas a higher n value resulted in less erosion for both DEM1 and DEM0.25. This trend is plausible because an increased flow velocity occurs with a smoother surface framework, resulting in higher forces acting on the soil. In Figure 5-3b, the sensitivity analysis of the median grain diameter d_{50} is shown. A reduction in d_{50} led to an increase in erosion, whereas an increase in d_{50} led to a decrease in erosion. This is again plausible because of the increased transport capacity of smaller soil particles. Contrary to expectations, two key trends emerged: i) Smaller rills (#7.10 < #7.6, #8) were more sensitive to the influence of changes in roughness or grain diameter, especially for rill #7.10, where the sensitivity to d_{50} was significant with variations of up to +61 % (reduced diameter) and -25 % (increased diameter); ii) Smaller rills were also more affected by grid resolution. Rill #7.10 showed significant differences between the 1 m and 0.25 m grids, ranging from -59 % for a reduced d_{50} and -39 % for an increased d_{50}. In contrast, for rill #8, the results for the 1 m and 0.25 m grids were almost identical (Table 5-7), and no clear trend could be derived. This can be attributed to the thalweg of rill #8. The grid resolution is a significant factor in estimating the erosion quantities for rills. In a 1 m grid, the discharge accumulates in one grid cell, while a 0.25 m grid provides four cells on the same grid width. Consequently, small rills were overestimated when a grid size of 1 m was used, whereas a higher grid resolution led to more accurate simulation results. This hypothesis is supported by the results for rill #8, which produced similar erosion quantities at both grid resolutions. However, high model resolutions can lead to a decrease in computational efficiency. The issue of computational efficiency was investigated by Hu et al. (2019) and Wu et al. (2023), although it was not the primary focus of

this study. The findings on the importance of DEM resolution are consistent with the results of Jia et al. (2023) who highlighted the advantages of using both high-resolution topography and numerical simulations.

The HydroAS GS–Govers model showed high sensitivity to both surface roughness and grain diameter. Modeling results were further influenced by grid resolution. Rill quantities derived from DEM0.25 matched the measured quantities more accurately than those derived from DEM1. However, a high-quality DEM with these grid resolutions is not always available for soil erosion modeling. Overall, the HydroAS GS–Govers model simulated less erosion than the observed values.

Therefore, the models were calibrated using a factor for TC_{Govers}. The models were calibrated to the measured rill quantities using this factor (Experiments named 'Cali'). Calibration was conducted for DEM1 because this database is commonly available.

Each field was calibrated to fit observed rill quantities (Exp. DEM 1, Cali). The factors in the TC_{Govers} equation (Eq. (5-8)) depend on the field and are 10, 1.2, and 3 for fields #4, #7, and #8, respectively.

Table 5-7: Rill erosion [t] for visible rills using different experimental runs.

Experiment	#4.1	#4.2	#7.6	#7.7	#7.8	#7.10	#8
DEM1	2.37	2.00	16.59	10.87	5.24	8.67	5.08
DEM1, Cali	11.25	8.16	19.57	13.17	6.22	10.32	15.42
DEM0.25	2.81	2.11	12.16	8.28	3.87	4.55	4.82
DEM1, n reduced (n=0.025)	2.87	2.44	19.98	12.69	6.16	9.61	6.09
DEM1, n increased (n=0.050)	1.74	1.46	12.18	7.17	3.81	6.31	3.18
DEM0.25, n reduced (n=0.025)	3.23	2.39	13.25	8.63	4.45	4.65	6.23
DEM0.25, n increased (n=0.050)	2.04	1.56	10.41	6.44	2.89	4.06	3.08
DEM1, d reduced (-30 – -40 %)	3.48	2.88	25.81	18.82	8.24	13.94	8.79
DEM1, d increased (+30 – +40 %)	1.76	1.49	12.64	7.66	3.99	6.51	3.56
DEM0.25, d reduced (-30 – -40 %)	3.68	2.75	14.83	9.50	4.84	5.73	7.86
DEM0.25, d increased (+30 – +40 %)	2.15	1.62	10.23	6.80	3.06	3.96	3.51

5.3.3.2 Total Erosion

The total erosion rate is the standard output of RUSLE2, which is part of the USLE family and a well-established method for erosion estimation. For the grid-based simulation models (E3D and HydroAS GS–Govers), elevation changes between the first and final time steps—as well as the bulk density—were used to calculate total field erosion. The simulation results for total erosion are listed in Table 5-8.

Table 5-8: Total erosion [t/ha] for each field using different experimental runs.

Experiment	#4	#7	#8
DEM1	22.94	81.43	4.07
DEM1, Cali	201.63	101.33	12.54
DEM 0.25	35.22	86.35	6.35

Figure 5-4 compares the erosion rates simulated using the HydroAS GS–Govers model (Exp. DEM1) with rates from RUSLE2 and E3D (Table 5-2). Both RUSLE2 and E3D predicted higher erosion rates in field #8 and lower erosion rates in fields #4 and #7. E3D, in particular, predicted significantly lower rates than RUSLE2 and HydroAS GS–Govers, whereas RUSLE2 values were only 14–40% lower than HydroAS GS–Govers for fields #4 and #7. Statistical values comparing RUSLE2 and HydroAS GS–Govers results (Table 5-9) revealed strong agreement. Field #8 may have been influenced by a relatively large d_{50} which exceeded the validity of the Govers approach (see Section 5.3.1), resulting in a TC that was too low to achieve sufficient erosion. In Exp. DEM1 (Cali), the model was calibrated to observed rill values. A comparison of the total erosion of the calibrated and RUSLE2 models shows strong deviations. In Table 5-9, the statistical values for a comparison of RUSLE2 and E3D with the uncalibrated and calibrated HydroAS-GS–Govers model indicate that the uncalibrated model fits RUSLE2 better. Because it is assumed that RUSLE2 provides plausible results for total erosion, the calibration of the rill quantities overestimates the total erosion.

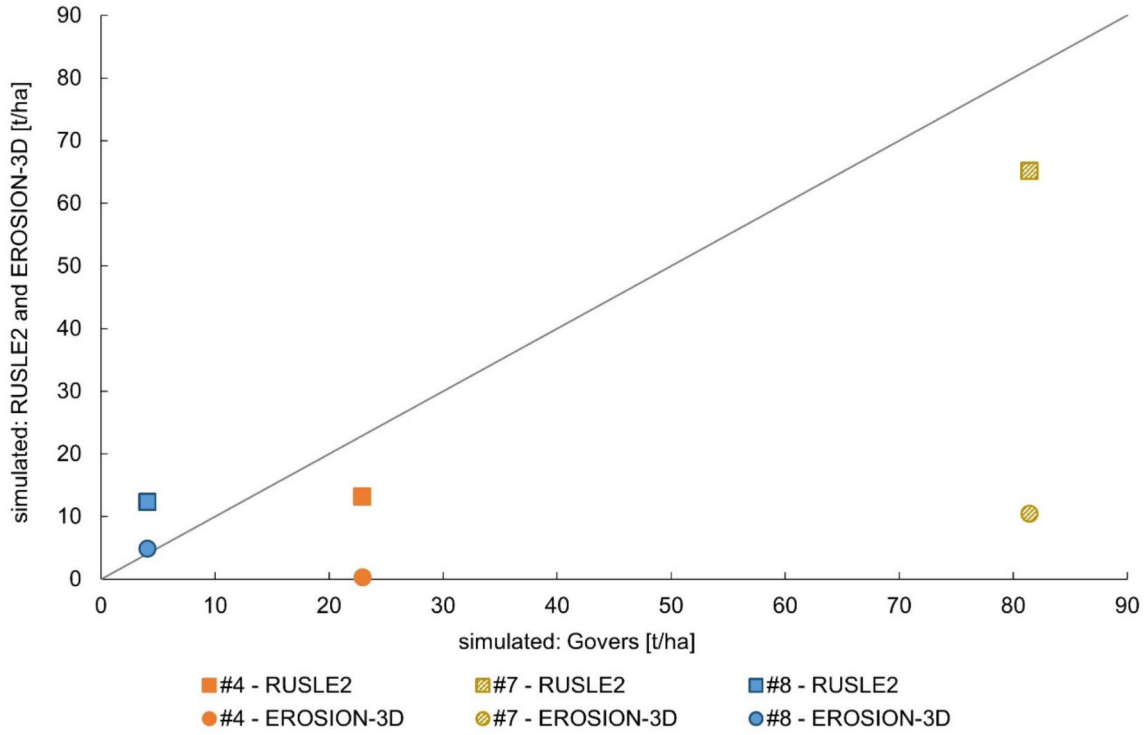

Figure 5-4: Comparison of the total erosion rate [t/ha] using the Govers approach (Exp. DEM1) (x-axis) and the RUSLE2 (y-axis, rectangle) or E3D (y-axis, dot) for different croplands (#4, #7, and #8).

Table 5-9: Statistics for the difference between the RUSLE2 and E3D model results and the results of the HydroAS GS–Govers model Exp. DEM1 and Exp. DEM1 Cali. Mean = Mean value, MAE = Mean Absolute Error, RMSE = Root Mean Square Error (all values in t/ha).

	RUSLE2 – HydroAS GS–Govers (Exp. DEM1)	**RUSLE2 – HydroAS GS–Govers (Exp. DEM1, Cali)**	**E3D – HydroAS GS–Govers (Exp. DEM1)**	**E3D – HydroAS GS–Govers (Exp. DEM1, Cali)**
Mean	-5.94	-74.96	-30.95	-99.97
MAE	11.44	74.96	31.46	99.97
RMSE	11.96	110.81	43.02	127.61

All simulations were conducted using standard parameter values. While HydroAS GS–Govers and RUSLE2 did not have many calibration parameters, E3D provided several opportunities to calibrate the model results. However, the comparative values were obtained from the literature, and the aim of this study was not to calibrate RUSLE2 or E3D.

In conclusion, the HydroAS GS–Govers and RUSLE2 models produced comparable results, although RUSLE2 was easier to apply and more time efficient. This overall good agreement with RUSLE2 aligns with the observations of Batista (2025), who reported on the prevalence of USLE family models in the literature on soil erosion modeling. However, RUSLE2 only provides an estimate for the entire field and offers no information on the occurrence of rill erosion. In contrast, grid-based models, such as E3D and HydroAS GS–Govers, can sim-

ulate accumulated discharge and resulting accumulate erosion. Here, computational efficiency is reduced when using a 2D hydraulic approach compared with the simplified hydraulics used in E3D. However, the focus of this study was to apply and analyze the impact of the 2D model, making the computational cost and efficiency less relevant.

5.3.3.3 Rill Erosion

In this study, both the HydroAS GS–Govers and E3D models indicated rill erosion. Rills were identified visually using varying symbologies and hillshades, following the method described by Hinsberger (2024). In field #4, E3D simulated one rill, whereas HydroAS GS–Govers simulated two naturally occurring rills (#4.1–4.2). In field #7, the natural event formed ten rills, of which E3D simulated two and HydroAS GS–Govers simulated four (#7.6–7.10). In field #8, both models simulated one rill that occurred in the thalweg during the rainfall event. The rill identifiers were assigned according to the system in Hinsberger (2024) and are shown in Figure 5-5.

The spatial distribution of simulated rills matched well with that of the orthophotos in both models. A comparison between the orthophotos and the HydroAS GS–Govers simulation results is presented in Figure 5-5. In field #4 (Figure 5-5a and b), both rill types–the two large rills (#4.1 and #4.2) and many smaller rills that occurred during the natural event–are visible in the HydroAS GS–Govers simulation. Field #7 (Figure 5-5c and d) reproduced many rills that occurred during the event in the simulation. In field #8, one large rill in the thalweg (#8) appeared in both the orthoimage (Figure 5-5e) and simulation results (Figure 5-5f).

Thus far, the HydroAS GS–Govers model has shown greater accuracy in simulating the spatial distribution of rills. RUSLE2 does not provide any information on rill distribution, and E3D consistently simulated fewer rills than observed. The advantage of simulating rills using a 2D hydraulic model was also demonstrated by Jia et al. (2023). They found that the evolution of the channel network was accurately simulated.

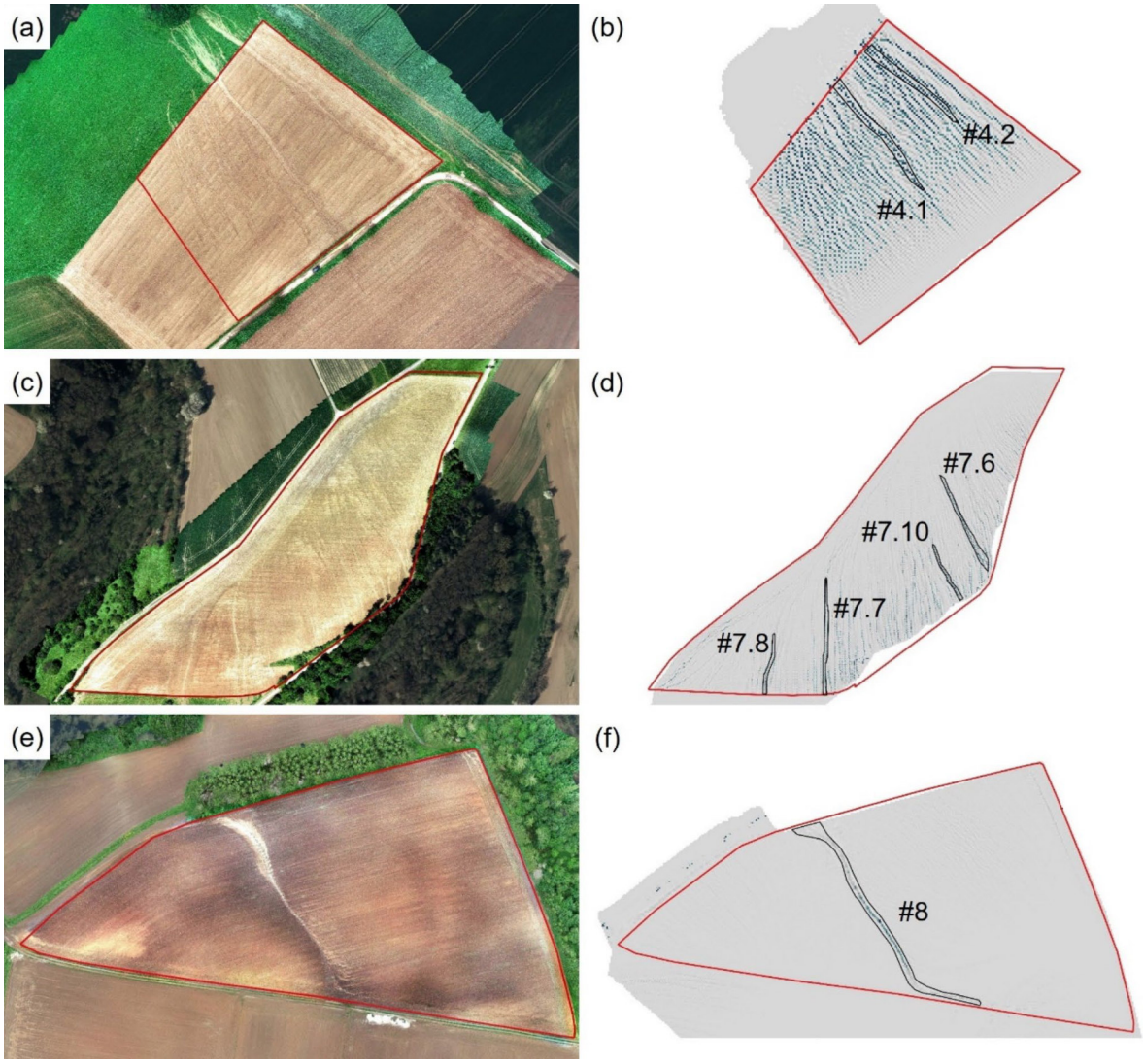

Figure 5-5: Orthophotos and simulation results of HydroAS GS–Govers (Exp. DEM1 Cali) shown as elevation changes using hillshades, with changes ≥ 1 cm for fields #4, (a) and (b); #7, (c) and (d); and #8, (e) and (f). The black outline indicates the identified rills and their corresponding names. Orthophotos (a), (c), and (e) are edited for better visibility of the rills.

The HydroAS GS–Govers model produced results for water depth, flow velocity, and discharge using the hydraulic approach, and sediment transport using the erosion approach. Figure 5-6 shows the discharge and sediment load hydrographs at the end of each rill. A comparison of rill erosion quantities in Table 5-7 with the cumulative sediment load reveals a significant discrepancy. For instance, rill #8 exhibited an erosion quantity of 15.42 tons as calculated from the erosion depth, whereas the sediment load reaching the end of the flume was only 1.66 tons for Exp. DEM1 (Cali). This indicates that a large portion of the eroded material was deposited in the field and did not reach the end of the rill. However, the simulation results imply that sedimentation mostly occurred in the field, rather than neighboring areas, contrary to the apparent erosion observed in the orthophotos.

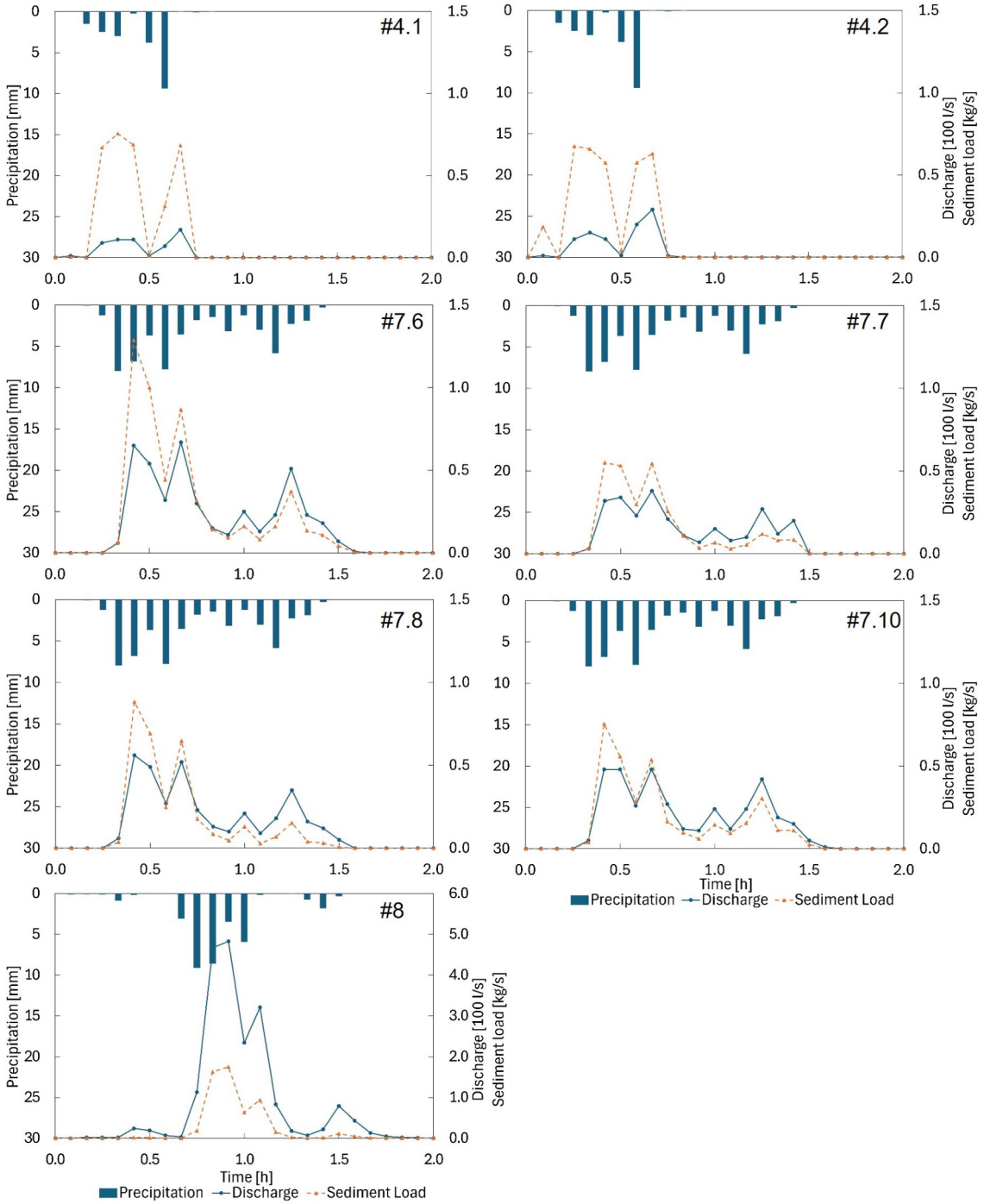

Figure 5-6: Results from simulations Exp. DEM1 (Cali): Discharge (blue line) and sediment load (orange, dashed line) hydrographs at the end of the rills and precipitation input of the model (blue bars). Discharge / Sediment load axis for #8 differs from the others.

In addition to the spatial distribution, the accuracy of rill erosion quantities is an important factor in evaluating model quality. To evaluate the rill erosion quantities, the results of HydroAS GS–Govers, E3D, and RUSLE2 (applied to the rill catchment area) were compared with the measured rill erosion for fields #4, #7, and #8. For the HydroAS GS–Govers model, the uncalibrated (Exp. DEM1) and the model calibrated using observed data (Exp. DEM1 Cali) were analyzed.

Figure 5-7 shows comparisons between the measured data with the model results of HydroAS GS–Govers Exp. DEM1, Cali (Figure 5-7a); Exp. DEM1 (Figure 5-7b); RUSLE2 (Figure 5-7c); and E3D (Figure 5-7d). The uncalibrated HydroAS GS–Govers model (Figure 5-7b) tended to underestimate rill erosion for most rills, particularly in fields #4 and #8, as well as rill #7.8. These rills were larger than others and suffered more erosion. Rill #7.10, which was smaller and less pronounced (Table 5-2; Figure 5-5d), was overestimated using the HydroAS GS–Govers model. Overall, the simulation resulted in a mean difference of -5 tons. The calibrated HydroAS GS–Govers achieved better results with a mean difference of -0.36 tons. RUSLE2 results were comparable, with large rills being overestimated and smaller rills aligning more closely to the measurements, showing a mean difference of -6.5 tons. In contrast, E3D results indicated an even greater underestimation of the measurements, with a mean difference of -13 tons in erosion. Overall, the statistical values of the observed and simulated erosion quantities (Table 5-10) show that HydroAS GS–Govers fits the measurements better than other models, particularly when calibrated.

A comparison of the rill erosion quantities of the HydroAS GS–Govers model with those of RUSLE2 and E3D showed that RUSLE2, applied to predefined rill catchments, delivered estimates of the same order of magnitude as HydroAS GS–Govers. In contrast, E3D produced much lower erosion estimates for both the total and rill erosion rates. Given that this study aims to assess the advantages of a 2D hydrodynamic numerical approach, a comparison of grid-based models is particularly relevant. HydroAS GS–Govers offers several advantages, including the consideration of precise hydraulics and adaptability to complex topography, improving flow and erosion calculations. Its superior ability to simulate rill formation in terms of spatial distribution and erosion quantities holds promise for future soil erosion modeling.

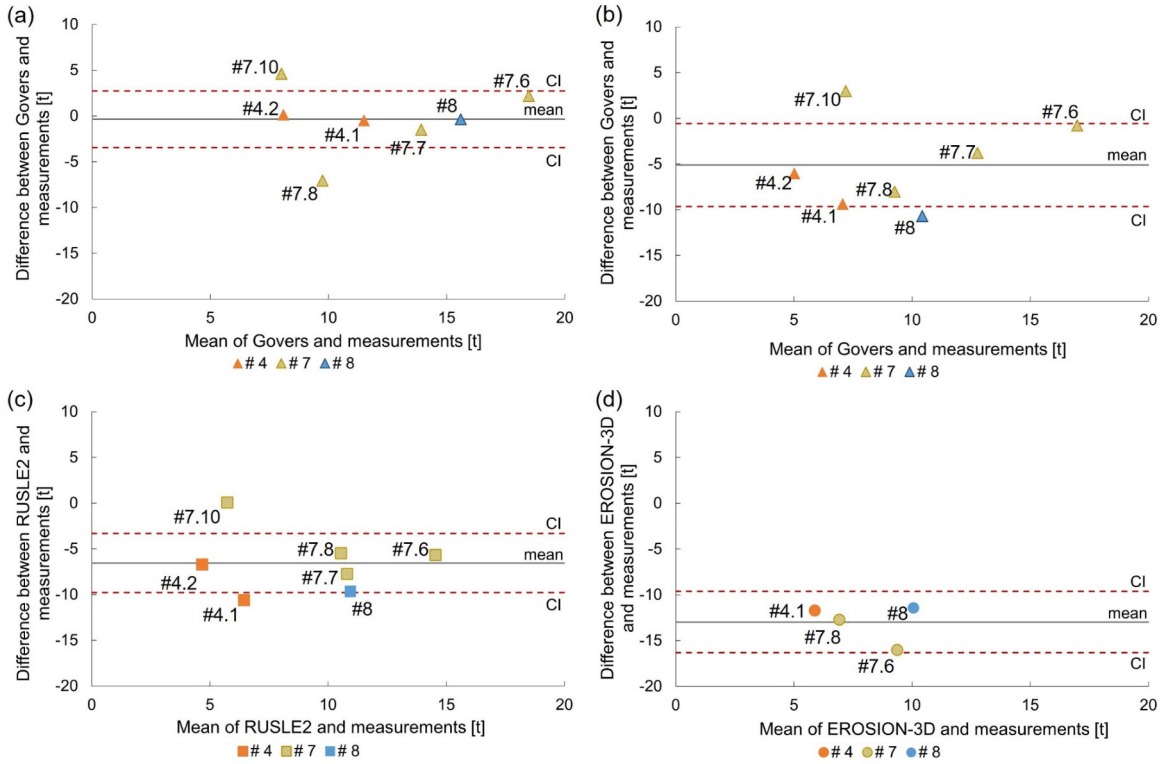

Figure 5-7: Bland-Altman plots comparing the calibrated HydroAS GS–Govers model (Exp. DEM1 Cali) (a), the uncalibrated HydroAS GS–Govers model (Exp. DEM1) (b), RUSLE2 (c), and E3D (d). Each data point represents one rill, with different colors representing different fields. The confidence interval (CI) was calculated as the sum of the mean and the quotient of the t distribution (95 %, n-1) *standard deviation and the square root of n.

Table 5-10: Statistics comparing the difference between the observed erosion and the results of the RUSLE2, E3D, and HydroAS GS–Govers model Exp. DEM1 and Exp. DEM1 Cali. Mean = Mean value, MAE = Mean Absolute Error, RMSE = Root Mean Square Error, NSE = Nash–Sutcliffe efficiency coefficient. (All values in tons)

	Observed – RUSLE2	**Observed – E3D**	**Observed – HydroAS GS–Govers (Exp. DEM1)**	**Observed – HydroAS GS–Govers (Exp. DEM1 Cali)**
Mean	-6.55	-12.98	5.11	-0.36
MAE	6.56	12.98	5.96	2.34
RMSE	7.30	13.11	6.84	3.35
NSE	0.86	0.77	0.85	0.94

5.4 Conclusions

This study investigated the Govers approach as a TC approach integrated with the 2D hydrodynamic numerical model HydroAS. Comparisons of the validity ranges for different TC confirmed that the Govers approach is suitable for soil erosion modeling. Using this combined 2D hydraulic and soil erosion model, plot-scale and event-scale data were successfully simulated. Comparisons between observed and simulated erosion plot data demonstrated that the approach is suitable for the entire validity range of the slope and for higher values as well as lower grain diameters than those shown in the validity range. However, the maximum grain diameter used by Govers should not be exceeded.

Simulations of event-based sheet and rill erosion showed substantial improvements over existing models. Regarding the spatial rill distribution, results corresponded well with the orthophotos of a natural event and outperformed E3D in simulating rill formation. Accurate rill formation and distribution modeling is important for planning and analyzing countermeasures against flooding and erosion, such as deriving nature-based solutions (e.g., agroforestry). The quantitative results of the uncalibrated HydroAS GS–Govers model indicated accurate sheet erosion quantity estimations compared to RUSLE2, and plausible estimations for small rills compared to observed data. However, erosion in large rills was often underestimated. This is consistent with conditions used in Govers (1990) experiments, at shallow water depths. For larger rills, calibration improved accuracy and demonstrated that observed data could be approximately simulated through parameter adjustment. However, calibration factors, such as soil properties, precipitation intensity, or quantity, needs to be investigated in more detail in order to improve the understanding of their influences.

Sensitivity analysis showed that grid resolution was a significant factor in determining erosion quantity, especially for small rills.

Unlike other models, such as EUROSEM and WEPP, this approach does not limit transport capacity based on the sediment load of the discharge. As the modeling results showed an underestimation of erosion compared to the measured data, the approach did not indicate any further limitations on the erosion rates.

The proposed method used a simple erosion approach to estimate the minimum erosion of croplands for a single heavy precipitation event. However, this approach should be enhanced by additional parameters and processes such as infiltration. It is also important to note that further erosion resulting from discharge pathways, such as at the wayside of a road and subsequent undercutting, was outside the scope of this study.

6 Synthesis

6.1 Summary of the Key Findings

Several research questions (RQ) were outlined in Section 1 of this thesis. To address this, various investigations, analyses, and assessments were conducted and results were provided in Sections 2 to 5.

In this thesis, the main objective was to simulate precisely calculated hydraulics and soil erosion. Section 2 focused on the accuracy of hydraulic modeling using the 2D HydroAS model. Surface roughness, a crucial factor in flow simulation, was empirically investigated for overland flow conditions to assess its transferability from channel flow. This investigation provided a basis for accurately modeling the hydraulics of overland flow. The main findings of this study are summarized in the responses to RQ1 and RQ2.

For the combination of hydraulic and soil erosion modeling, a transport capacity approach suitable for overland flow conditions, particularly for large slope gradients, was selected. The approach by Govers (1990) met all requirements and was integrated into the HydroAS model. The combined model is referred to as HydroAS GS–Govers. Details on the selection criteria are presented in the response to RQ3.

A significant part of this work involved calibrating, validating, and evaluating the new model. To achieve this, erosion data were collected using a UAV. The UAV's capability to record tilled and untilled cropland soils, as well as rill erosion, was examined. These findings were crucial in determining the accuracy of the UAV-generated DEMs, which served as the foundation for erosion quantity analyses. The key findings of this study are outlined in response to RQ4.

Erosion resulting from heavy precipitation was monitored using a UAV over three years, and the spatial distribution and quantities of erosion were analyzed. The observed data were used to assess and compare the soil erosion modeling capabilities of existing erosion models, such as RUSLE2 and EROSION-3D, which employ simplified hydraulic approaches, alongside the new HydroAS GS–Govers model. This comparison aimed to explore the impact of enhanced hydraulics on soil erosion prediction. The outcomes of this analysis are presented in response to RQ5 and RQ6. Furthermore, the ability of the HydroAS GS–Govers model to simulate erosion rills was evaluated. While existing models like WEPP differentiate between rill and interrill areas, the new model does not. Given the significance of rill formation in modeling, this aspect was thoroughly investigated and discussed in response to RQ7.

The subsequent sections provide a summary of the main findings and responses to the research questions.

RQ1: How do water depth and slope influence roughness parameters for hydraulic modeling?

Until now, roughness values derived from channel flow conditions, specifically high water depths and low slopes, have been applied to overland flow calculations with low water depths and high slopes. In this study, laboratory experiments were conducted with different surface roughness, various discharges, water depths, and slopes to examine the impact of water depth and slope on roughness values. The experimental results showed that roughness does not exhibit a clear dependence on slope but is dependent on water depth for certain surfaces. Two main surface conditions were distinguished:

- Solid surfaces consistently exhibited a smooth roughness with a reasonable roughness coefficient k_N. There was no observed correlation between water depth and roughness coefficients.
- Vegetated surfaces showed a significant correlation between water depth and roughness coefficients.

Vegetated surfaces showed different influences on roughness depending on the degree of submergence. There is a distinction in roughness values for i) submerged vegetation, where water depth is greater than the vegetation height (submergence > 1), and ii) emergent vegetation, where water depth is lower than the vegetation height (submergence < 1).

- For submerged vegetation (such as artificial grass), roughness values (Darcy-Weisbach's f, Manning's n) decrease with increasing water depth and submergence. Therefore, increasing water depth results in a smoother roughness value, while decreasing water depth leads to a rougher value.
- For emergent vegetation (such as wheat), roughness values (Darcy-Weisbach's f, Manning's n) increase with increasing water depth. The effect is opposite to that of submerged vegetation.

Figure 6-1 summarizes these findings schematically. The results of this study and the literature (Abrahams et al., 1990, 1994; Nepf, 2012) indicate that the influence of water depth on roughness changes with a submergence of 1 (change from submerged to emergent). Therefore, the maximum roughness is reached when the water depth is equal to the vegetation height.

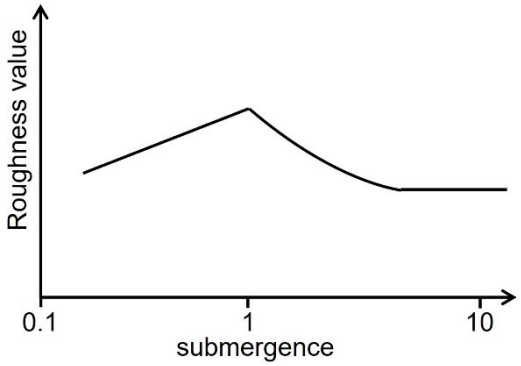

Figure 6-1: Principle of the influence of submergence (water depth/vegetation height) on roughness (Darcy-Weisbach's f, Manning's n) for vegetated surfaces (Nepf, 2012; modified).

According to previous studies (Augustijn et al., 2008; Gualtieri et al., 2018; Huthoff et al., 2007), the roughness approaches a constant value when the water depth is significantly greater than the vegetation height. A submergence greater than 5 is mentioned in the literature referenced. The results of the present study indicate that roughness remains constant at a submergence greater than 6 or 7.

RQ2: Which roughness values are most suitable for an accurate calculation?

No dependency of slope or water depth was detected for solid surfaces. Therefore, assuming constant roughness values based on existing literature for channel flow conditions is reasonable.

For vegetated surfaces, it is appropriate to consider roughness coefficients that are related to water depth. Simulations using a 2D model showed that water depth–dependent roughness values for submerged vegetation lead to retention and translation effects, as opposed to using constant values from the literature. This is because shallow water with low submergence flows with more resistance and at a slower rate. Therefore, accurate consideration of roughness plays a crucial role in the catchment response. In practice, roughness values for submerged vegetation are adjusted based on water depth. However, emergent vegetation has not been taken into account yet, even though its influence can be just as significant as submerged vegetation, but in the opposite direction.

RQ3: Which erosion approach is suitable for heavy precipitation framework conditions?

In Section 5, the hydraulic model HydroAS was combined with an erosion approach. The process of selecting a suitable erosion approach was discussed.

In the literature, several erosion approaches have been developed to estimate transport capacity (TC). These approaches are usually derived from experiments conducted under specific setups and soil properties. Therefore, each approach is only valid within the experimental conditions for which it was designed (Brazier et al., 2011). A comparison of the validity ranges for grain diameter and slope showed that the TC approaches, commonly used in existing soil erosion models, are not always suitable for overland flow conditions. For example, the Meyer–Peter and Müller (MPM), Ackers-White, and Engelund-Hansen approaches are valid mainly for small slopes (<4 %), indicating river conditions and a wide range of grain diameters. In contrast, the Govers approach is valid across a much wider slope range (<21 %), including overland flow conditions, and a more limited range of grain diameters. Additionally, an evaluation of slopes of natural erosion fields showed that the slope conditions fit the validity range of Govers significantly more.

One shortcoming shown in the simulation results using the HydroAS GS–Govers model was the influence of grain diameter exceeding the validity range of the Govers approach.

RQ4: How accurately can soil erosion be recorded using a UAV?

Calibration data were generated to evaluate the combined hydraulic and erosion model. In Section 3, UAV-generated data was analyzed and compared with manual measurements to assess data quality. Results were obtained in terms of the accuracy of recording i) the soil surface with different conditions (untilled/tilled) and ii) rill erosion width and depth.

The results revealed that untilled, even soil surfaces (low microrelief) can be accurately detected with an RMSE of 1.91 cm (using GCP). The detection error rates of tilled soils were higher, with an RMSE of 4.63 cm. The surface conditions of croplands investigated in Section 4 were comparable to the conditions for untilled, even soil surfaces.

The accuracy of linear erosion in UAV-based DEMs showed different results for rill width and depth:

- The rill widths were accurately recorded with an RMSE of 10.8 cm for rills up to 350 cm wide. The values are scattered, showing both underestimation and overestimation, with a total mean of 3.7 mm.
- The rill depths were underestimated by the digital elevation model (DEM) generated from UAV data, with an RMSE of 2.1 cm for rills up to 20 cm deep.

This underestimation of rill depth in UAV-generated DEMs results in a corresponding underestimation of observed erosion volume and quantity by approximately 10 % and up to a

maximum of 20 %. Therefore, the erosion quantities used for calibration should be considered as minimum erosion estimates.

RQ5: How well can existing erosion models using simplified hydraulics simulate erosion caused by heavy precipitation?

Two existing erosion models, RUSLE2 and E3D, were used to simulate heavy precipitation-induced soil erosion. The erosion data observed in this study were applied to these models and used to evaluate the models in Section 4.

RUSLE2 is a member of the USLE family and uses empirically derived relationships for rainfall erosivity, soil erodibility, slope length and gradient, crop management and protection factors. Hydraulics are not considered separately from the soil erosion process in this model. The RUSLE2 model allows for the calculation of total erosion and only the sheet erosion share (USDA, 2013). Consequently, it is possible to draw conclusions about the share of rill erosion. Since RUSLE2 is a lumped model, the spatial distribution of the modeling results is not available. Therefore, only the erosion quantities were analyzed for this model. To evaluate the suitability of the RUSLE2 model for calculating erosion due to heavy precipitation, observed erosion data were used for comparison. As only rill erosion data could be provided due to the methods of recording erosion, the rill share of RUSLE2 was compared to the observed rill erosion data. The comparison revealed that for most rills, the erosion rate of the natural events was higher than the calculated rate using RUSLE2. The analysis showed that the rill expansion was decisive for the differences in the suitability of RUSLE2 to simulate fitting results. Larger and more pronounced rills led to higher deviations between RUSLE2 and observed data, while smaller rills resulted in lower deviations. Strong erosion caused a higher error in RUSLE2, as larger rill systems were formed. This may have been because many small rills showed a similar amount of erosion, or the erosion type recorded by the calibration data of the RUSLE2. Erosion rates obtained using the RUSLE2 underestimated the linear erosion quantities because linear erosion was not considered.

E3D calculates hydraulic and erosion processes on a grid basis. The simplified hydraulic approach for E3D was employed in this study, utilizing a series of GIS applications to calculate flow. E3D produced both sheet erosion and rill erosion. Sheet erosion occurred across the entire field, while rills were formed in flow paths. However, the number of rills and the amount of rill erosion were only a fraction of what was observed in natural events. The erosion quantities observed in natural events were always higher than those calculated using E3D, resulting in a significant underestimation of rill erosion quantities in E3D. This underestimation is evident in both the formation of rills and the quantity of rill erosion.

Both the RUSLE2 and E3D models underestimated the occurrence of erosion rills. Overall, linear erosion was not adequately reproduced by the existing erosion models used in this study.

RQ6: Can the use of an improved hydraulic approach also enhance soil erosion predictions compared with existing erosion models?

In Section 5, the HydroAS GS–Govers model was presented and applied to natural erosion events. The simulation results were then compared with those of existing erosion models, RUSLE2 and E3D.

Compared to RUSLE2 and E3D, the HydroAS GS–Govers model accurately calculates hydraulics and represents an improvement in erosion simulation. Erosion quantities were compared among observed data and simulation results to evaluate i) the total erosion quantity in the field, ii) the rill erosion quantity, and iii) the spatial distribution of rills.

Total erosion rates were not directly observed; therefore, only simulation results using different models were compared at this stage. Results from RUSLE2 and the uncalibrated HydroAS GS–Govers model were in the same order of magnitude, likely due to the experimental conditions underlying the Govers equation. Overland flow conditions with high slopes and shallow water depth were used, similar to data used for USLE family models. E3D showed significantly lower total erosion rates.

While the RUSLE2 model provided good results and is easy to use, it does not provide spatial distribution for rill erosion and sedimentation. In HydroAS GS–Govers, rills were formed during the simulation, indicating an improvement in existing models. These rill formations are attributed to the driving forces of accumulated flow and the adaptation of the topography at each time step using the Exner equation. The spatial distribution of the rills closely matched that of observed rills after a natural event, with more rills generated compared to the previously models mentioned. However, not all rills from the natural rill system were replicated.

The accuracy of erosion quantity simulated in HydroAS GS–Govers, when compared to observed data, relied on rill expansion. Small rills were accurately reproduced, but large rills were underestimated. A calibration factor, specific to cropland types, was necessary for more accurate results. Despite this, statistical analysis of observed and simulated erosion quantities indicated that HydroAS GS–Govers align better with measurements than other models, especially when calibrated.

RQ7: Can rills be simulated in terms of their location and quantity without differentiating between rill and interrill areas, as in existing models?

In the evaluation of the HydroAS GS–Govers model, total and rill erosion were analyzed in Section 5. The results of the HydroAS GS–Govers model showed erosion occurring as sheet erosion and in deepened rills. A low erosion depth was evident across the entire field, and the deepening rills, influences by changes in topography (Exner equation), indicated the impact of flow paths and driving forces on the soil in those areas. Qualitatively, the location of the rills aligns well with observed rills from natural events.

The grid resolution proved to be a significant factor when estimating rill quantities. Small rills were overestimated with a 1 m grid size, while a higher resolution of 0.25 m resulted in more accurate simulation results compared to the observed data.

Additionally, erosion quantities in large rills were often underestimated, consistent with conditions observed in Govers (1990) experiments at shallow water depths. Calibration for larger rills improved accuracy and demonstrated that observed data could be approximated through parameter adjustments. This suggests that a distinction between rill and interrill areas is reasonable, even if it has not yet been implemented. A practical, empirical approach could involve the use of a water depth-dependent or flow velocity-dependent calibration factor for rill areas. A more process-oriented approach could involve utilizing another TC approach in rill areas that shows better validity for high water depths, potentially even an approach for channel flow. However, the validity ranges for large slopes and small grain diameters, as explored in this study (Section 5.3.1), should be taken into consideration. Further studies should investigate suitable water depths or flow velocities as threshold values for changing TC approaches.

6.2 Assessment of the Research Results

Section 2 focused on improving hydraulic modeling by adopting a precise approach for roughness values. At present, a constant roughness value is applied for solid surfaces, which aligns with the findings of this study. In recent years, water depth-dependent roughness values have been introduced for submerged vegetation (LUBW, 2020). However, the guidelines for flash flood modeling in Germany (LUBW, 2020) do not currently account for an increase in roughness with increasing water depth for emergent vegetation. With this approach, emergent vegetation like wheat fields could potentially slow overland flow more than currently assumed.

Section 5 investigated a combined hydraulic and erosion modeling approach. The aim of using a 2D model for hydraulic modeling was to accurately calculate the hydraulic forces

acting on the soil. Roughness investigations from Section 2 were conducted based on this. However, no laboratory experiments were conducted for bare soil surfaces due to limitations in the model layout. Therefore, roughness coefficients to model soil surfaces were assumed based on values from the literature.

The comparison of observed erosion data and simulation results using the HydroAS–GS Govers model revealed an underestimation of the soil erosion quantity in the modeling results. However, there are various indications that the underestimation of observed erosion quantities is even higher than simulations suggest. The reasons for this are as follows:

- Inaccuracy of observed erosion data
  Investigations into the accuracy of DEM data generated by the UAV have shown that rill erosion can be up to 20 % higher than observed. Thus, the differences between observed and simulated data using the Govers approach would likely be even greater than indicated in this study.
- Total precipitation as provided for an event as simulation input
  Since no discharge measurements were taken for the recorded erosion events, no hydraulic calibration was performed. The precipitation data, provided by the DWD, was used unmodified for the simulations. While this is reasonable considering that the soil may dry out in early summer and during events, incorporating a discharge coefficient would result in less surface runoff and reduced erosive forces on the soil.

The main objective of this thesis was to develop a soil erosion model using accurately calculated hydraulics with a 2D model. The evaluation of total erosion quantities, rill erosion quantities, and rill distribution showed that the HydroAS GS–Govers model improved the soil erosion model compared to existing models and provided plausible results for small rills. However, large rills are underestimated in the model and require calibration. In a broader view, accurate rill formation and distribution modeling is important for planning and analyzing countermeasures against flooding and erosion, such as deriving nature-based solutions (e.g., agroforestry).

Section 5 primarily focused on the correct calculation of erosion quantities. However, comparisons of soil erosion quantities and transport rates at the end of the flume indicated that soil deposition primarily occurred in the field and only a small fraction of sediment was transported to neighboring areas. This contrasts with observed UAV-orthoimages, where sedimentation areas downstream of the erosion fields are apparent. Therefore, detachment was not sufficiently represented in the current version of the HydroAS GS–Govers model. This may be attributed to the implemented erosion and transport processes, where sediment is only treated as bedload. This assumption is a simplified approach, as sediment is

transported as suspended load to a large extent. Further investigations have already shown an improvement in sedimentation processes by treating sediment as both bedload and suspended load. However, special attention must be given to the sink velocity value for sediments to accurately consider sedimentation processes.

6.3 Research Limitations

Several limitations were acknowledged in the studies conducted for this thesis.

In overland flow simulations, hillslopes are of particular interest, especially considering the high gradients in the catchment area. However, the 2D model uses depth-averaged shallow water equations that are only valid for slopes ≤ 0.1 (Maniak, 2016; Yörük, 2008) (see Section 1.2.2.1). These circumstances were neglected in this work, as well as in practice.

In the study on roughness values suitable for overland flow simulations, both solid and vegetated surfaces were investigated in laboratory experiments. However, no experiments on the roughness of bare soil surfaces were carried out. Therefore, no suitable values were derived, and all simulations using the HydroAS GS–Govers model were conducted with roughness coefficients mentioned in the literature. Additionally, since no information was available on the differences between surface roughness and sediment roughness, this distinction was neglected.

The erosion processes of detachment, transport, and deposition are introduced in Section 1 of this thesis. The TC approach by Govers (1990) was selected for implementing erosion processes in the 2D model. This approach is used in the model to consider flow-induced forces acting on the soil, focusing on the detachment and transport of sediment caused by flow. Splash erosion detachment is not considered in the HydroAS GS–Govers model, but it is assumed that the splash effect breaks down soil aggregates, providing loose soil particles for sediment transport. The median grain diameter d_{50} of the fine soil was used as an input parameter for the simulations, without making assumptions about aggregate sizes.

Furthermore, the Govers approach is empirically derived and includes a threshold value for detachment that is valid for specific grain diameters. In some conditions, this threshold value was exceeded, but the impact of this limitation was addressed in the subsequent studies.

The usability of the HydroAS GS–Govers model was investigated in Section 5. It is important to note that the new model was only tested on three croplands with rill erosion. While efforts were made to include different topographies and rill types, the model's applicability is limited by the small number of tests. Additionally, applying the model to cropland affected by heavy

precipitation but without visible rills could also be reasonable to evaluate the model accuracy. Furthermore, the sensitivity of the HydroAS GS–Govers model was analyzed in terms of mesh resolution. Simulations were conducted using grid resolutions of 1 m and 0.25 m. In overland flow simulations, water depth can be relatively small. A smaller grid resolution of 0.25 m may result in a combination of small values that could lead to numerical instabilities.

6.4 Practical Applications

The results of the studies in Sections 2–5 have wide applicability as they cover various topics.

In Section 2, roughness values were empirically derived for submerged and emergent vegetation as well as solid surfaces. These values can be utilized to enhance the accuracy of flash flood simulations and produce rainfall hazard maps. In this study, a novel approach for the sand-grain roughness k_N, where resistance decreases with increasing water depth, was proposed for submerged vegetation. Based on the findings of the experimental work, this approach has already been implemented in practice (LUBW, 2019). Currently, all vegetation approaches consider a decrease in resistance with increasing water depth. However, this work and previous studies showed an increase in resistance with increased water depth for emergent vegetation. In practice, the application of these findings could slow overland flow on croplands and lead to retention effects.

Additionally, this thesis introduced the novel HydroAS GS–Govers model. Soil detachment, transport, and deposition can be simulated using this model.
For model calibration and validation, erosion data were generated using a UAV. The workflow for recording and analyzing erosion compiled in this study can be applied to further croplands affected by erosion. An expansion of high-quality erosion data can be used to further improve the HydroAS GS–Govers model and to address additional research questions. Simulation results of the HydroAS GS–Govers model can be used to assess areas of soil erosion and sedimentation on croplands, neighboring areas, adjoining ecosystems, and receiving waters. Both the spatial and quantitative damaging effects of erosion and sedimentation can be evaluated to identify croplands prone to erosion. The spatial distribution of areas at risk for erosion and sedimentation can be detected. Furthermore, the amount of soil loss can be quantified. Soil loss not only reduces cultivation potential but can also have a negative impact on other ecosystems. Furthermore, estimating the associated transport of pesticides and nutrients from the eroded sediment can help identify potential sources of environmental damage.

In addition to the hazard assessment of erosion and sedimentation, the model can serve as the basis for assessing and proving the functionality of potential countermeasures. Section 4 determined that a soil cover of more than 25 % is sufficient to protect the soil from erosion. Hence, an effective countermeasure could be reducing bare soil in identified vulnerable areas. Cornfields, in particular, are known for providing bare soil in early summer when heavy precipitation occurs. Thus, reducing these arable crops in hazard and risk areas can be a useful option to minimize erosion damage.

When erosion cannot be prevented, rill erosion, in particular, leads to a high sediment transport rate and, consequently, to a high share of soil loss. These areas require particular attention. The influence of countermeasures can be verified using the knowledge about the spatial distribution and amount of rill erosion. Possible countermeasures include implementing agroforestry to reduce cropland slope lengths or establishing riparian zones to protect streams from the influx of sediment. These zones can help slow sediment transport and decrease the influx of pesticides and nutrients.

6.5 Future Research

This thesis demonstrates that using a 2D hydraulic model significantly enhances the accuracy of soil erosion modeling results. However, the soil erosion approach is founded on numerous simplifications and assumptions. These simplifications facilitate the determination of relevant input parameters. Incorporating more sub-processes in the erosion approach may increase the complexity of parameterization, but it could also enhance the accuracy of soil erosion detachment, transport, and deposition processes. Striking a balance between practicality and effort is essential for an effective model.

One aspect relevant to multiple parts of this work is the consideration of vegetation. Both surface roughness (Section 2) and erosion processes (Sections 4 and 5) are affected. In Section 4, 456 croplands were investigated after heavy precipitation events. The analysis revealed that erosion occurred in croplands with a land cover of up to 25 %. Consequently, vegetation coverage protects the soil from erosion and represents resistance to hydraulic forces acting on the soil. In the current study and version of the HydroAS GS–Govers model, bare soil fields were investigated, presenting only a scenario for possible consequences. However, the risk of erosion can be reduced when croplands are covered with vegetation or mulch, and under such conditions, the simulations may not align with real-world outcomes. Therefore, it is reasonable to investigate how erosion evolves with vegetation conditions and to extend the erosion approach by incorporation a vegetation term or the thresh-

old value for detachment must be adapted accordingly. A first approach could be to investigate the differences in shear stress on a surface with and without vegetation. The groundwork for these analyses has been laid in Section 2.

Another important aspect to consider is the impact of soil management. Previous studies have indicated that conventional and conservation tillage have different effects on soil erosion (Dugan et al., 2024). This influence was neglected in this study and presents an opportunity for further investigation.

One primary objective of erosion studies is to gain knowledge about the occurrence and quantity of soil erosion in order to implement effective countermeasures. One objective for future research can be the protection of neighboring ecosystems, such as streams. The influx of soil into streams can lead to the enrichment of the water with nutrients, potentially leading to eutrophication and fish mortality. A sufficient width of riparian stripes can counteract this sediment influx into streams. One application area for soil erosion simulation can be the determination of these widths.

References

Abderrezzak, K.E.K.; Paquier, A.; Mignot, E. (2009). Modelling flash flood propagation in urban areas using a two-dimensional numerical model. Nat. Hazards 2009, 50, 433–460. https://doi.org/10.1007/s11069-008-9300-0

Abood, M.M.; Yusuf, B.; Mohammed, T.A.; Ghazali, A.H. (2006). Manning Roughness Coefficient for Grass-Lined Channel. Suranaree J. Sci. Technol. 2006, 13 (4), 317–330.

Abrahams, A.D.; Parsons, A.J.; Luk, S.-H. (1990). Field experiments on the resistance to overland flow on desert hillslopes. In Erosion, Transport and Deposition Processes, Proceedings of the Jerusalem Workshop, Jerusalem, Israel, March-April 1987; IAHS Publications: Wallingford, UK.

Abrahams, A.D.; Parsons, A.J.; Wainwright, J. (1994). Resistance to overland flow on semiarid grassland and shrubland hillslopes, Walnut Gulch, southern Ariona. J. Hydrol. 1994, 156, 431–446. https://doi.org/10.1016/0022-1694(94)90088-4

Ackers, P.; White, W.R, (1973). Sediment Transport: New Approach and Analysis. J. Hydraul. Div., 99, 11, 2041–2060. https://doi.org/10.1061/JYCEAJ.0003791

Agisoft LLC (n.d.). Software Agisoft Metashape Professional, Version 1.7.1, St. Petersburg, Russia

Aigner, D.; Bollrich, G. (2015) Handbuch der Hydraulik für Wasserbau und Wasserwirtschaft, 1st ed.; Beuth Verlag GmbH: Berlin, Germany, ISBN: 978-3-410-21341-3.

Aksoy, H.; Unal, N.E.; Cokgor, S.; Gedikli, A.; Yoon, J.; Koca, K.; Inci, S.B.; Eris, E.; Pak, G. (2013). Laboratory experiments of sediment transport from bare soil with a rill. Hydrological Sciences Journal, 58 (7). https://doi.org/10.1080/02626667.2013.824085

Al-Fugara, A.; Mabdeh, A.N.; Alayyash, S.; Khasawneh, A. (2023). Hydrological and Hydrodynamic Modeling for Flash Flood and Embankment Dam Break Scenario: Hazard Mapping of Extreme Storm Events. Sustainability, 15, 1758. https://doi.org/10.3390/su15031758

Albert, A. (2020). Schneider–Bautabellen für Ingenieure mit Berechnungshinweisen und Beispielen; 24., revised edition; Reguvis: Köln, Germany. ISBN: 978-3-8462-1140-3.

Amelung, W.; Blume, H.-P.; Fleige, H. et al. (2018). Scheffer/Schachtschnabel Lehrbuch der Bodenkunde, 17., überarbeitete und ergänzte Auflage, Springer Spektrum, Berlin. https://doi.org/10.1007/978-3-662-55871-3

Andualem, T.G.; Hewa, G.A.; Myers, B.R.; Peters, S.; Boland, J. (2023). Erosion and Sediment Transport Modeling: A Systematic Review. Land, 12, 1396. https://doi.org/10.3390/land12071396

Aquaveo LLC (n.d.). Software SMS, Version 13.1.0, Provo, UT, United States

Aquaveo. XMS Wiki. SMS: Mesh Node Triangulation. https://www.xms-wiki.com/wiki/SMS:Mesh_Node_Triangulation (last accessed: 10.03.2023)

Armand, R.; Bockstaller, C.; Auzet, A.-V.; Van Dijk, P. (2009). Runoff generation related to intra-field soil surface characteristics variability. Application to conservation tillage context. Soil & Tillage Research, 102, 27–37. https://doi.org/10.1016/j.still.2008.07.009

Auerswald, K.; von Perger, P. (1998). Bodenerosion durch Wasser – Ursachen, Schutzmaßnahmen und Prognose mit PC-ABAG. Editor: Auswertungs- und Informationsdienst für Ernährung, Landwirtschaft und Forsten (aid) e.V., Bonn, ISBN 3-89661-769-9

Auerswald, K.; Geist, J.; Quinton, J.N.; and Fiener, P. (2025). HESS Opinions: Floods and droughts – are land use, soil management, and landscape hydrology more significant drivers than increasing CO2?, Hydrol. Earth Syst. Sci., 29, 2185–2200, https://doi.org/10.5194/hess-29-2185-2025

Augustijn, D.C.M.; Huthoff, F.; van Velzen, E.H. (2008). Comparison of vegetation roughness description. In Proceedings of Inter-national Conferences on Fluvial Hydraulics (River Flow), Cezme, Izmir, Turkey, 3–5 September 2008; pp. 343–350.

Báčová, M.; Krása, J.; Devátý, J.; Kavka, P. (2018). A GIS method for volumetric assessments of erosion rills from digital surface models. European Journal of Remote Sensing, 52, S1, 96–107. https://doi.org/10.1080/22797254.2018.1543556

Baptist, M.J.; Babovic, V.; Rodríguez Uthurburu, J.; Keijzer, M.; Uittenbogaard, R.E.; Mynett, A., Verwey, A. (2007). On inducing equations for vegetation resistance. J. Hydraul. Res., 45, 435–450. https://doi.org/10.1080/00221686.2007.9521778.

Barbero, G.; Costabile, P.; Costanzo, C.; Ferraro, D.; Petaccia, G. (2022). 2D hydrodynamic approach supporting evaluations of hydrological response in small watersheds: Implications for lag time estimation. J. Hydrol. 2022, 610, 127870. https://doi.org/10.1016/j.jhydrol.2022.127870

Batista, P.V.G., Davies, J., Silva, M.L.N. et al. (2019). On the evaluation of soil erosion models: Are we doing enough?, Earth-Science Reviews, 197, 102898, https://doi.org/10.1016/j.earscirev.2019.102898

Batista, P. (2025). A Lakatosian history of soil-erosion modelling as a scientific research programme, EGU General Assembly 2025, Vienna, Austria, 27 Apr–2 May 2025, EGU25-18554, https://doi.org/10.5194/egusphere-egu25-18554, 2025.

Beasley, D.; Huggins, L.; Monke, A. (1980). ANSWERS: A model for watershed planning. Trans. ASAE, 23, 938–0944. https://doi.org/10.13031/2013.34692

Bellos, V.; Papageorgaki, I.; Kourtis, I.; Vangelis, H.; Kalogiros, I.; Tsakiris, G. (2020). Reconstruction of a flash flood event using a 2D hydrodynamic model under spatial and temporal variability of storm. Nat. Hazards, 101, 711–726. https://doi.org/10.1007/s11069-020-03891-3

Biswas, T.R.; Begam, S.; Dey, S.; Sen, D. (2021). Equilibrium approach for modeling erosional failure of granular dams. Phys. Fluids 33, 043306. https://doi.org/10.1063/5.0039140

Boardman, J.; Favis-Mortlock, D. (Ed.) (1998). Modelling Soil Erosion by Water. NATO ASI Subseries I. Vol. 55. https://doi.org/10.1007/978-3-642-58913-3

Bond, S.; Kirkby, M.J.; Johnston, J.; Crowle, A.; Holden, J. (2020). Seasonal vegetation and management influence overland flow velocity and roughness in upland grassland. Hydrol. Process., 34, 3777–3791. https://doi.org/10.1002/hyp.13842.

Borelli, B.; Alewell, C.; Alvarez, P. et al. (2021). Soil erosion modelling: A global review and statistical analysis. Science of the Total Environment, 780, 146494. https://doi.org/10.1016/j.scitotenv.2021.146494

Brazier, R.E.; Hutton, C.J.; Parsons, A.J.; Wainwright, J. (2011). Scaling Soil Erosion Models in Space and Time. In: Morgan RPC; Nearing MA (Ed.) (2011) Handbook of Erosion Modelling. John Wiley & Sons ISBN: 978-1-4051-9010-7, pp 289–312

Bruno, C.; Di Stefano, C.; Ferro, V. (2008). Field investigation on rilling in the experimental Sparacia area, South Italy. Earth Surf. Process. Landforms, 33, 263–279. https://doi.org/10.1002/esp.1544

Bryan (Ed.) (1990). Soil Erosion – Experiments and Models. Catena Supplement 17.

Bundesministerium für Land- und Forstwirtschaft, Umwelt und Wasserwirtschaft (BMLFUW) and Österreichischer Wasser- und Abfallwirtschaftsverband (ÖWAV) (Ed.) (2011) Fließgewässermodellierung – Arbeitsbehelf Feststofftransport und Gewässermorphologie. AV+Astoria Druckzentrum GmbH, Wien

Cândido, B. M.; Quinton, J. N.; James, M. R.; Silva, M. L. N.; de Carvalho, T. S.; de Lima, W.; Beniaich, A.; Eltner, A. (2020). High-resolution monitoring of diffuse (sheet or interrill) erosion using structure-from-motion. Geoderma, 375, 114477. https://doi.org/10.1016/j.geoderma.2020.114477

Carollo, F.G.; Di Stefano, C.; Ferro, V.; Pampalone, V. (2015). Measuring rill erosion at plot scale by a drone-based technology. Hydrol. Process., 29, 3802–3811. https://doi.org/10.1002/hyp.10479

Carollo, F.G.; Di Stefano, C.; Nicosia, A.; Palmeri, V.; Pampalone, V.; Ferro, V. (2021). Flow resistance in mobile bed rills shaped in soils with different texture. Eur. J. Soil Sci., 72, 2062–2075. https://doi.org/10.1111/ejss.13093.

Carollo, F.G.; Serio, M.A.; Pampalone, V.; Ferro, V. (2024). The unit plot of the Universal soil loss equation (USLE): Myth or reality? Journal of Hydrology, 632, 130880. https://doi.org/10.1016/j.jhydrol.2024.130880

Casalí, J.; López, J.J.; Giráldez, J.V. (1999). Ephemeral gully erosion in southern Navarra (Spain). Catena, 36(1–2):65–84. https://doi.org/10.1016/s0341-8162(99)00013-2

Casalí, J.; Loizu, J.; Campo, M.A.; De Santisteban, L.M.; Álvarez-Mozos, J. (2006). Accuracy of methods for field assessment of rill and ephemeral gully erosion. Catena, 67(2):128–38. https://doi.org/10.1016/j.catena.2006.03.005

Castillo, C.; Pérez, R.; James, M.R.; Quinton, J.N.; Taguas, E.V.; Gómez, J.A. (2012). Comparing the Accuracy of Several Field Methods for Measuring Gully Erosion. Soil Science Society of America Journal, 76(4):1319–32. https://doi.org/10.2136/sssaj2011.0390

Caviedes-Vouillème, D.; García-Navarro, P.; Murillo, J. (2012). Influence of mesh structure on 2D full shallow water equations and SCS Curve Number simulation of rainfall/runoff events. J. Hydrol., 448–449, 39–59. https://doi.org/10.1016/j.jhydrol.2012.04.006

Cea, L.; Legout, C.; Darboux, F.; Esteves, M.; Nord, G. (2014). Experimental validation of a 2D overland flow model using high resolution water depth and velocity data. J. Hydrol., 513, 142–153. https://doi.org/10.1016/j.jhydrol.2014.03.052

Cheng, N.-S. (2011). Representative roughness height of submerged vegetation. Water Resources Research, 47, W08517. https://doi.org/10.1029/2011WR010590.

Chow, V.T. (1959). Open-Channel Hydraulics; McGraw-Hill Book Company: New York, NY, USA.

Comiti, F.; Mao, L.; Wilcox, A.; Wohl, E.E.; Lenzi, M.A. (2007). Field-derived relationships for flow velocity and resistance in high-gradient streams. J. Hydrol., 340, 48–62. https://doi.org/10.1016/j.jhydrol.2007.03.021.

Cook, K.L. (2017). An evaluation of the effectiveness of low-cost UAVs and structure from motion for geomorphic change detection. Geomorphology, 278:195–208. https://doi.org/10.1016/j.geomorph.2016.11.009

Costabile, P.; Costanzo, C.; Ferraro, D.; Barco, P. (2021). Is HEC-RAS 2D accurate enough for storm-event hazard assessment? Lessons learnt from a benchmarking study based on rain-on-grid modelling. J. Hydrol., 603, 126962. https://doi.org/10.1016/j.jhydrol.2021.126962

Costabile, P.; Cea, L.; Barbaro, G.; Costanzo, C.; Llena, M.; Vericat, D. (2024). Evaluation of 2D hydrodynamic-based rainfall/runoff modelling for soil erosion assessment at a seasonal scale, J. Hydrol., 632, 130778. https://doi.org/10.1016/j.jhydrol.2024.130778

David, A.; Schmalz, B. (2020). Flood hazard analysis in small catchments: Comparison of hydrological and hydrodynamic approaches by the use of direct rainfall. J. Flood Risk Manag., 13, e12639. https://doi.org/10.1111/jfr3.12639.

Deltares (n.d.). Software Delft-FEWS, Version 2019.02, Delft, The Netherlands

Deutscher Wetterdienst (DWD). Wetter- und Klimalexikon. Starkregen. https://www.dwd.de/DE/service/lexikon/Functions/glossar.html?nn=103346&lv2=102248&lv3=102572 (last accessed: 02.08.2024)

Deutscher Wetterdienst (DWD). Projekt RADOLAN, Routineverfahren zur Online-Aneichung der Radarniederschlagsdaten mit Hilfe von automatischen Bodenniederschlagsstationen (Ombrometer). Zusammenfassender Abschlussbericht für die Projektlaufzeit von 1997 bis 2004, 2004. https://www.dwd.de/DE/leistungen/radolan/radolan_info/abschlussbericht_pdf.pdf?__blob=publicationFile&v=2 (last accessed: 10.03.2023)

Deutscher Wetterdienst (DWD). RADOLAN: Radar Online Adjustment, Radar based quantitative precipitation estimation products, poster, 2017. https://www.google.com/url?sa=t&rct=j&q=&esrc=s&source=web&cd=&ved=2ahUKEwjK_duoodH9AhX-aSPEDHe6VCRQQFnoECBcQAQ&url=https%3A%2F%2Fwww.dwd.de%2FDE%2Fleistungen%2Fradolan%2Fradolan_info%2Frado-lan_poster_201711_en_pdf.pdf%3F__blob%3DpublicationFile%26v%3D2&usg=AOv-Vaw2xtcS2EXfUWE9LQtc7RuPV (last accessed: 10.03.2023)

De Roo, A.P.J.; Wesseling, C.G.; Cremers, N.H.D.T.; Offermans, R.J.E. (1994). LISEM: a new physically-based hydrological and soil erosion model in a GIS-environment, theory and implementation. In: Variability in Stream Erosion and Sediment Transport (Proceedings of the Canberra Symposium, December 1994). IAHS Publ. no. 224, pp 439–448

DIN Deutsches Institut für Normung (2020). DIN 18125–2:2020-11, Baugrund, Untersuchung von Bodenproben - Bestimmung der Dichte des Bodens - Teil 2: Feldversuche [Soil, investigation and testing - Determination of density of soil - Part 2: Field tests], Beuth, Berlin

DIN Deutsches Institut für Normung (2017). DIN 19708:2017-08, Bodenbeschaffenheit – Ermittlung der Erosionsgefährdung von Böden durch Wasser mit Hilfe der ABAG [Soil quality – Predicting soil erosion by water by means of ABAG], Beuth, Berlin

DIN Deutsches Institut für Normung (2017). DIN EN ISO 17892-4:2017-04, Geotechnische Erkundung und Untersuchung - Laborversuche an Bodenproben - Teil 4: Bestimmung der Korngrößenverteilung [Geotechnical investigation and testing - Laboratory testing of soil - Part 4: Determination of particle size distribution], Beuth, Berlin

Di Stefano, C.; Ferro, V.; Palmeri, V.; Pampalone, V. (2017). Measuring rill erosion using structure from motion: A plot experiment. Catena, 156, 383–392. https://doi.org/10.1016/j.catena.2017.04.023

Di Stefano, C.; Nicosia, A.; Pampalone, V.; Palmeri, V.; Ferro, V. (2019a). Rill flow resistance law under equilibrium bed-load transport conditions. Hydrol. Process., 33, 1317–1323. https://doi.org/10.1002/hyp.13402.

Di Stefano, C.; Nicosia, A.; Palmeri, V.; Pampalone, V.; Ferro, V. (2019b). Comparing flow resistance law for fixed and mobile bed rills. Hydrol. Process., 33, 3330–3348. https://doi.org/10.1002/hyp.13561.

Di Stefano, C.; Palmeri, V.; Pampalone, V. (2019c). An automatic approach for rill network extraction to measure rill erosion by terrestrial and low-cost unmanned aerial vehicle photogrammetry. Hydrological Processes, 33:1883–1895. https://doi.org/10.1002/hyp.13444

Di Stefano, C.; Nicosia, A.; Palmeri, V.; Pampalone, V.; Ferro, V. (2021). Estimating flow resistance in steep slope rills. Hydrol. Process., 35, e14296. https://doi.org/10.1002/hyp.14296.

DJI (2021). PHANTOM 4 RTK: User Manual, v2.4, 2021.07. https://www.dji.com/downloads/products/phantom-4-rtk

D'Oleire-Oltmanns, S.; Marzolff, I.; Peter, K. D.; Ries, J. B. (2012). Unmanned Aerial Vehicle (UAV) for Monitoring Soil Erosion in Morocco. Remote Sensing, 4(11), pp. 3390–3416. https://doi.org/10.3390/rs4113390

DroneDeploy; DJI; Trimble (2019). Measurement Accuracy of the DJI Phantom 4 RTK & Photogrammetry. https://www.dronedeploy.com/resources/ebooks/measurement-accuracy-dji-phantom-4-rtk-drone-photogrammetry/

Dugan, I.; Pereira, P.; Kisic, I. et al. (2024). Temporal Dynamics of Soil Erosion and Nutrient Loss in Croatian Orchard: Experimental Insights into Resilience Mechanisms. Environ. Process., 11, 53. https://doi.org/10.1007/s40710-024-00735-1

Dunn, C.; López, F.; García, M. (1996). Mean Flow and Turbulence in a Laboratory Channel With Simulated Vegetation; Civil Engineering Studies, Hydraulic Engineering Series; University of Illinois: Illinois, USA. http://hdl.handle.net/2142/12229.

Duttmann, R. (2001). Die Bodenfeuchte als Steuergröße der Bodenerosion. Geogr. Rundsch. 53(5), 24–32

DWA Deutsche Vereinigung für Wasserwirtschaft Abwasser und Abfall e. V. (2020). DWA-Regelwerk, Merkblatt DWA-M 921. Bodenerosion durch Wasser – Kartieranleitung zur Erfassung aktueller Erosionsformen [Soil erosion by water – Mapping guideline to record current erosion forms], Entwurf. Druckhaus köthen GmbH & Co KG. Hennef. ISBN: 978-3-88721-853-9

Eltner, A.; Baumgart, P.; Maas, H.-G.; Faust, D. (2014). Multi-temporal UAV data for automatic measurement of rill and interrill erosion on loess soil. Earth Surf. Process. Landforms, 40, pp. 741–755. https://doi.org/10.1002/esp.3673

Engelund, F.; Hansen, E. (1967). A monograph on sediment transport in alluvial streams, teknisk forlag, Copenhagen

Feuerwehr Eppelborn (n.d.). Unwetter: Dramatische Szenen in Dirmingen. https://www.feuerwehr-eppelborn.de/index.php?page=einsatz_details&einsatz_id=3290 (accessed on 09.09.2025).

Ferguson, R. (2021a). Limits to scale invariance in alluvial rivers. Earth Surf. Process. Landf., 46, 173–187. https://doi.org/10.1002/esp.5006.

Ferguson, R.I. (2021b). Roughness calibration to improve flow predictions in coarse-bed streams. Water Resour. Res., 57, e2021WR029979. https://doi.org/10.1029/2021WR029979

Ferro, V. (2017). New Flow-Resistance Law for Steep Mountain Streams Based on Velocity Profile. J. Irrig. Drain. Eng., 143, 1208. https://doi.org/10.1061/(ASCE)IR.1943-4774.0001208.

Ferro, V. (2019). Assessing flow resistance law in vegetated channels by dimensional analysis and self-similarity. Flow Meas. Instrum., 69, 101610. https://doi.org/10.1016/j.flowmeasinst.2019.101610

Ferro, V.; Guida, G. (2022). A theoretically-based overland flow resistance law for upland grassland habitats. Catena, 210, 105863. https://doi.org/10.1016/j.catena.2021.105863.

Forlani, G.; Dall'Asta, E.; Diotri, F.; Di Cella, U.M.; Roncella, R.; Santise, M. (2018). Quality Assessment of DSMs Produced from UAV Flights Georeferenced with On-Board RTK Positioning. Remote Sensing, 10(2):311. https://doi.org/10.3390/rs10020311

García-Feal, O.; González-Cao, J.; Gómez-Gesteira, M.; Cea, L.; Domínguez, J.M.; Formella, A. (2018). An Accelerated Tool for Flood Modelling Based on Iber. Water, 10, 1459. https://doi.org/10.3390/w10101459

García-Pintado, J.; Barberá, G.G.; Erena, M.; Castillo, V.M. (2009). Calibration of structure in a distributed forecasting model for a semiarid flash flood: Dynamic surface storage and channel roughness. J. Hydrol., 377, 165–184. https://doi.org/10.1016/j.jhydrol.2009.08.024.

GeoGnostics (n.d., a). EROSION-3D. Zusatzmodul 'Kinematische Welle'. http://geognostics.de/e3d_kin_wave.html (accessed on 22.08.2025).

GeoGnostics (n.d., b). Software EROSION-3D, Version 3.3.2.3.32, Berlin, Germany

Gerlinger, K. (1997). Erosionsprozesse auf Lößboden: Experimente und Modellierung. Dissertation, Universität Fridericiana zu Karlsruhe (TH)

Gibson, M.J.; Savic, D.A.; Djordjevic, S.; Chen, A.S.; Fraser, S.; Watson, T. (2016). Accuracy and computational efficiency of 2D urban surface flood modelling based on cellular automata. Procedia Eng., 154, 801–810. https://doi.org/10.1016/j.proeng.2016.07.409

Giménez, R.; Marzolff, I.; Campo, M. A.; Seeger, M.; Ries, J. B.; Casalí, J.; Álvarez-Mozos, J. (2009). Accuracy of high-resolution photogrammetric measurements of gullies with contrasting morphology. Earth Surf. Process. Landforms, 34, pp. 1915–1926. https://doi.org/10.1002/esp.1868

Glendell, M.; McShane, G.; Farrow, L.; James, M.R.; Quinton, J.; Anderson, K. et al. (2017). Testing the utility of structure-from-motion photogrammetry reconstructions using small unmanned aerial vehicles and ground photography to estimate the extent of upland soil erosion. Earth Surf Processes Landf, 42(12):1860–71. https://doi.org/10.1002/esp.4142

Gómez-Gutiérrez, Á.; Schnabel, S.; Berenguer-Sempere, F.; Lavado-Contador, F.; Rubio-Delgado, J. (2014). Using 3D photo-reconstruction methods to estimate gully headcut erosion. Catena, 120:91–101. https://doi.org/10.1016/j.catena.2014.04.004

Govers, G. (1990). Empirical relationships for the transport capacity of overland flow. Erosion, Transport and Deposition Processes (Proceedings of the Jerusalem Workshop, March-April 1987). IAHS Publ. no. 189,1990.

Govers, G.; Poesen, J. (1988). Assessment of the interrill and rill contributions to total soil loss from an upland field plot. Geomorphology, 1, 4, pp. 343–354. https://doi.org/10.1016/0169-555X(88)90006-2

Gualtieri, P.; De Felice, S.; Pasquino, V.; Doria, G.P. (2018). Use of conventional flow resistance equations and a model for the Nikuradse roughness in vegetated flows at high submergence. J. Hydrol. Hydromech., 66, 107–120. https://doi.org/10.1515/johh-2017-0028

Hebel, B. (2003). Validierung numerischer Erosionsmodelle in Einzelhang- und Einzugsgebiet-Dimension. In: Basler Beiträge zur Physiogeographie: Physiogeographica, Bd. 32

Held, I.M.; Soden, B.J. (2006). Robust Responses of the Hydrological Cycle to Global Warming. Journal of Climate, 19 (21) pp. 5686–5699. https://doi.org/10.1175/JCLI3990.1

Hessel, R.; Jetten, V.G.; Liu, B.; Qiu, Y. (2011). Evaluating Effects of Soil and Water Management and Land Use Change on the Loess Plateau of China using LISEM. In: Morgan, R.P.C.; Nearing, M.A. (Eds.). Handbook of Erosion Modelling, John Wiley and Sons, chapter 12, pp. 223–248 https://doi.org/10.1002/9781444328455.ch12

Hinsberger, R. (2024). Analysis of heavy precipitation-induced rill erosion. Environ Earth Sci, 83, 354. https://doi.org/10.1007/s12665-024-11671-6

Hinsberger, R.; Biehler, A.; Yörük, A. (2022). Influence of Water Depth and Slope on Roughness—Experiments and Roughness Approach for Rain-on-Grid Modeling. Water, 14, 4017. https://doi.org/10.3390/w14244017

Hu, P.; Lei, Y.; Han, J.; Cao, Z.; Liu, H.; He, Z. (2019). Computationally efficient modeling of hydro-sediment-morphodynamic processes using a hybrid local time step/global maximum time step. Adv Water Resour, 127, pp 26–38. https://doi.org/10.1016/j.advwatres.2019.03.006

Hu, P.; Ji, A.; Li, W.; Tang, X.; Xiao, W.; Cao, Z. (2025). Capacity and Noncapacity Sediment Transport Characteristics in the Overtopping-Induced Dam-Breaching Process. J. Hydraul. Eng., 151(2): 04025001. https://doi.org/10.1061/JHEND8.HYENG-13985

Hu, X.; Song, L. (2018). Hydrodynamic modeling of flash flood in mountain watersheds based on high-performance GPU computing. Nat Hazards, 91, pp. 567–586. https://doi.org/10.1007/s11069-017-3141-7

Huang, W.; Cao, Z.-x.; Qi, W.-j.; Pender, G.; Zhao, K. (2015). Full 2D Hydrodynamic Modelling of Rainfall-induced Flash Floods. J. Mt. Sci., 12, 1203–1218. https://doi.org/10.1007/s11629-015-3466-1

Huang, R.; Ni, Y.; Cao, Z. (2022). Coupled modeling of rainfall-induced floods and sediment transport at the catchment scale. International Journal of Sediment Research, 37, pp 715–728. https://doi.org/10.1016/j.ijsrc.2022.05.002

Huber, A.; Lumassegger, S.; Kohl, B.; Spira, Y.; Weingraber, F.; Achleitner, S. (2021). Modellierung pluvialer Sturzfluten – Anforderungen und Sensitivitäten der 2D-hydraulischenModellierung. Österr. Wasser- und Abfallw., 73, pp 116–133. https://doi.org/10.1007/s00506-021-00749-1

Huthoff, F. (2012). Theory for flow resistance caused by submerged roughness elements. J. Hydraul. Res., 50, 10–17. https://doi.org/10.1080/00221686.2011.636635.

Huthoff, F.; Augistijn, D.C.M. (2006). Hydraulic Resistance of Vegetation: Predictions of Average Flow Velocities Based on a Rigid-Cylinders Analogy; Final Project Report; Planungsmanagement für Auen, University of Twente, The Netherlands.

Huthoff, F.; Augistijn, D.C.M.; Hulscher, S.J.M.H. (2007). Analytical solution of the depth-averaged flow velocity in case of submerged rigid cylindrical vegetation. Water Resour. Res., 43, W06413. https://doi.org/10.1029/2006WR005625.

Hodson, T.O. (2022). Root-mean-square error (RMSE) or mean absolute error (MAE): when to use them or not. Geosci Model Dev, 15(14):5481–7. https://doi.org/10.5194/gmd-15-5481-2022

Hydrotec (2021). Reference Manual, HYDRO_AS-2D, 2D-Flow Model for Water Management Applications, Version 5.2.5; Hydrotec Ingenieurgesellschaft für Wasser und Umwelt mbH: Aachen, Germany.

Hydrotec (2025a) HydroAS, Reference manual, 2D-flow model for water management applications, version 6.2.5, Aachen. https://www.hydrotec.de/wp-content/uploads/HydroAS-Manual.pdf. (accessed on 28.07.2025)

Hydrotec (2025b) HydroAS FT, Reference manual, Add-ons for simulating sediment transport, version 6.2.5, Aachen. https://www.hydrotec.de/wp-content/uploads/HydroAS-Sedimenttransport-Manual.pdf. (accessed on 28.07.2025)

Hydrotec (2025c) HydroAS RiverMesh, User manual, Extension for the generation of a river channel for 2D modeling, version 2.2.1, Aachen. https://www.hydrotec.de/wp-content/uploads/HydroAS-RiverMesh-Manual.pdf. (accessed on 28.07.2025)

Hydrotec (n.d.). Software HYDRO_AS-2D, Version 5.3.4, Ingenieurgesellschaft für Wasser und Umwelt mbH, Aachen, Germany

IPCC (2021). Summary for Policymakers. In Climate Change 2021: The Physical Science Basis. Contribution of Working Group I to the Sixth Assessment Report of the Intergovernmental Panel on Climate Change; Masson-Delmotte, V., Zhai, P., Pirani, A., Connors, S.L., Péan, C., Berger, S., Caud, N., Chen, Y., Goldfarb, L., Gomis, M.I., et al., Eds.; Cambridge University Press: Cambridge, UK; New York, NY, USA, pp. 3–32. https://doi.org/10.1017/9781009157896.001

IPCC (2023). Summary for Policymakers. In: Climate Change 2023: Synthesis Report. Contribution of Working Groups I, II and III to the Sixth Assessment Report of the Intergovernmental Panel on Climate Change [Core Writing Team, H. Lee and J. Romero (eds.)]. IPCC, Geneva, Switzerland, pp. 1-34, https://doi.org/10.59327/IPCC/AR6-9789291691647.001

Järvelä, J. (2004). Determination of flow resistance cause by non-submerged woody vegetation. Int. J. River Basin Manag., 2, 61–70. https://doi.org/10.1080/15715124.2004.9635222

Jia, Y.; Wells, R.R.; Momm, H.G.; Zhang, Y.; Bennett, S.J. (2023). Physically based numerical model for the landscape evolution of soil-mantled watersheds driven by rainfall and overland flow. J. Hydrol., 620, 129419. https://doi.org/10.1016/j.jhydrol.2023.129419

Kaiser, A.; Neugirg, F.; Rock, G.; Müller, C.; Haas, F.; Ries, J. et al. (2014). Small-Scale Surface Reconstruction and Volume Calculation of Soil Erosion in Complex Moroccan Gully Morphology Using Structure from Motion. Remote Sensing, 6(8):7050–80. https://doi.org/10.3390/rs6087050

Karantounias, G. (1972). Dünnschichtabfluss auf Stark Geneigter Ebene. Ph.D. Thesis, University Karlsruhe (TH), Germany.

Khanal, M.; Hasan, M.; Sterbentz, N.; Johnson, R.; Weatherly, J. (2020). Accuracy Comparison of Aerial Lidar, Mobile-Terrestrial Lidar, and UAV Photogrammetric Capture Data Elevations over Different Terrain Types. Infrastructures, 5(8):65. https://doi.org/10.3390/infrastructures5080065

Kilinc, M.; Richardson, E.V. (1973). Mechanics of soil erosion from overland flow generated by simulated rainfall. Hydrology Papers, no. 63, Colorado State University, Fort Collins, Colorado. http://hdl.handle.net/10217/61574

Knisel, W. G. (Ed.) (1980). CREAMS: A field scale model for chemicals, runoff and erosion from agricultural managed systems. USDA, Conservation Research Report 26.

Kou, P.; Xu, Q.; Yunus, A. P.; Ju, Y.; Guo, C.; Wang, C.; Zhao, K. (2020). Multi-temporal UAV data for assessing rapid rill erosion in typical gully heads on the largest tableland of the Loess Plateau, China. Bulletin of Engineering Geology and the Environment, 79, pp. 1861–1877. https://doi.org/10.1007/s10064-019-01631-x

Laflen, J.M., Lane, L.J., Foster, G.R. (1991). WEPP: a new generation of erosion prediction technology. J. Soil Water Conserv., 46, 34–38.

Lavoie, B.; Mahdi, T.F. (2017). Comparison of two-dimensional flood propagation models: SRH-2D and Hydro_AS-2D. Nat Hazards, 86, pp 1207–1222. https://doi.org/10.1007/s11069-016-2737-7

LfU Bayerisches Landesamt für Umwelt (2018). Publ. Handbuch Hydraulische Modellierung. Vorgehensweisen und Standards für die 2-D-hydraulische Modellierung von Fließgewässern in Bayern. 2018. Available online: https://www.bestellen.bayern.de/application/applstarter?APPL=eshop&DIR=eshop&ACTIONxSETVAL(artdtl.htm,APGxNODENR:3779,AARTxNR:lfu_was_00134,AARTxNODENR:351717,USERxBODYURL:artdtl.htm,KATALOG:StMUG,AKATxNAME:StMUG,ALLE:x)=X (accessed on 07.12.2022).

Liang, Q.; Xia, X.; Hou, J. (2016). Catchment-scale High-resolution Flash Flood Simulation Using the GPU-based Technology. Procedia Engineering, 154, pp 975–981. https://doi.org/10.1016/j.proeng.2016.07.585

Liu, K.; Ding, H.; Tang, G.; Na, J.; Huang, X.; Xue, Z. et al. (2016). Detection of Catchment-Scale Gully-Affected Areas Using Unmanned Aerial Vehicle (UAV) on the Chinese Loess Plateau. ISPRS International Journal of Geo-Information, 5(12):238. https://doi.org/10.3390/ijgi5120238

LUBW Landesanstalt für Umwelt, Messungen und Naturschutz Baden-Württemberg (2016). Leitfaden Kommunales Starkregenrisikomanagement in Baden-Württemberg. Available online: https://pudi.lubw.de/detailseite/-/publication/47871 (accessed on 09.09.2025).

LUBW Landesanstalt für Umwelt, Messungen und Naturschutz Baden-Württemberg (2020). Publ. Anhänge 1 a, b, c zum Leitfaden Kommunales Starkregenrisikomanagement in Baden-Württemberg. Available online: https://pudi.lubw.de/detailseite/-/publication/47871 (accessed on 07.09.2024).

LVGL Landesamt für Vermessung, Geoinformation und Landentwicklung (2019). Digitale Geländemodelle [Digital elevation models]. https://www.saarland.de/lvgl/DE/themenaufgaben/themen/geotopographie/digitalegelaendemodelle/digitalegelaendemodelle.html (last accessed: 12.01.2022)

LVGL Landesamt für Vermessung; Geoinformation und Landentwicklung (n.d.): Geoportal Saarland, ALKIS Bodenschätzung (Ressourcenidentifikator: 41583)

Malinowski, R.; Heckrath, G.; Rybicki, M.; Eltner, A. (2022). Mapping rill soil erosion in agricultural fields with UAV-borne remote sensing data. Earth Surf. Process. Landforms., 1–17. https://doi.org/10.1002/esp.5505

Maniak, U. (2016). Hydrologie und Wasserwirtschaft, Eine Einführung für Ingenieure, 7., neu bearbeitete Auflage, Springer Vieweg, pp. 301–414. https://doi.org/10.1007/978-3-662-49087-7

Martínez-Carricondo, P.; Agüera-Vega, F.; Carvajal-Ramírez, F.; Mesas-Carrascosa, F.-J.; García-Ferrer, A.; Pérez-Porras, F.-J. (2018). Assessment of UAV-photogrammetric mapping accuracy based on variation of ground control points. International Journal of Applied Earth Observation and Geoinformation, 72:1–10. https://doi.org/10.1016/j.jag.2018.05.015

Maugnard, A.; Cordonnier, H.; Degre, A.; Demarcin, P.; Pineux, N.; Bielders, C.L. (2014). Uncertainty assessment of ephemeral gully identification, characteristics and topographic threshold when using aerial photographs in agricultural settings. Earth Surf Processes Landf, 39(10):1319–30. https://doi.org/10.1002/esp.3526

Meyer-Peter, E.; Müller, R. (1948). Formulas for Bed-Load Transport. International Association for Hydraulic Structures Research, Second Meeting, 7. – 9.06.1948, Stockholm

Michael, A. (2000). Anwendung des physikalisch begründeten Erosionsprognosemodells EROSION 2D/3D – Empirische Ansätze zur Ableitung der Modellparameter. Dissertation, Technische Universität Bergakademie Freiberg

Michael. A., Schmidt, J., Schmidt, W.A. (1996). EROSION 2D/3D. EIN COMPUTERMODELL ZUR SIMULATION DER BODENEROSION DURCH WASSER. PARAMETERKATALOG SACHSEN. ANWENDUNGEN.

Morgan, R.P.C., Nearing, M.A. (Ed.) (2011). Handbook of Erosion Modelling. Blackwell Publishing Ltd. https://doi.org/ 10.1002/9781444328455

Morgan, R.P.C., Quinton, J.N., Smith, R.E., Govers, G., Poesen, J.W.A., Auerswald, K., Chisci, G., Torri, D., Styczen, M.E. (1998a). The European soil erosion model (EUROSEM): a process-based approach for predicting soil loss from fields and small catchments. Earth Surf. Process. Landforms, 23, 527–544. https://doi.org/10.1002/(SICI)1096-9837(199806)23:6<527::AID-ESP868>3.0.CO;2-5

Morgan, R.P.C., Quinton, J.N., Smith, R.E., Govers, G., Poesen, J.W.A., Auerswald, K., Chisci, G., Torri, D., Styczen, M.E.; Folly, A.J.V. (1998b). The European Soil Erosion Model (EUROSEM): documentation and user guide. Version 3.6, Silsoe College, Cranfield University.

Murphy, E.; Ghisalberti, M.; Nepf, H. (2007). Model and laboratory study of dispersion in flows with submerged vegetation. Water Resour. Res., 43, W05438. https://doi.org/10.1029/2006WR005229.

Nepf, H.M. (2012). Hydrodynamics of vegetated channels. J. Hydraul. Res., 50, 262–279. https://doi.org/10.1080/00221686.2012.696559.

Nepf, H.M.; Vivoni, E.R. (2000). Flow structure in depth-limited, vegetated flow. J. Geophys. Res., 105, 28547–28557. https://doi.org/10.1029/2000JC900145.

Nicosia, A.; Di Stefano, C.; Pampalone, V.; Palmeri, V.; Ferro, V.; Nearing, M.A. (2019). Testing a new rill flow resistance approach using the Water Erosion Prediction Project experimental database. Hydrol. Process., 33, 616–626. https://doi.org/10.1002/hyp.13348.

Nicosia, A.; Di Stefano, C.; Palmeri, V.; Pampalone, V.; Ferro, V. (2020). Flow resistance of overland flow on a smooth bed under simulated rainfall. Catena, 187, 104351. https://doi.org/10.1016/j.catena.2019.104351.

Nicosia, A.; Bischetti, G.B.; Chiaradia, E.; Gandolfi, C.; Ferro, V. (2021). A full-scale study of Darcy-Weisbach friction factor for channels vegetated by riparian species. Hydrol. Process., 35, e14009. https://doi.org/10.1002/hyp.14009.

Nikuradse, J. (1933). Strömungsgesetze in Rauhen Rohren; VDI: Berlin, Germany.

Nunes, J.P.; Nearing, M.A. (2011). Modelling Impacts of Climate Change: Case Studies using the New Generation of Erosion Models. In: Morgan RPC, Nearing MA (Ed.) (2011) Handbook of Erosion Modelling. John Wiley & Sons ISBN: 978-1-4051-9010-7, pp 289–312

Oberle, P.; Kron, A.; Kerlin, T.; Ruiz Rodriguez, E. Nestmann, F. (2021). Diskussionsbeitrag zur Fließwiderstandsparametrisierung zur Simulation der Oberflächenabflüsse bei Starkregen. WasserWirtschaft, 4, 12–21.

Palmeri, V.; Pampalone, V.; Di Stefano, C.; Nicosia, A.; Ferro, V. (2018). Experiments for testing soil texture effects on flow resistance in mobile bed rills. Catena, 171, 176–184. https://doi.org/10.1016/j.catena.2018.07.016.

Parkin, G.W.; Gardner, W.H.; Auerswald, K. (2008). Water Erosion. In: Chesworth W. (eds) Encyclopedia of Soil Science. Encyclopedia of Earth Sciences Series. Springer, Dordrecht. https://doi.org/10.1007/978-1-4020-3995-9_625

Peter, K. D.; d'Oleire-Oltmanns, S.; Ries, J. B.; Marzolff, I.; Aït Hssaine, A. (2014). Soil erosion in gully catchments affected by land-levelling measures in the Souss Basin, Morocco, analysed by rainfall simulation and UAV remote sensing data. Catena, 113, pp. 24–40. http://dx.doi.org/10.1016/j.catena.2013.09.004

Pineux, N.; Lisein, J.; Swerts, G.; Bielders, C.L.; Lejeune, P.; Colinet, G.; Degré, A. (2017). Can DEM time series produced by UAV be used to quantify diffuse erosion in an agricultural watershed? Geomorphology, 280, pp. 122–136. http://dx.doi.org/10.1016/j.geomorph.2016.12.003

Polyakov, V.; Stone, J.; Holifield Collins, C.; Nearing, M.A.; Paige, G.; Buono, J.; Gomez-Pond, R.-L. (2018). Rainfall simulation experiments in the southwestern USA using the Walnut Gulch Rainfall Simulator. Earth Syst. Sci. Data, 10, 19–26. https://doi.org/10.5194/essd-10-19-2018.

Pourali, S.; Arrowsmith, C.; Chrisman, N.; Matkan, A. (2014). Vertical accuracy assessment of LiDAR ground points using minimum distance approach. CEUR Workshop Proc. 2014, 1142, 86–96. In: Winter S and Rizos C, Editors. Research@Locate'14, Canberra, Australia, 07-09 April 2014, published at http://ceur-ws.org

Prandtl, L. (2009). II. Theoretischer Teil. Zur turbulenten Strömung in Rohren und längs Platten. In Ergebnisse der Aerodynamischen Versuchsanstalt zu Göttingen. IV. Lieferung; Dillmann, A., Ed.; Göttinger Klassiker der Strömungsmechanik: Göttingen, Germany, https://doi.org/10.17875/gup2009-104

Prasuhn, V. (1991). Bodenerosionsformen und -prozesse auf tonreichen Böden des Basler Tafeljura (Raum Anwil, BL) und ihre Auswirkungen auf den Landschaftshaushalt. In: Basler Beiträge zur Physiogeographie: Physiogeographica, Bd. 16

Przybilla, H.-J.; Bäumker, M. (2020). Untersuchungen zur Qualität des Realtime Kinematic GNSS Systems der DJI Phantom 4 RTK Quality control of the realtime kinematic GNSS systems of DJI Phantom 4 RTK. Conference Paper, 40. Wissenschaftlich-Technische Jahrestagung der DGPF in Stuttgart – Publikationen der DGPF, 2020, Band 29, pp. 47–61.

QGIS (n.d.). Software QGIS, Version 3.26.2

Quan, X.; He, J.; Cai, Q.; Sun, L.; Li, X.; Wang, S. (2020). Soil erosion and deposition characteristics of slope surfaces for two loess soils using indoor simulated rainfall experiment. Soil Till. Res., 204, 104714. https://doi.org/10.1016/j.still.2020.104714

Robinson, A.; Lehmann, J.; Barriopedro, D. et al. (2021). Increasing heat and rainfall extremes now far outside the historical climate. npj Clim Atmos Sci 4, 45. https://doi.org/10.1038/s41612-021-00202-w

Römkens, M.J.M.; Helming, K.; Prasad, S.N. (2001). Soil erosion under different rainfall intensities, surface roughness, and soil water regimes. Catena, 46, pp. 103–123. https://doi.org/10.1016/S0341-8162(01)00161-8

Ruiz Rodriguez, E. Trost, L. (2017). Umgang mit Starkniederschlägen in Hessen. Auszug aus dem 3. Zwischenbericht. KLIMPRAX Starkregen Arbeitspaket 2. Hochschule RheinMain: Wiesbaden, Germany.

Sanz-Ramos, M.; Bladé, E.; González-Escalona, F.; Olivares, G.; Aragón-Hernández, J.L. (2021). Interpreting the Manning Roughness Coefficient in Overland Flow Simulations with Coupled Hydrological-Hydraulic Distributed Models. Water, 13, 3433. https://doi.org/10.3390/w13233433

Scherer, U.; Zehe, E.; Träbing, K.; Gerlinger, K. (2012). Prediction of soil detachment in agricultural loess catchments: Model development and parameterization. Catena, 90, 63–75. https://doi.org/10.1016/j.catena.2011.11.003

Scheres, B.; Schüttrumpf, H.; Felder, S. (2020). Flow Resistance and Energy Dissipation in Supercritical Air-Water Flows Down Vegetated Chutes. Water Resour. Res., 56, e2019WR026686. https://doi.org/10.1029/2019WR026686.

Schmidt, J. (1984). Experimentelle Untersuchungen und Modellvorstellungen zur Bodenerosion durch Wasser. Mitteilg. Dtsch. Bodenkdl. Gesellsch., Bd. 39, S. 139–144

Schmidt, J. (1988). Wasserhaushalt und Feststofftransport an geneigten, landwirtschaftlich bearbeiteten Nutzflächen. Dissertation, FU Berlin

Schmidt, J. (1996). Entwicklung und Anwendung eines physikalisch begründeten Simulationsmodells für die Erosion geneigter landwirtschaftlicher Nutzflächen. Berliner Geogr. Abb., Heft 61: 1–148, Berlin.

Schröder, R. (1990). Hydraulische Methoden zur Erfassung von Rauheiten; Schriftenreihe des DVWK: Parey, Germany, Volume 92. ISBN: 978-3-490-09297-7.

Schubert, J.E.; Sanders, B.F.; Smith, M.J. Wright, N.G. (2008). Unstructured mesh generation and landcover-based resistance for hydrodynamic modeling of urban flooding. Adv. Water Resour., 31, 1603–1621. https://doi.org/10.1016/j.advwatres.2008.07.012.

Schwertmann, U., Vogl, W., Kainz, M. (1987). Bodenerosion durch Wasser. Vorhersage des Abtrags und Bewertung von Gegenmaßnahmen. 2. Auflage. Stuttgart.

Semwal, P.; Khobragade, S.D.; Nainwal, H.C. (2017). Modelling of Recent Erosion Rates in a Lake Catchment in the North-Western Siwalik Himalayas. Environ Process, 4, 355–374. https://doi.org/10.1007/s40710-017-0234-y

Smith, R.E.; Goodrich, D.C.; Unkrich, C.L. (1999). Simulation of selected events on the Catsop catchment by KINEROS2 A report for the GCTE conference on catchment scale erosion models. Catena, 37, pp. 457–475. https://doi.org/10.1016/S0341-8162(99)00033-8

Soininen, V.; Hyyppä, E.; Muhojoki, J.; Luoma, V.; Kaartinen, H.; Lehtomäki, M. et al. (2024). Accuracy comparison of terrestrial and airborne laser scanning and manual measurements for stem curve-based growth measurements of individual trees. Science of Remote Sensing, 9:100125. https://doi.org/10.1016/j.srs.2024.100125

Stone, J.J.; Lane, L.J., Shirley, E.D.; Hernandez, M. (1995). HILLSLOPE SURFACE HYDROLOGY. In: Flanagan, D.C.; Nearing, M.A. (Eds.) USDA - WATER EROSION PREDICTION PROJECT HILLSLOPE PROFILE AND WATERSHED MODEL DOCUMENTATION. NSERL Report No. 10. Chapter 4, pp. 4.1–4.20

Štroner, M.; Urban, R.; Reindl, T.; Seidl, J.; Brouček, J. (2020). Evaluation of the Georeferencing Accuracy of a Photogrammetric Model Using a Quadrocopter with Onboard GNSS RTK. Sensors, 20(8):2318. https://doi.org/10.3390/s20082318

Taccone, F.; Antoine, G.; Delestre, O.; Goutal, N. (2020). A new criterion for the evaluation of the velocity field for rainfall-runoff modelling using a shallow-water model. Adv. Water Resour., 140, 103581. https://doi.org/10.1016/j.advwatres.2020.103581

Tackmann, R. (2010). Analysis of rill erosion in cohesive soils. Doctoral thesis.

Taddia, Y.; González-García, L.; Zambello, E.; Pellegrinelli, A. (2020). Quality Assessment of Photogrammetric Models for Façade and Building Reconstruction Using DJI Phantom 4 RTK. Remote Sensing, 12(19):3144. https://doi.org/10.3390/rs12193144

Tang, X.; Wu, S.; Rahimi, H.; Xue, W.; Lei, Y. (2018). Experimental Study of Open Channel Flows with Two Layers Vegetation. In Proceedings of the 2nd International Symposium on Hydraulic Modelling and Measuring Technology Congress, 30 May–1 June 2018, Nanjing, China.

Trenberth, K.E.; Dai, A.; Rasmussen, R.M.; Parsons, D.B. (2003). The Changing Character of Precipitation. Bulletin of the American Meteorological Society, 84 (9), pp. 1205–1218. https://doi.org/10.1175/BAMS-84-9-1205

Tügel, F. (2023). Flash flood modeling with a specific focus on arid regions and infiltration. Dissertation, Technische Universität Berlin

Tyrna, B.; Assmann, A.; Fritsch, K. Johann, G. (2018). Large-scale high-resolution pluvial flood hazard mapping using the raster-based hydrodynamic two-dimensional model FloodAreaHPC. J. Flood Risk Manag., 11, 1024–1037. https://doi.org/10.1111/jfr3.12287.

USDA (2008). DRAFT USER'S REFERENCE GUIDE. Revised Universal Soil Loss Equation Version 2 (RUSLE2). USDA-Agricultural Research Service. Washington, D.C. https://www.ars.usda.gov/southeast-area/oxford-ms/national-sedimentation-laboratory/watershed-physical-processes-research/research/rusle2/revised-universal-soil-loss-equation-2-rusle2-documentation/

USDA (2013). Science Documentation: Revised Universal Soil Loss Equation Version 2 (RUSLE2) (for the model with release date of May 20, 2008). USDA-Agricultural Research Service. Washington, D.C. https://www.ars.usda.gov/southeast-area/oxford-ms/national-sedimentation-laboratory/watershed-physical-processes-research/research/rusle2/revised-universal-soil-loss-equation-2-rusle2-documentation/

Van Velzen, E.H.; Jesse, P.; Cornelissen, P.; Coops, H. (2003). Stromingsweerstand Vegetatie in Uiterwaarden; Handboek. Part 1 and 2. RIZA Reports, 2003.028 and 2003.029; Directoraat-Generaal Rijkswaterstaat, RIZA: Arnhem, The Netherlands.

Vargas-Luna, A.; Crosato, A.; Uijttewaal, W.S.J. (2015). Effects of vegetation on flow and sediment transport: Comparative analyses and validation of predicting models. Earth Surf. Process. Landf., 40, 157–176. https://doi.org/10.1002/esp.3633

Wainwright, J.; Parsons, A.J.; Cooper, J.R.; Gao, P.; Gillies, J.A.; Mao, L.; Orford, J.D.; Knight, P.G. (2015). The concept of transport capacity in geomorphology, Rev Geophys, 53, 1155–1202, https://doi.org/10.1002/2014RG000474

Wang, S.; Flanagan, D.C.; Engel, B.A. (2019a). Estimating Sediment Transport Capacity for Overland Flow, J. Hydrol., 578. https://doi.org/10.1016/j.jhydrol.2019.123985

Wang, W.-J.; Peng, W.-Q.; Huai, W.-X.; Katul, G.G.; Liu, X.-B.; Qu, X.-D.; Dong, F. (2019b). Friction factor for turbulent open channel flow covered by vegetation. Sci. Rep., 9, 5178. https://doi.org/10.1038/s41598-019-41477-7.

Wilson, C.A.M.E.; Horritt, M.S. (2002). Measuring the flow resistance of submerged grass. Hydrol. Process., 16, 2589–2598. https://doi.org/10.1002/hyp.1049.

Winterrath, T.; Brendel, C.; Hafer, M.; Junghänel, T.; Klameth, A.; Lengfeld, K.; Walawender, E.; Weigl, E.; Becker, A. (2018). RADKLIM Version 2017.002: Reprocessed quasi gauge-adjusted radar data, 5-minute precipitation sums (YW). https://doi.org/10.5676/DWD/RADKLIM_YW_V2017.002

Wirtz, S.; Seeger, M.; Ries, J.B. (2010). The rill experiment as a method to approach a quantification of rill erosion process activity. Z. Geomorphologie, 54, 1, 47–64. https://doi.org/10.1127/0372-8854/2010/0054-0004

Wirtz, S.; Seeger, M.; Ries, J.B. (2012). Field experiments for understanding and quantification of rill erosion processes. Catena, 91, 21–34. https://doi.org/10.1016/j.catena.2010.12.002

Wischmeier, W.H., Smith, D.D. (1978). Predicting rainfall erosion losses. Agric. Handb. no. 537, 285–291. https://doi.org/10.1029/TR039i002p00285

Woolhiser, D.A.; Smith, R.E.; Goodrich, D.C. (1990). KINEROS: A kinematic runoff and erosion model: documentation and user manual. USDA., Agric. Res. Service, ARS-77

Wu, J.; Hu, P.; Zhao, Z.; Lin, Y.-T.; He, Z. (2023). A GPU-accelerated and LTS-based 2D hydrodynamic model for the simulation of rainfall-runoff processes, J. Hydrol., 623, 129735. https://doi.org/10.1016/j.jhydrol.2023.129735

Yalin, M.S. (1963). An Expression for Bed-Load Transportation. J. Hydraul. Div., 89, 3, 221–250. https://doi.org/10.1061/JYCEAJ.0000874

Yörük, A. (2008). Unsicherheiten bei der hydrodynamischen Modellierung von Überschwemmungsgebieten. Dissertation, Universität der Bundeswehr München

Yörük, A., Sacher, H. (2014). Methoden und Qualität von Modellrechnungen für HW-Gefahrenkarten. In Technische Universität Dresden, Institut für Wasserbau und technische Hydromechanik (Ed.): Simulationsverfahren und Modelle für Wasserbau und Wasserwirtschaft. Dresdner Wasserbauliche Mitt., 50, 55–64.

Zanke, U. (2013). Hydraulik für Wasserbau, 3rd ed.; Springer Vieweg: Berlin/Heidelberg, Germany. https://doi.org/10.1007/978-3-642-05489-1

Zeiger, S.J.; Hubbart, J.A. (2021). Measuring and modeling event-based environmental flows: An assessment of HEC-RAS 2D rain-on-grid simulations. J. Environ. Manag., 285, 112125. https://doi.org/10.1016/j.jenvman.2021.112125.

Zhang, S.; Li, F.; Li, T.; Yang, J.; Bu, K.; Chang, L. et al. (2015). Remote sensing monitoring of gullies on a regional scale: A case study of Kebai region in Heilongjiang Province, China. Chin Geogr Sci, 25(5):602–11. https://doi.org/10.1007/s11769-015-0780-z

Zhang, L.; Liu, X.; Song, Y.; Li, J.; Cai, C.; Zhao, X.; Li, Z. (2021). Characterization of Surface Runoff Pathways and Erosion Using Hydrological Attributes Under Simulated Rainfall. Front. Earth Sci., 9:683473. https://doi.org/10.3389/feart.2021.683473

Appendices

Appendix A: Publications

Appendix A.1: Peer-Reviewed Publications – Scientific Journals

Hinsberger, R., Biehler, A.; Yörük, A. (2022). Influence of Water Depth and Slope on Roughness – Experiments and Roughness Approach for Rain-on-Grid Modeling, *Water*, 14(24), 4017. https://doi.org/10.3390/w14244017

Hinsberger, R. (2024). Analysis of heavy precipitation-induced rill erosion, *Environ. Earth Sci*. 83, 354, 2024. https://doi.org/10.1007/s12665-024-11671-6

Hinsberger, R.; Yörük, A. (2025). Accuracy of recording linear erosion using an unmanned aerial vehicle (UAV). PLoS One, 20 (9): e0329286. https://doi.org/10.1371/journal.pone.0329286

Hinsberger, R.; Yörük, A. (2025). Application of a 2D Hydrodynamic Numerical Model for Heavy Precipitation-Induced Soil Erosion. Accepted for Publication in Environmental Processes. https://doi.org/10.1007/s40710-025-00797-9

Appendix A.2: Non Peer-Reviewed Publications

Yörük, A., Buchholz, O.; Hinsberger, R. (2021). Digitale Daseinsvorsorge im Bereich des Starkregenrisiko-Managements, ASG, Ländlicher Raum, 03/2021

Hinsberger, R.; Yörük, A. (2023). Notwendigkeit und Realisierung von Erosionssimulationen auf Grundlage von Starkregenereignissen, KW Korrespondenz Wasserwirtschaft, 2023 (16), Nr. 11

Appendix B: Conference Contributions

Hinsberger, R.; Yörük, A. (2022). Notwendigkeit und Realisierung von Erosionssimulationen auf Grundlage von Starkregenereignissen, 23. Tag der Hydrologie, 22./23. März 2022, München – Presentation (Book of Abstracts TdH 2022, S. 10 ff)

Hinsberger, R.; Yörük, A. (2024). Simulation starkregenbasierter, linearer Erosion mit 2D-Modellen, 24. Tag der Hydrologie 2024, 19. – 21.03.2024, Berlin – Poster

Hinsberger, R. (2024). F+E Projekt: Bodenerosion und Starkregengefahrenkarten Saarland, Saarländische Wassertage, 10./11. April 2024, Saarbrücken – Presentation (Tagungsband, ISBN 978-3-00-079244-1, S. 26-32, https://www.fg-wasser.de/saarl%C3%A4ndische-wassertage-2024/)

Hinsberger, R.; Yörük, A. (2024). Application of a 2D hydrodynamic numerical model to simulate erosion caused by heavy precipitation, ICCE symposium, 23. – 26. Juli 2024, Eichstätt – Presentation

Hinsberger, R.; Yörük, A. (2025). Numerische Simulation flächiger und linearer Bodenerosion mittels 2D-Modellierung, 25. Tag der Hydrologie 2025, 19. – 21.03.2025, Augsburg – Poster

Hinsberger, R.; Yörük, A. (2025). Numerical Simulation of Sheet and Rill Erosion using 2D Modelling, EGU General Assembly 2025, Vienna, Austria, 27 Apr–2 May 2025, EGU25-5175, https://doi.org/10.5194/egusphere-egu25-5175. – Presentation

Hinsberger, R.; Yörük, A. (2025). Evaluation of the new HydroAS–Govers Model using Erosion Data Resulting from Natural Rainfall, 41st IAHR World Congress, Singapur, 22–27 June 2025 – Poster